Lithospheric Deformations in Central Asia derived from Gravity Data

Dissertation

zur Erlangung des Doktorgrades
der Naturwissenschaften im Fachbereich
Geowissenschaften
der Universität Hamburg

vorgelegt von

Xiaodian Jiang
aus Qingdao, China

Hamburg
Dezember 2004

Als Dissertation angenommen vom Fachbereich Geowissenschaften der Universität Hamburg

auf Grund der Gutachten von Prof. Dr. H. K. Wong

und Dr. T. Lüdmann

Hamburg, den 15.Dez. 2004

Prof. Dr. H. Schleicher
Dekan
des Fachbereichs Geowissenschaften

Contents

Abstract

Central Asia is characterized by a number of spectacular tectonic units such as the Tibetan Plateau, the Tien Shan intra-continental mountain belt and the Altyn Tagh strike-slip fault. Deformation of the lithosphere of these units is not well understood. In this dissertation, an attempt is made to answer the following tectonic questions: To what extent do the tectonic units formed in the upper crust in the course of the convergence between India and Eurasia weaken the underlying lithosphere? How is the Tibetan Plateau gravitationally compensated along its northern boundary? Do the Altyn Tagh and/or West Kunlun faults persist as vertical strike-slips throughout the crust and mantle lithosphere, thus representing a fundamental plate boundary? Which dynamic processes in the crust and mantle of the Tien Shan are responsible for intra-continental mountain building? What characterizes the local stress field in the Tien Shan and what causes the deformation of these mountains?

To answer these questions, the elastic plate theory is used to interpret gravity and topography data, and in turn to derive specific characteristics of the lithospheric structure in Central Asia. Theoretical deflection of the elastic plate or plates were calculated using the 3D and 2D finite-difference methods. Variable-rigidity elastic plates are subjected to vertical and horizontal loads, shear forces, and terminal bending moments. Surface topographic data from the Topo30 dataset is used as vertical surface loading to calculate the flexure of the elastic lithosphere. Most of the gravity data used were digitized from the 1:4,000,000 map "Regional Bouguer Gravity of China". The resulting dataset is supplemented by 468 new gravity stations surveyed in 1997 and 1998 across the northern edge of Tibet.

Our results show that the mechanical strength of the lithosphere in Central Asia varies significantly from a small elastic thickness of less than 15 km to a moderate thickness of 40-50 km. Weak zones exist in the major mountain building areas such as the Tien Shan, Altyn Shan, West Kunlun Shan, Qilian Shan and the Indus-Zhangbo suture zone. Stronger zones are located in the less deformed basinal areas such as the Tarim, Qaidam and Sichuan basins as well as in certain topographically low areas (< 2500 m). Of particular interest is the central and eastern Tibetan plateau. Here, the elastic strength is high, namely close to that of the lowlands. Even the steep transition from the eastern high plateau to its adjacent lowland (Sichuan Basin) does not significantly weaken the lithosphere underneath.

A number of plausible models of crustal structure were constructed in an effort to reproduce the main features of the Bouguer gravity and topographic data by integrating information on the sedimentary column derived from exploration seismology in the Tarim and Qaidam basins. Based on the gravity fit, it was found that elastic strength across the Altyn Tagh Fault is zero, allowing for the possibility that this fault cuts through the entire lithosphere and has a negligible thrust component currently or in the past. This result is consistent with tectonic models that assume the creation of a thickened crust in northern Tibet through thick-skinned thrust sheets progressively overriding Asia to the northeast as the Altyn Tagh, behaving as a classical transform fault, propagates in that direction. Farther west, the gravity observations across the West Kunlun Fault are best explained by significant underthrusting of the high topography by an elastic plate with effective thicknesses between 30 and 40 km, in agreement with geological interpretations and modelling of earlier, but very sparse gravity observations.

Sediment corrections in the Zungar and Tarim basins north and south of the Tien Shan respectively as well as 2D modelling along four profiles were carried out. A number of plausible models of lithospheric structure were also tested in order to reproduce the main features of the Bouguer gravity and topography in the space domain. Our results indicate that the lithospheric elastic strength across the western Tien Shan is zero, suggesting that the Southern Tien Shan Thrust Fault cuts through the entire lithosphere. In contrast, the gravity data are best fitted by an underthrusting elastic plate with an effective thickness of 40-45 km in the Tarim and Zungar basins, decreasing to 20-25 km beneath the Tien Shan. Deformations of the Tien Shan are dominated by underthrusting of a rigid plate beneath the mountain range.

We examined the local stress field in the Tien Shan and analysed how the older orogenic event is related to the reactivation of the Tien Shan under the present tectonic regime. We calculated the sum of the stress fields from (1) interaction between the Indian and Eurasian plates, (2) the elevated gravitational potential energy, and (3) bending of the lithosphere in the Tien Shan area. This composite stress field is consistent with the stress derived from seismic focal solutions, GPS measurements and surface geology. Our results show that the flexural stress field resulting from bending of the lithosphere beneath the Tien Shan contributes the most to the total stress field. Furthermore, they suggest that the Tien Shan uplifted in response to a local intra-continental stress field rather than to the regional stress caused by the collision between India and Eurasia.

Chapter 1. Introduction

The study of lithospheric deformations in this dissertation is focused on Central Asia, which includes western People's Republic of China, northern part of India, and southern Mongolia (Fig. 1). The relief in the study area has been significantly changed and is still changing due to convergence between India and Eurasia. Topographic highs include the Tibetan Plateau and the Tien Shan. The Tibetan Plateau is the largest high plateau in the world with an average elevation of about 5000 m and a crustal thickness of 70 km. The Tien Shan is one of the highest, young and seismically active intra-continental mountain belts in Central Asia. Topographic lows include the Tarim, Zungar, and Sichuan basins. The Tarim Basin is centred at the vast sandy Takla Makan, the driest desert in Asia. Dune ridges in its interior rise to local heights of as much as 100 m. The Zungar and Sichuan basins which contain some sandy and stony deserts are primarily a region of fertile steppe (*Xia and Fang*, 2000*; Zhou*, 1992).

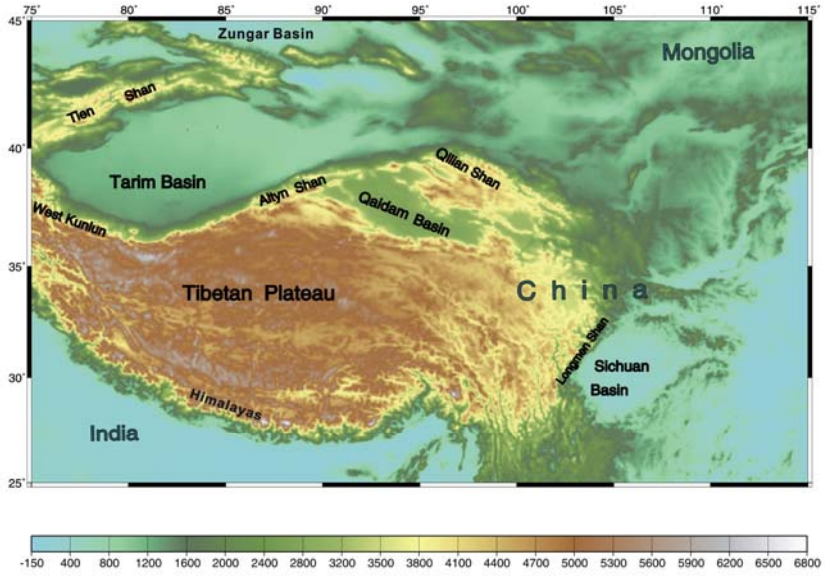

Figure 1. Regional physiography of the study area. Topography is from the Topo30 database. The names of major geographic features are also shown. The word *Shan* in Chinese means mountain. The colour bar is elevation in meters.

The Tibetan Plateau is bordered by the Himalaya mountains in the south, the Qilian, Kunlun and Altyn faults in the north, and Longman Shan in the east (Fig. 1). The Himalayas are the highest mountains in the world. The Altyn Tagh is one of the largest intra-continental strike-slip faults on Earth. The surface of the Tibetan Plateau is covered with salt lakes and marshes, and is transected by several low relief mountain ranges (*Larson et al.,* 1999; *Leven et al.,* 2000*; Rong and Jackson,* 2000). Many large rivers in Asia, such as the Indus, Yangtze, and Yellow River, originate from this high plateau (*Harrison et al.,* 1992). A large range of vertical ecosystem zones exists from the high Himalayas to the low Indian subcontinent.

With the closure of the Tethys and the collision between the Indian subcontinent and Eurasia in the Paleogene (*Allegre et al.,* 1984*; Dewey and Burke,* 1973*; Gansser,* 1974*; Molnar and Tapponnier,* 1975), spectacular deformation belts were formed. This collision is still active today, making Tibet an unique natural laboratory for geologists and geophysicists to study continental lithospheric composition, inter- and intra-plate deformation, the geological processes involved in continent-continent collision, and the effects of mountain building and highland formation.

Geoscientists have been focusing on Central Asia for the last three decades. The studies carried out aim at a better understanding of the mechanisms of uplift of the Tibetan Plateau, the deep structure of the continental crust in this collision zone, and the interactions between crust and mantle in a rapidly evolving mountain. More general aims include major tectonic processes shaping the Earth, tectonic evolution of the continental lithosphere and its relationship to global tectonics.

In our study area, many tectonic questions are still under debate. For example, is the plateau uplifted uniformly and what mechanisms thickened the Tibetan crust? What are the crust and mantle features in the continent-continent collision zone? To what extent are these upper crustal features coupled with deformations of the upper mantle lithosphere beneath them? Does the Tarim Basin subduct beneath the Tibetan Plateau anywhere along the Altyn Tagh or Western Kunlun faults? Although our understanding of Central Asian tectonics has significantly improved through numerous scientific expeditions to Tibet in the past two decades, the data collected in this area are still very limited relative to the size of the region.

Because large-scale lithospheric deformations usually define regional tectonic features, we will focus on three questions in this dissertation. Firstly, is the upper crustal flexure in Central Asia coupled with or decoupled from the deformation of the upper mantle litho-

sphere? Here, we hope to derive information on the laterally inhomogeneous lithosphere in Central Asia and determine the elastic strengths of the different tectonic units. Secondly, how is the plateau compensated along its northern boundary? Is there evidence that the Altyn Tagh persists as a vertical strike-slip fault throughout the crust and mantle lithosphere, thus representing a fundamental plate boundary? Thirdly, what are the major tectonic consequences of uplift of the Tien Shan? And fourthly, what are the deep structure and kinematics of the deformations in the Tien Shen? Our ultimate goal is to better understand the dynamic processes responsible for intra-continental mountain building.

Chapter 2. General geological setting of Central Asia

Tectonics in Central Asia is characterized by relative convergence of the Indian, Pacific and Philippine plates toward the Eurasian plate. Our study area lies in as well as near this convergence zone, and includes the majority of the Yangtze block, the Sino-Korean platform, the Tarim block, the Qaidam block, the Tibetan Plateau and the Mongolian block (*Sengör,* 1996*; Yin and Harrison* 2000). These blocks are separated by suture zones, the geometry and distribution of which have been significantly modified by various tectonic events (Fig. 2). The Yangtze block and the Sino-Korean platform were sutured in the Late Triassic along the Qilian-Qinling suture zone (*Yin and Nie,* 1996). The Mongolian and Sino-Korean blocks were sutured along the Tien Shan-Yin Shan suture zone in the Permian and the Jurassic (*Calais et al.,* 2002*; Petit et al.,* 2002). The Tien Shan also separates the Tarim block from Mongolia (*Neil and Houseman,* 1997). The Altyn Tagh Fault separates the Tarim block from the Qaidam block. The Indian subcontinent underthrusts the Tibet block along the Indus-Zhangbo suture zone (*Tapponnier et al.,* 2001).

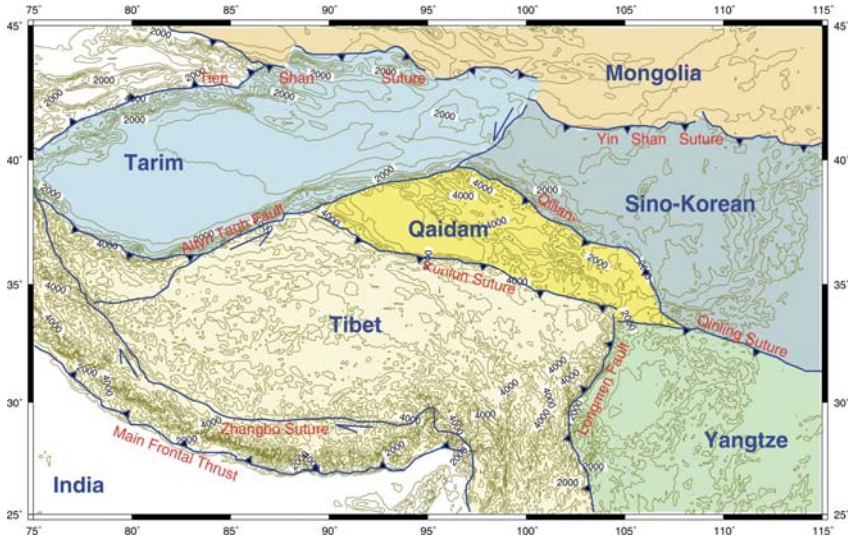

Figure 2. Simplified map of the major tectonic blocks and tectonic boundaries of the study area, modified from *Yin and Harrison* (2000) *and Tapponnier et al.* (2001). Blue lines are major faults. The background lines are topography in meters. The arrows indicate strike-slip direction.

The following discussion outlines the geological framework of these regions, especially their tectono-stratigraphic and tectonic features.

The Yangtze block

The Yangtze block is bounded by the Qinling Fault to the north, and the Longmen and Xian Shuihe faults to the west. To the east, it extends into the East China Sea (Fig. 3). Sichuan Basin is the major sedimentary basin in this block.

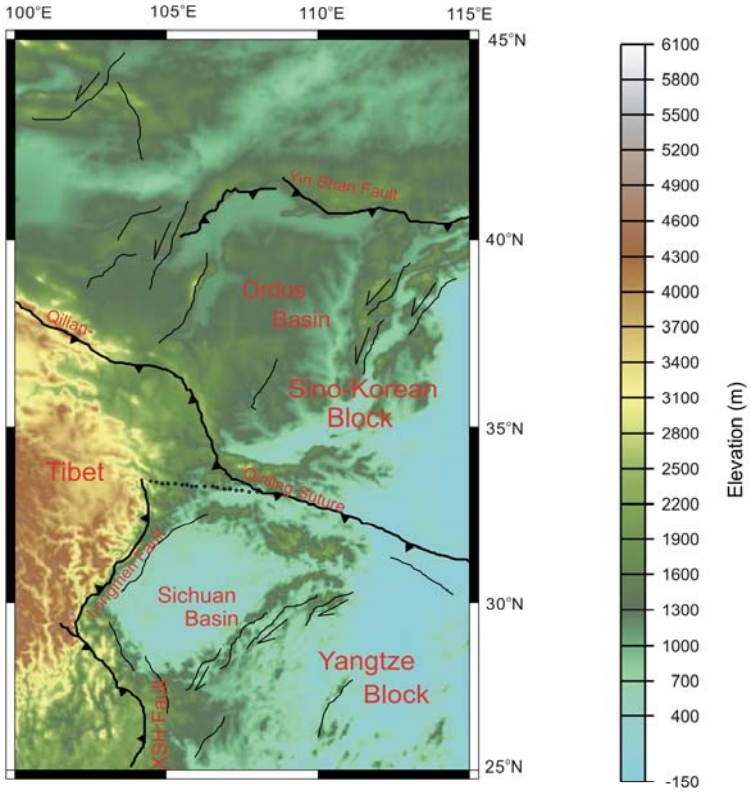

Figure 3. Tectonic framework of the Yangtze and Sino-Korean blocks. Bold lines are boundary faults that usually reach the mantle, and thin lines are crustal faults within the blocks. Adapted from *Ren et al.* (1999). The colour bar is elevation in meters.

The basement of the Yangtze Platform consists primarily of two types of rocks: high-grade metamorphic crystalline rocks of Lower Archean to Upper Proterozoic age and low-grade metamorphic folded rocks of Middle and Upper Proterozoic age. Deep-marine shales, cherts, and thick sandy mudstone beds were deposited from the Sinian to the Lower Palaeozoic (*Yang et al.*, 1986). In the Late Precambrian, the Yangtze block was a passive continental margin as evidenced by continuous shallow marine sedimentation (*Ji and Coney*, 1985*; Yang et al.*, 1986*; Yin and Nie*, 1993). Because this block was rifted and uplifted during the Silurian, unmetamorphosed sedimentary sequences of this age are generally

absent. The Devonian and Carboniferous sediments are confined to the edge of this block. Limestones, mudstones and interbedded basalts were deposited in the Permian. Between the Upper Permian and the Triassic, the sedimentation pattern changed on the Yangtze block, with dominantly shallow marine sedimentation giving way to terrestrial clastic sedimentation. This marine to terrestrial transition may be a result of the collision between the Yangtze and Sino-Korean blocks (*Yin and Nie,* 1996). The Jurassic fluvial sediments conformably overlie a Triassic series (*Yang and Besse,* 2001). The unconformity at the base of the Eocene indicates a pre-Eocene phase of deformation related to the last phase of orogeny from Late Cretaceous to Early Tertiary. The Cenozoic sediments consist of a sequence of terrestrial fluvial and alluvial deposits (Fig. 4).

After occasional connections with East Gondwanaland up to the Devonian, the Yangtze block was left at low-latitude positions, while East Gondwanaland drifted rapidly towards the South Pole during the mid-Carboniferous (*Hacker et al.,* 1996*; Yin and Nie,* 1996). The Yangtze block acted as a stable unit with relatively little internal deformations until Mesozoic time. The Mesozoic continent-continent collision and contemporaneous northward subduction and subsequent exhumation of the continental Yangtze plate (*Hacker et al., 1996;* 2000) led to complex, large-scale crustal shortening along the Qilian-Qinling suture (*Ratschbacher et al.,* 2000). This deformation is reflected in major changes in depositional patterns: from shallow marine to non-marine in character. As a result of the collision of India with Eurasia in the Cenozoic, deformations occurred along the western margin of the Yangtze block. A series of NE trending folds and faults appeared in the southwestern Yangtze block (Fig. 3).

The Sino-Korean block

The Sino-Korean block is bounded by the Qilian-Qinling Fault to the south and west, and the Yin Shan Fault to the north (Fig. 3). The Yangtze and Mongolia blocks lie to its south and north, respectively. It extends into the Gulf of Bohai and the northern Yellow Sea.

The Sino-Korean block is the oldest block in China and consists of high-grade metamorphic Lower Archean basement rocks with complicated superimposed folds. The Sino-Korean block and the Yangtze block are similar stable cratons, but their stratigraphies are significantly different (Fig. 4). From the Proterozoic to the Lower Palaeozoic, stable shallow water clastics and carbonates were widely distributed in the Sino-Korean block,

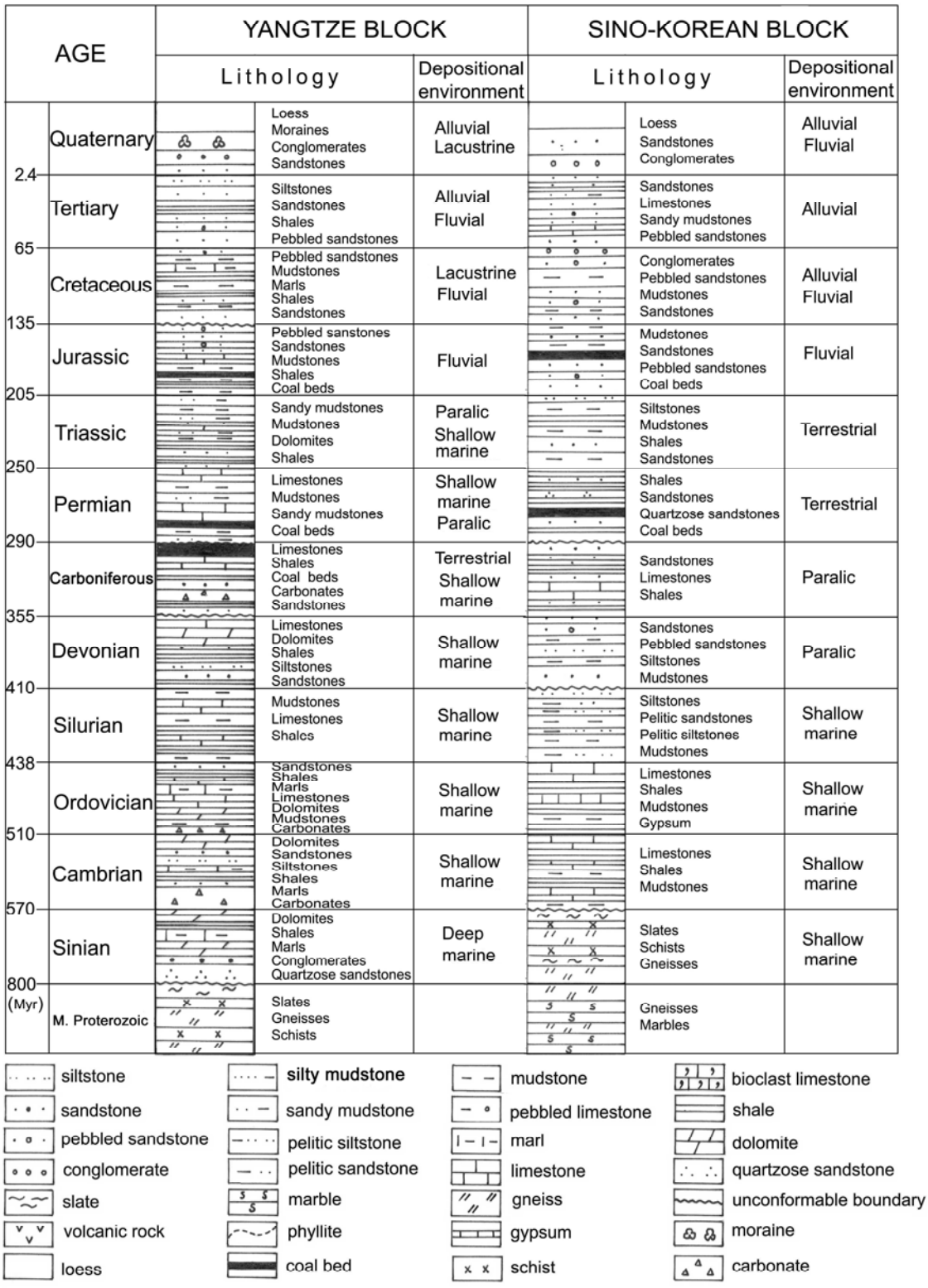

Figure 4. Schematic stratigraphic columns and facies interpretations from the Archean to the Cenozoic of the Yangtze and Sino-Korean blocks. Adapted from *Yang and Besse* (2001).

and Sinian strata were rare except in the marginal areas. There are abundant volcanic rocks in the Precambrian sequences (*Rong et al.,* 2001; *Wang,* 1985; *Yang et al.,* 1986; *Yin and Nie,* 1993). During the Carboniferous to the Permian, a transition from marine to terrestrial deposition occurred. This terrestrial deposition continued to the Triassic. Sandstones, mudstones and interbedded conglomerates were deposited in the Mesozoic. The Cenozoic sediments are alluvial, fluvial and lacustrine.

Analogous to the Yangtze block, the Sino-Korean block was also at equatorial latitudes but at a different longitude in the Palaeozoic, and it drifted northward at the beginning of the Carboniferous (*Wu et al.,* 1990). Collision between the Yangtze and Sino-Korean blocks started during the Mesozoic, and was completed before the Cretaceous (*Wang et al.,* 2001*; Gilder and Courtillot,* 1997). The two blocks were sutured along the Qilian-Qinling orogenic zone with large-scale crustal overthrusting (*Li et al.,* 1978; *Mattauer et al.,* 1985; *Meng and Zhang,* 1999; *Oberhänsli et al.,* 2002). In the Permian and the Jurassic, both subduction of the Qaidam block from the southwest (*Ritts et al.,* 2001; *Yin and Nie,* 1996) and underthrusting of the Siberia block from the north resulted in NE-trending folds and faults in the Sino-Korean block with significant crustal shortening (*Burov et al.,* 1993; *Darby and Ritts* 2002) (Fig. 3). Various basins (e.g., the Ordos Basin) developed in the Sino-Korean block from the Mesozoic to the Cenozoic.

The Tarim block

The Tarim block is bounded by the Tien Shan Fault to the north, the West Kunlun Fault to the southwest and the Altyn Tagh Fault to south (Fig. 5). This isolated rigid block is surrounded on all sides by active intraplate or interplate orogenic zones.

The Tarim Basin has a Neogene sediment cover with a maximum thickness of 15 km (*Jia et al.,* 1991). Its basement consists of strata of Sinian age or older, including high-grade metamorphic rocks of Archean age, intermediate-grade metamorphic rocks of Lower Proterozoic age and low-grade metamorphic rocks of Middle and Upper Proterozoic age (*Zhou and Chen,* 1990). The basin was in a stable, deep marine depositional environment with carbonates and sandstones during the Lower Palaeozoic (*Zhou and Chen,* 1990). During the Silurian, the passive continental margin changed into a volcanic arc in the northern Tarim block and the southern Tarim block was subjected to regional uplift, so that Silurian sediments are absent. The Tarim block was characterized by shallow marine

deposition during the Devonian and the Carboniferous (*Carroll et al.*, 1995; *Zhou and Chen*, 1990). It began to receive terrestrial sediments during Mesozoic time (Fig. 6). Fluvial and alluvial strata with dominant sandstones were deposited in the Triassic. The Jurassic and Cretaceous strata unconformably overlie older units of siltstones and mudstones (*Sobel* 1995; *Sobel et al.*, 2001). The Cenozoic sediments are characterized by a series of red mudstones, siltstones, sandstones and red beds which were deposited in alluvial and lacustrine environments (*Jolivet et al.*, 2001).

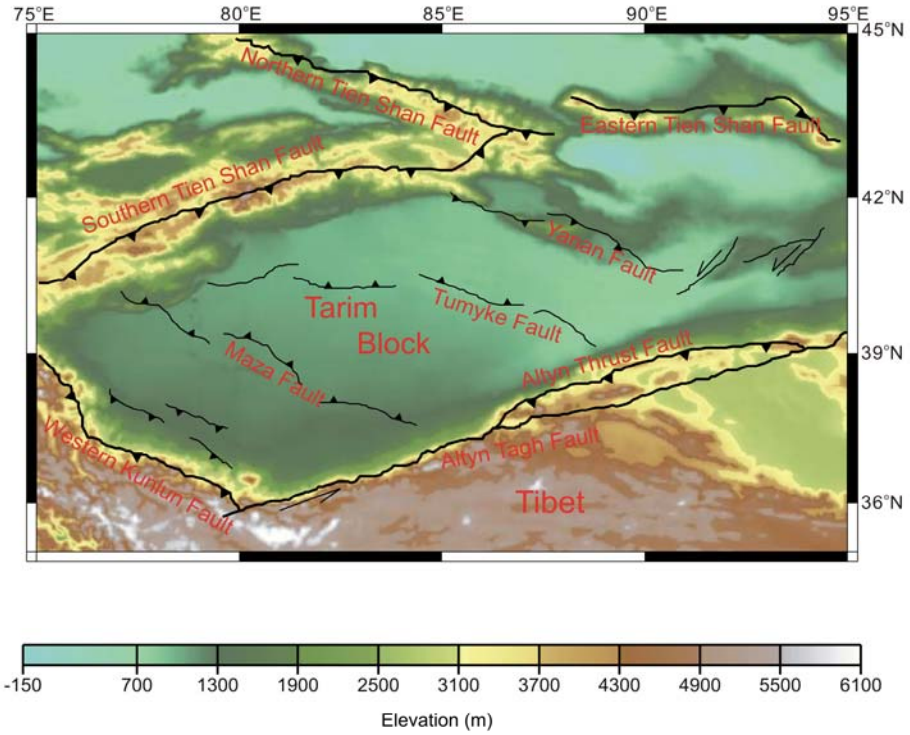

Figure 5. Simplified tectonic framework of the Tarim block. Bold lines are boundary faults, and thin lines are faults within the basin. Adapted from *Yin and Nie* (1993) *and Zhai* (1992). The colour bar is elevation in meters.

The Tarim block was stable and rigid with little internal deformations until the Upper Palaeozoic. Paleomagnetic studies shows that it was located in low latitudes in the Devonian, and that it moved northwards during the Devonian and the Carboniferous (*Li*, 1990). Closure of the residual ocean basin between the Tarim block and the Kazakhstan block that was located to its northwest occurred from the Late Carboniferous to the Permian (*Jia et al.*, 1991). Marine basins in the present-day Tien Shan and West Kunlun Shan were folded into mountains. In the Late Permian, the Tarim block was under strong compression, and was

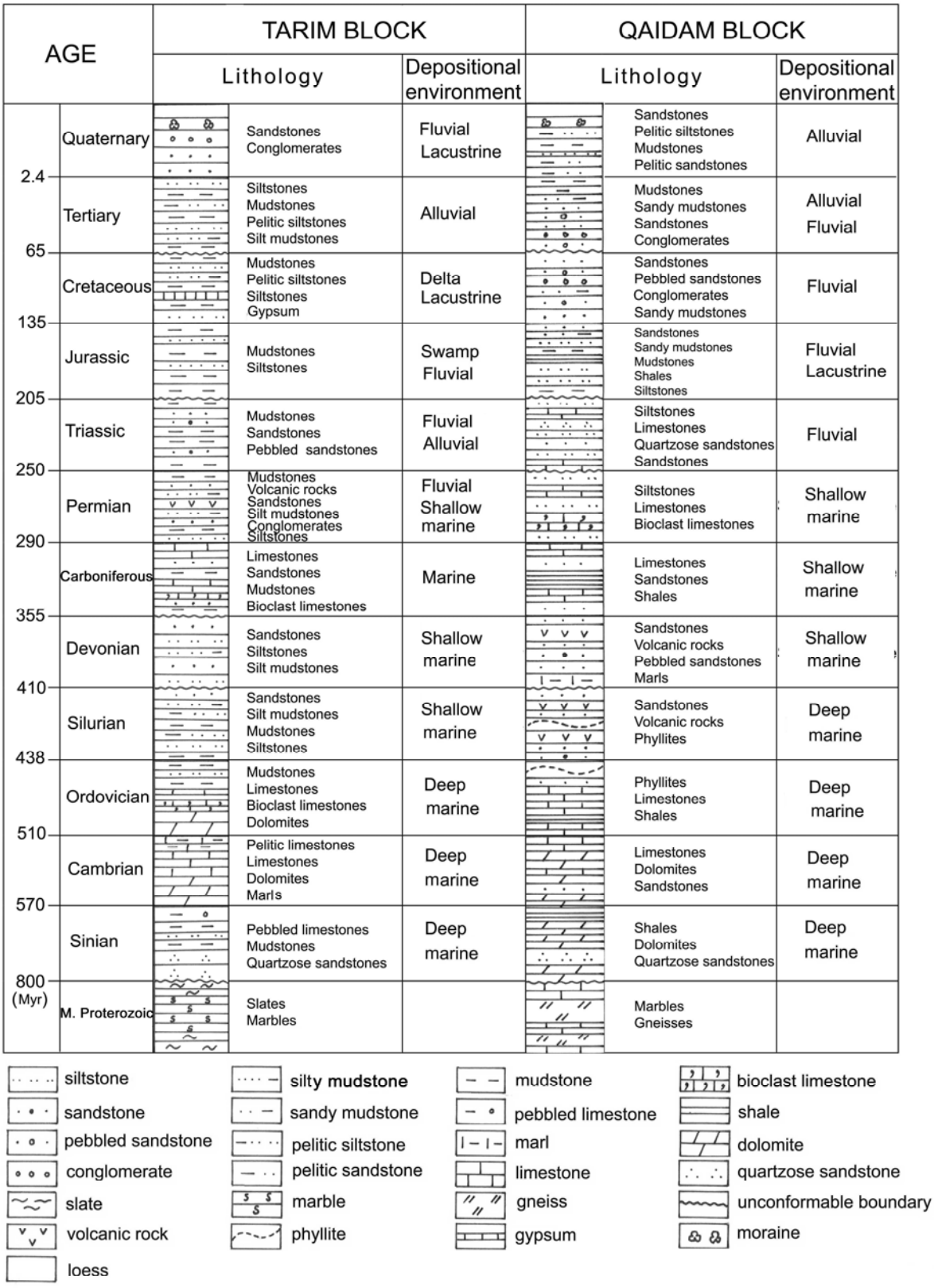

Figure 6. Schematic stratigraphic columns and facies interpretations from the Archean to the Cenozoic of the Tarim and Qaidam blocks. Adapted from *Zhai* (1992).

folded and uplifted at its edges. During the Cenozoic, a series of flexural foreland basins developed along the northern and southern edges of the Tarim Basin (*Sobel and Dumitru*, 1997) in response to the collision between India and Eurasia (*Yin and Nie*, 1996). Although the Tarim Basin has remained relatively undeformed during this collision, the large N-S directed compression in both the Mesozoic and the Cenozoic generated a series of near east-west trending faults, such as the Yanan Fault and the Maza Fault (Fig. 5).

The Qaidam block

The Qaidam block lies at the northeastern margin of the Tibetan Plateau, and has an average elevation of 3000 m. It is bordered by the Altyn Tagh Fault to the north and the Kunlun and Qilian faults to the south and east, respectively (Fig. 7).

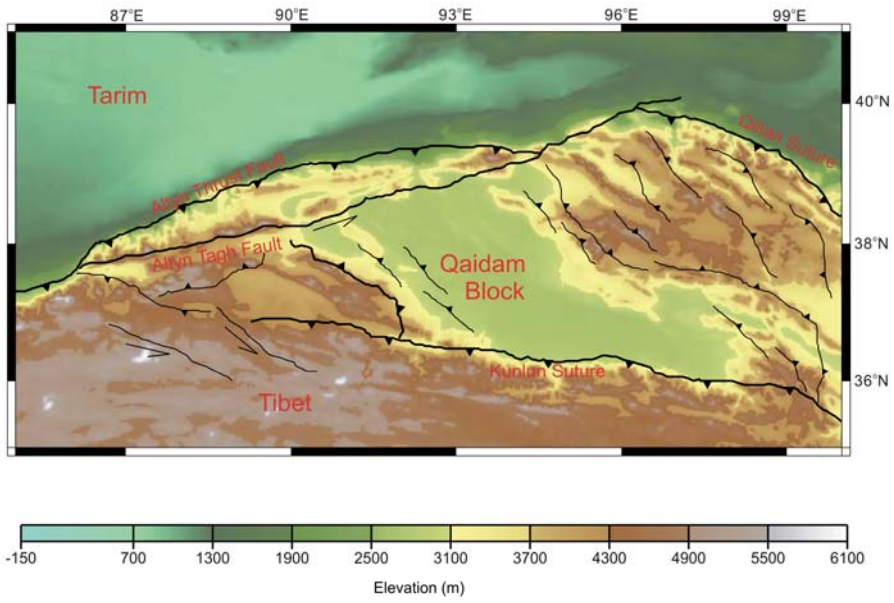

Figure 7. Simplified tectonic framework of the Qaidam block. Bold lines are boundary faults, and thin lines are internal basinal faults. Adapted from *Yin and Nie* (1993). The colour bar is elevation in meters.

The present outline of the Qaidam Basin reflects its development during the Cenozoic (*Song and Wang*, 1993). It is partially filled by the thick sequence of Late Cenozoic sediments, and its basement consists of high-grade Lower Proterozoic metamorphic rocks and low-grade Middle and Upper Proterozoic metamorphic rocks (*Song and Wang*, 1993). Lower Proterozoic-Sinian metamorphic rocks together with Cambrian to Silurian highly-

deformed deep-marine and volcanic rocks are exposed along the southeastern margin of this block (*Delville et al.*, 2001; *Yin and Nie*, 1993). The Devonian strata are clastic and the Carboniferous and Permian sections consist of shallow marine limestones. The Mesozoic strata are entirely non-marine (*Ritt and Biffi*, 2001). During the Triassic and the Lower Jurassic, lacustrine sediments (mudstones and shales) were deposited. These are overlain by a fluvial and alluvial sequence (Fig. 6). The Upper Jurassic and Cretaceous strata in this block are dominated by sandy and conglomeratic red beds which overlie the older units unconformably. The Tertiary strata are saline lacustrine deposits interbedded with terrestrial sedimentary rocks, in particular hematite-rich sandstones (*Song and Wang*, 1993). A thick Quaternary sequence also occurs in the Qaidam Basin (*Qinghai BGM*, 1989).

The Qaidam block was stable and suffered only limited deformations until the Mesozoic, when it underthrusted the Sino-Korean block along the Qilian mountain range and developed a series of folds and faults in front of the thrust (*Ritt and Biffi*, 2001). Three unconformities of Paleocene-Eocene, Early Pliocene, and Early Quaternary age have been recognized in the Cenozoic sequences of the Qaidam Basin. These unconformities are possibly related to phases of the India-Eurasian collision (*Hacker et al.*, 2000; *Yin and Nie*, 1996). At the end of the Pliocene, the Qaidam Basin was uplifted by renewed tectonic movements (*Métivier and Gaudemer*, 1997; *Métivier et al.*, 1998). Cenozoic tectonic activity documented in the basin is weak (*Bailey and Anderson*, 1982; *Jolivet et al.*, 2001; *Dupont-Nivet et al.*, 2002; *Zhu and Helmberger*, 1998), only NW-SE trending folds are occasionally developed between the thrust faults.

The Tibetan block and the Himalaya fold belt

The Tibetan block (Tibetan Plateau) is bounded by the Himalayas to the southwest, and the Kunlun and Altyn Tagh faults to the north (Fig. 8). A series of alternating, deep, forested valleys and high mountain ranges such as the Longmen Mountains define its eastern margin (Fig. 2). Significant crustal shortening (at least 1400 km) occurred in the Tibetan Plateau. The Indian-Eurasian collision starting 50 million years ago is responsible for the formation of the highest mountains (the Himalaya Mountains) and the largest plateau on Earth (the Tibetan Plateau) as well as many present-day tectonic features in large parts of Central Asia.

From south to north, the Tibetan Plateau is divided into: the Himalaya fold belt, Lhasa micro-block, Qiangtang micro-block and the Songpan-Gangzi fold belt (Fig. 8) (*Brown et*

al., 1996; *Chen and Molnar*, 1981; *Kind et al.*, 2002; *Patzelt et al.*, 1996; *Yin et al.*, 1994). The Main Boundary Thrust constitutes the southern edge and the Indus-Zhangbo suture marks the northern edge of the Himalaya fold belt. The Lhasa micro-block is located between the Indus-Zhangbo suture and the Bangong-Nujiang suture. The Bangong-Nujiang and Jinsha sutures form the southern and northern edges of the Qiangtang micro-block respectively. The Songpan-Gangzi fold belt in northern Tibet is bounded by the Kunlun Fault to the north, and the Jinsha suture to the south (*McNamara et al.*, 1995; *Molnar*, 1988; *Yin*, 2000).

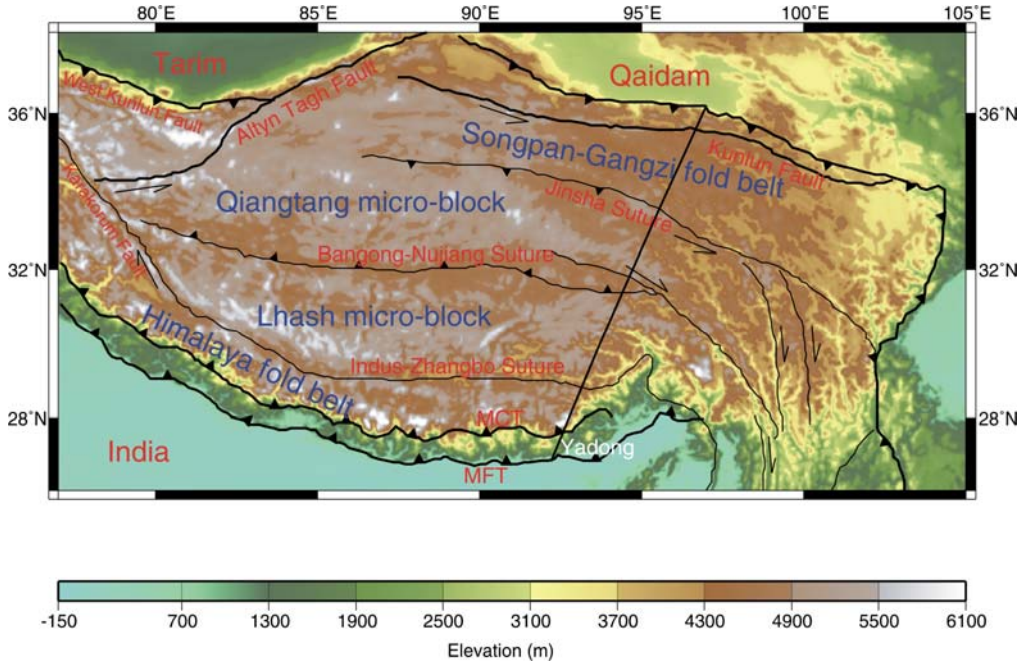

Figure 8. Map of major tectonic micro-blocks, fold belts and tectonic boundaries of the Tibet block. MFT: Main Frontal Thrust, MCT: Main Central Thrust. The black solid line gives the location of a geological profile from Yadong to the Kunlun Mountains shown in Fig. 11. Adapted from *Kind et al.* (2002) *and Tapponnier et al.* (2001). The colour bar is elevation in meters.

The basement of the Himalaya fold belt comprises crystalline gneiss of Lower Cambrian age (*Finlayson et al.*, 2002; *Gahagan et al.*, 1988; *Grujic et al.*, 1996; *Hoffman*, 1991; *Vannay and Steck*, 1995). The Palaeozoic strata are characteristic of stable, continuous and shallow marine deposition. The Devonian formations consist of littoral to shallow marine quartzose sandstones, and the Carboniferous and Permian beds comprise terrestrial deposits of conglomerates, sands and shales. Shallow marine conditions also

prevailed during the Mesozoic until the Early Cretaceous (*Derry and France-Lanord,* 1996). Large-scale emplacement of basic magma occurred in the Cretaceous. The Himalaya orogeny resulted in thick terrestrial molasse deposits in the foreland basins (*An et al.,* 2001*; Coleman and Hodges,* 1998; *Lavé and Avouac,* 2000; *Molnar,* 1984). The Quaternary is represented by glacial sediments interbedded with material of the fluvial-lacustrine facies (*Burbank et al.,* 1993; *Harrison et al.,* 1997; *Pêcher,* 1991). The sutures and major thrusts from north to south across the Himalayas are: the Indus-Zhangbo Suture, the Main Central Thrust (MCT) that brings the High Himalayas over the Lower Himalayas, the Main Boundary Thrust (MBT), and the Main Frontal Thrust (MFT) that separates the Indian subcontinent from the Himalayan Mountains (Fig. 9) (*Hodges,* 2000). Most models proposed for the evolution of the Himalayas assume that the zone of plate convergence shifted progressively towards the foreland during the mountain building process (Fig. 9) (*Bendick and Bilham,* 2001; *Harris and Massey,* 1994; *Hodges et al.,* 1998; *Meigs et al.,* 1995; *Yeats et al.,* 1992).

About 225 million years ago, India was a micro-continent situated off Australia, and the Tethys separated India from the Asian continent. When Gondwana broke apart about 200 million years ago, India began to forge northward (*Bird,* 1978; *Chemenda et al.,* 2000; *Gansser,* 1974; *Molnar and Tapponnier,* 1975*).* This resulted in closure of the Tethys, and finally in the collision between India and Eurasia about 50 million years ago (*Klootwijk et al.,* 1992; *Rowley,* 1996; *Van der Voo et al.,* 1999). About 25 million years ago, the Lower

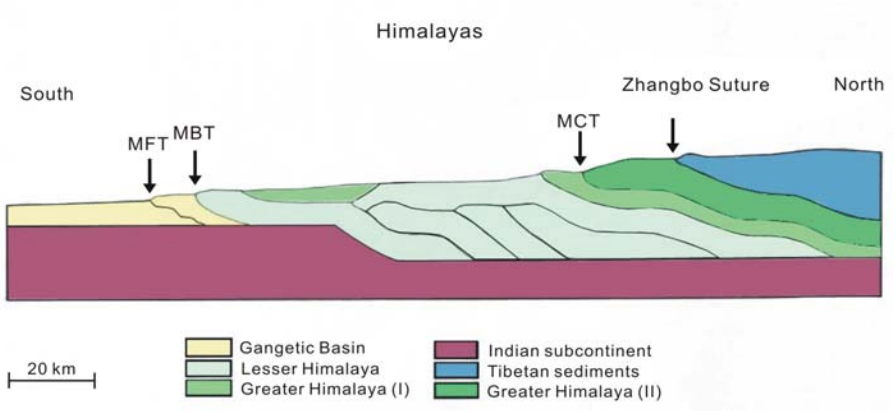

Figure 9. Model of subduction of the Indian plate beneath the Himalayan orogen, with several distinct sequences and fault zones. MCT: Main Central Thrust , MBT: Main Boundary Thrust, MFT: Main Frontal Thrust. After *Wittke* (2002).

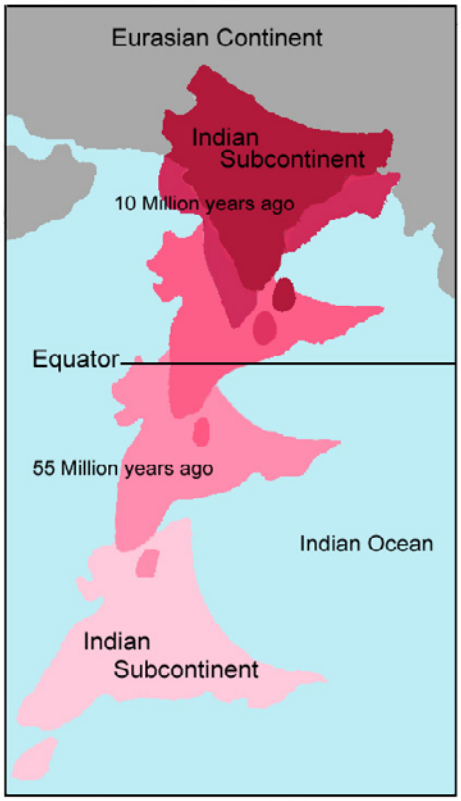

Figure 10. Sequence showing the collision that formed Tibet and the Himalayas. After *Burbank* (1996) *and Burbank et al.* (1993).

Himalayas were formed, and by about 0.6 million years ago, the present-day geomorphic form of the Himalayan system came into existence (*Allegre et al.*, 1984; *Le Fort*, 1996; *Rothery and Drury*, 1984; *Rowley*, 1996) (Fig.10). GPS measurements show that the Himalayas are growing in height by more than 1 cm/year (*Bilham et al.*, 1997; *DeMets et al.*, 1990; *Holt et al.*, 2000; *Powers et al.*, 1998).

The Lower Precambrian basement of the Lhasa micro-block consists of mica-schists, phyllites and quartzites mixed with granitic rocks (*Barth et al.*, 1994; *Kaneoka and Kono*, 1981). The overlying Palaeozoic sequence is shallow marine. The slates, sandstones and quartzites are considered to be of Cambrian age. The Ordovician and Silurian are represented by conglomerates, quartzites, sandstones, shales, limestones and dolomites (*Garzanti et al.*, 1986), and the Devonian to the Perminan by limestones, shales and quartzites. The Mesozoic rocks consist of a large thickness of limestones and shales (*Edwards and Harrison*, 1997; *Patzelt et al.*, 1996). Granites were intruded during the Late Jurassic and Early Cretaceous, which implies that the Lhasa micro-block became part of the Asian continent

during the Late Yanshan movement (*Hirn et al.,* 1984; *Patzelt et al.,* 1996). The Cenozoic is represented by sandstones and shales in this area (*Jain et al.,* 2000; *Noble and Searle,* 1995).

The Qiangtang micro-block is a stable tectonic unit with a metamorphic Lower Precambrian crystalline basement (*Shen et al.,* 2001; *Yin and Harrison,* 2000). Stable shallow marine deposition occurred during the Ordovician to the Carboniferous. The older zircon ages are similar to those of the gneisses within the Lhasa micro-block and the Himalaya belt, implying that the Qiangtang micro-block was contiguous with them along the northern margin of Gondwana during Earliest Paleozoic time. Flysch was laid down in the Permian, and carbonates and clastic rocks in the Triassic. The Late Triassic-Early Jurassic metamorphic core complex consists of rocks of the amphibolite facies. From the Cretaceous to the Tertiary, this block was characterized by terrestrial sedimentation.

The Songpan-Gangze fold belt formed during Jurassic time (*Dewey et al.,* 1988). Stable Palaeozoic strata overlie the Precambrian basement. This area subsided in the Permian, and a thick, clastic, marine sequence was deposited in the Triassic. It is characterized by an intensely deformed Triassic-Jurassic sequence of deep marine deposits. This area was folded during the Indosinian movement. Terrestrial sedimentation occurred at the margin of the Kunlun Fault and in the intermontane basins.

The fold belts and micro-blocks discussed above are characterized by fold-and-thrust belts, which developed over a large area with regional decolléments (Fig. 11) since the Indo-Asian collision at about 50 Ma (*Yin and Harrison,* 2000). Deformations in the mantle lithosphere of Tibet is possibly decoupled from surface faulting (*Chen et al.,* 2000; *McNamara et al.,* 1995; *Molnar and Lyon-Caen,* 1989; *Wei et al.*, 2001). The upper crust and the upper mantle deform at their own characteristic wavelengths (*Alsdorf and Nelson,* 1999; *Herquel et al.,* 1995; *Holt and Wallace,* 1990; *Jin et al.,* 1994, 1996; *Royden et al.*, 1997). A weak, low viscosity lower crust exists between the strong upper crust and the upper mantle. The lower crust absorbs the advancing Indian lithosphere through thickening, and with it uplift of the Tibetan Plateau (*Nelson et al.,* 1996).

The evolution of the Tibetan Plateau may be divided into the following stages: The first stage is closure of the Tethys and initiation of subduction of the Indian continent beneath the Eurasian plate (*Barazangi and Ni,* 1982; *Jin et al.,* 1996; *Lyon-Caen and Molnar,* 1983; *Tapponnier et al.,* 2001; *Zhao et al.,* 1993). Indian underplating reaches to the Banggong suture (*Chen et al.,* 1996; *Jin et al.,* 1996; *Nie et al.,* 1990; *Royden and Burchfiel* 1995). The second stage is crustal shortening (*Avouac and Peltzer,* 1993). Strain along the

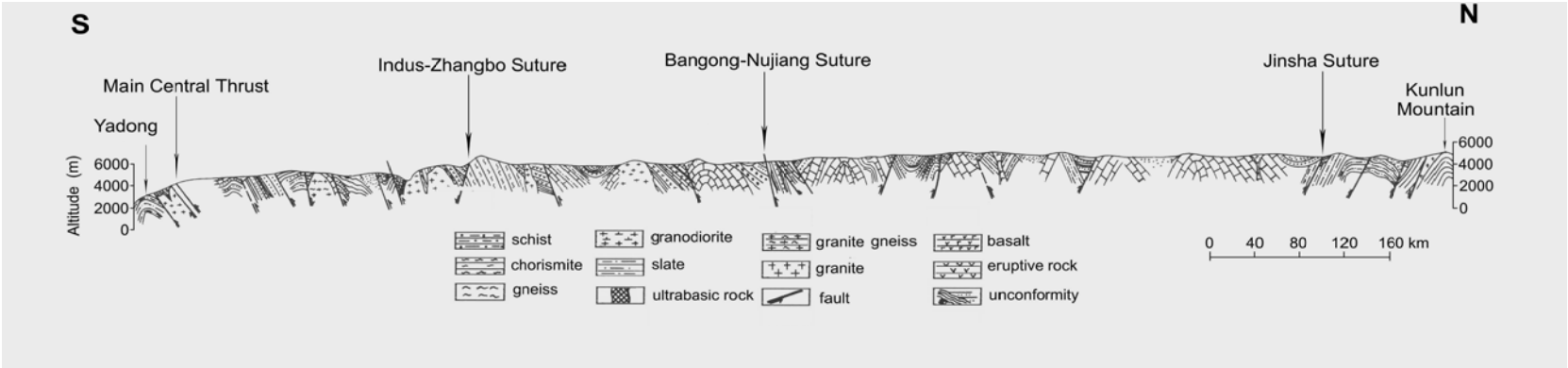

Figure 11. Geological profile crossing Tibet from Yadong to the Kunlun Mountains. See Fig. 8 for profile location. After *Zhai* (1992).

southern edge of the Tibetan Plateau accommodates 80% of the convergence between India and Eurasia (*Bilham et al.,* 2001*; Harrison et al.,* 1992). GPS measurements show that India and southern Tibet converge at a rate of about 20 mm/year (*Bilham et al.,* 1997; *Holt et al.,* 2000; *Larson et al.,* 1999; *Rong and Jackson,* 2000). The third stage is uplift of the Tibetan Plateau, which occurs following crustal shortening. The fourth stage is strike-slip faulting. A series of large, roughly east-west trending, left-lateral strike-slip faults formed within the Tibetan Plateau (*Jain et al.,* 2000; *Molnar,* 1984; *Tapponnier et al.,* 1982). These strike-slips accommodate the regional north-south shortening by eastward mass translation, whereby mass from the Tibetan Plateau is transferred to the southeast along these major strike-slip faults (*England and Molnar,* 1997; *Holt and Haines,* 1993; *Tapponnier et al.,* 2001).

The origin of the Tibetan Plateau is still under debate. There are three major theories on its uplift. The first is basement reactivation (*Dewey and Burke,* 1973). The continental crust may have been simply shortened by folding and thrusting, and lithospheric deformation may have been distributed throughout the Himalayas and Tibet (*Masek et al.,* 1994). The second model is continental subduction (*Fielding et al.,* 1994; *Kong et al.,* 1997; *Ni and Barazangi,* 1984; *Willett and Beaumount,* 1994). The Indian lithosphere subducted beneath the entire Tibetan Plateau and produced subsequent uplift. The third is continental injection (*Zhao and Morgen,* 1987). The fact that the area of weakening of the Indian plate coincides with the edge of the plateau suggests that it marks the location where Indian crust is skinned off the mantle lithosphere and injected into the Tibetan lower crust.

The Tien Shan orogenic belt

1000-1800 km north of the convergent boundary between the Indian and Eurasian plates lies the intra-continental Tien Shan orogenic belt. It extends east-west for approximately 2500 km. It is flanked by the Tarim Basin to the south and the mountain range is divided into the north and south Tien Shan respectively (Fig. 2).

Granite gneisses of Lower Proterozoic age form the basement of the Tien Shan (*Bukharin,* 1978). They are unconformably overlain by marine sediments including calcareous shales, dolomites and limestones of Cambrian age (*Mukhin,* 1989). Deep-marine deposition of sandstones and shales dominated in the Ordovician. From the Silurian to the Devonian, carbonates and shallow marine successions accumulated, especially in the Tien Shan foreland basin (*Akhber and Mushkin,* 1976*; Chen,* 1985). There, an unconformable,

thick molasse sequence was laid down in the Carboniferous, probably as a result of the continuing uplift of this area (*Bukharin,* 1978; *Moore, et al.,* 1991*).* Throughout the Permian, volcanism with the extrusion of rhyolites was widespread. Mesozoic rocks include red conglomerates, carbonaceous sandstones and mudstones, followed by gypsum, mudstones and limestones (*Yin and Nie,* 1996). They are overlain by Paleogene gypsum, dolomites and limestones, which are separated from the lower Neogene conglomerates by an unconformity (*Bullen et al.,* 2001; *Chen et al.,* 2002). Shortening in the Tien Shan began in early Neogene time (*Burchfiel et al.,* 1999). This is documented by the marked unconformity separating marine Paleogene strata from continental Neogene strata (*Yin and Nie,* 1996).

The Tien Shan is a Paleozoic orogenic belt reactivated by folding and faulting in the Tertiary under the present tectonic regime (*Beloussov et al.,* 1980; *Carrol et al.,* 1995; *Gao et al.,* 1998; *Hendrix et al.,* 1994). Since the Late Carboniferous and Early Permian, marine basins in the present-day Tien Shan were closed and folded into mountains. The Mongolia block underthrusted southward, and suturing along the Tien Shan in the Last Permian produced much of the structural and metamorphic fabric of the mountain interior (*Dewey and Burke,* 1973; *Gansser* 1974; *Gao et al.,* 1998). After a period of quiescence in the Mesozoic and Early Tertiary, tectonic activity resumed in the Eocene in response to the collision of India with Eurasia (*Avouac et al.,* 1993; *Molnar and Tapponnier,* 1975). Even though the Tien Shan is about 1000 km away from this collision zone, active folding and thrusting are contemporaneous with the collision. During the last 10 m.y., the Tien Shan has been uplifted about 3 km on the average (*Abdraknmatov et al.,* 1996; *Burov et al.,* 1990, 1998; *Jin,* 1997; *Stephen et al.,* 2002).

The Altyn Tagh Fault

The Altyn Tagh Fault is one of the most striking structural features attributed to the Cenozoic collision between India and Asia (*Molnar and Tapponnier,* 1975). It is predominantly a left-lateral strike-slip fault that extends at least 1600 km along the northern edge of the Tibetan Plateau (Fig. 2). It separates the Tarim Basin to the north from the Qaidam Basin in the south, and lies between the Western Kunlun thrust belt to the west and the Qilian thrust zone to the east. North of the Altyn Tagh Fault is the Altyn Thrust Fault, which joins the Altyn Tagh Fault at a depth of 80 km, then continues to underthrust steeply

southward to 150 km (*Wittlinger et al.,* 1998). The Altyn Mountain Range is located between the Altyn Tagh Fault and the Altyn Thrust Fault (Fig. 12).

Rocks throughout the Altyn Tagh Fault and the Altyn Mountain Range are dominantly marine. They include also ophiolite and eclogite formations as well as high-pressure metamorphic rocks (Fig. 11) (*Sobel et al.,* 2001). The Precambrian basement is metamorphic and is overlain by thick carbonates and clastic rocks deposited in the Proterozoic. Marine sedimentation lasted to the Upper Palaeozoic. Permian and Triassic strata are absent. There are organic-rich lacustrine and alluvial facies rocks (sandstones and siltstones) in the Jurassic strata along the southern flank of the Altyn Tagh Fault. Cenozoic strata, including continental conglomerates and sandstones, unconformably overlie older units along the margins of the mountains and within an intermontane basin along the eastern Altyn Tagh Fault (*Yin et al.,* 2000).

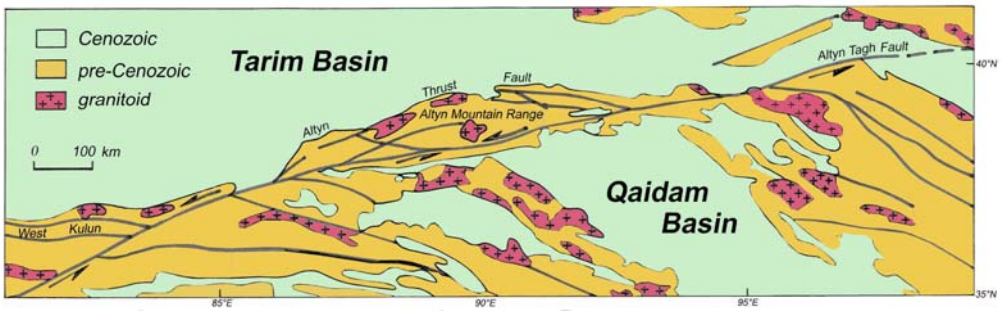

Figure 12. Simplified geological map of the Altyn Tagh Fault and adjacent regions. Adapted from *Sobel et al.* (2001).

Deformation of the Precambrian basement and Proterozoic formations within the Altyn Tagh area is intense. During the Triassic and Cretaceous, this area was uplifted into a mountain belt. The frontal parts of the mountain range both in the north and in the south are very active at present. Several push-up structures developed between nearly parallel segments of the transcurrent fault (*Jolivet et al.,* 2001). From the Late Oligocene to the Miocene, left-lateral strike-slip displacements on the Altyn Tagh Fault were initiated (*Hanson,* 1999; *Ritts and Biffi,* 2001; *Rumelhart,* 1999; *Peltzer and Tapponnier,* 1988; *Yue et al.,* 2001). Its total slip is about 400-1200 km on the basis of common offset and a long-term average slip rate of approximately 12–16 mm/year (*Bendick et al.,* 2000; *Shen et al.,* 2001). Some kinematic models for the evolution of the Altyn Tagh Fault predict a systematic decrease in the amount of strike-slip from the southwest to the northeast (*Burchfiel et al.,* 1989; *Yue and Liou,* 1999; *Gehrels et al.,* 2000). The left-lateral offset accommodates the

northeastward extrusion of the Tibetan Plateau (*Tapponnier and Molnar,* 1977; *Peltzer and Tapponnier,* 1988; *Yue and Liou,* 1999). The total offset along the Altyn Tagh Fault may provide an answer to the question of whether the convergence between India and Asia has been largely accommodated by the extrusion of Asia towards Indochina (*Avouac et al.,* 1993; *Peltzer and Tapponnier,* 1988; *Peltzer et al.,* 1989), or by shortening within the crust and mantle (*Burchfiel et al.,* 1989), perhaps even including subduction of mantle lithosphere (*Jin et al.,* 1996; *Wittlinger et al.,* 1998).

The evolution of Central Asia

Based on the description above, we discuss here the general geological evolution of Central Asia, beginning in the Proterozoic and continuing through the Cenozoic.

During the Proterozoic and Lower Palaeozoic, the Yangtze, Sino-Korean, Tarim, Qaidam and Tibet blocks were at low-latitude positions, or they lie in the southern hemisphere (*Scotese and Sager,* 1988; *Scotese and Barrett,* 1990; *Sengör,* 1996). The Mongolia block was in the western hemisphere (*Powell* 1993). These blocks were characterized by a stable, continuous, deep-marine depositional environment at that time (*Ji and Coney,* 1985; *Zhou and Chen,* 1990).

During the Devonian, the Tarim block and the Sino-Korean block drifted together northward (*Wu et al.,* 1990; *Yin and Nie,* 1996), while the Mongolia block drifted eastward (Fig. 13a). In the Carboniferous, the residual ocean basin between the Tarim and Kazakhstan blocks closed and the Tarim and Sino-Korean micro-continents formerly in this ocean collided with the Kazakhstan-Siberia continent (Fig. 13b). The Qaidam and Tarim blocks formed a single unit at that time (*Yin and Nie,* 1996). The Yangtze block drifted rapidly northward during the mid-Carboniferous (*Hacker et al.,* 1996; 1998; 2000). From the Devonian to the Carboniferous, the Tarim, Qaidam and Sino-Korean blocks were characterized by shallow marine deposition, and only the Yangtze block received sediments at its edge (*Yang and Besse,* 2001). The Qiangtang micro-block (the northern part of the Tibet block) drifted northward at the beginning of the Permian. During the Late Permian, the Sino-Korean block collided with the Mongolia block along the Yin Shan suture zone, closing the ocean between them (*Webb et al.,* 1999).

During the Triassic, the Yangtze block collided with the Sino-Korean block along the Qilian-Qinling suture zone (*Faure et al.,* 2001). Simultaneously, the Qaidam block

underthrusted the Sino-Korean block along the Qilian mountain range (*Ritt and Biffi,* 2001). Collision between the Yangtze and Sino-Korean blocks squeezed the northern part of the Qaidam block westward, extruding it from its original position (*Mattauer et al.,* 1985). The Qiangtang micro-block and Indochina drifted northward continuously and the Lhasa micro-block (the southern part of the Tibet block), began to drift northward (Fig. 13c). During the Jurassic, the Siberia block collided with the Mongolia block along the Mongolo-Okhotsk suture, closing the Solonker Ocean between them (*Powell,* 1993). At that time, the Qiangtang micro-block and Indochina collided with the combined Qaidam-Tarim-Yangtze-Sino-Korean continent along the Kunlun suture. During the Late Cretaceous, the Lhasa micro-block collided with the Qiangtang micro-block along the Bangong-Nujiang suture. Meanwhile, the India subcontinent began to drift northward (Fig. 13d). In the Mesozoic, shallow marine sedimentation succeeded by terrestrial clastic sedimentation took place in the Yangtze, Sino-Korean, Tarim and Qaidam blocks (*Yin and Nie,* 1996; *Sobel et al.,* 2001; *Ritt and Biffi,* 2001).

During the Tertiary, the Tethys Ocean closed and the Indian subcontinent started to collide with the Eurasian continent. The Himalaya Mountains and the Tibetan Plateau were formed, the Tien Shan (a Palaeozoic orogenic belt) was reactivated, and Altyn Tagh (an approximately 1000 km long left-lateral strike-slip) and a series of NE-trending folds and faults appeared in Central Asia (Fig. 13e). Terrestrial fluvial and alluvial sediments of Cenozoic age are found in the Yangtze and Sino-Korean blocks. Thick Tertiary and Quaternary deposits were laid down in the Tarim, Qaidam, Zugguer and Ordos basins.

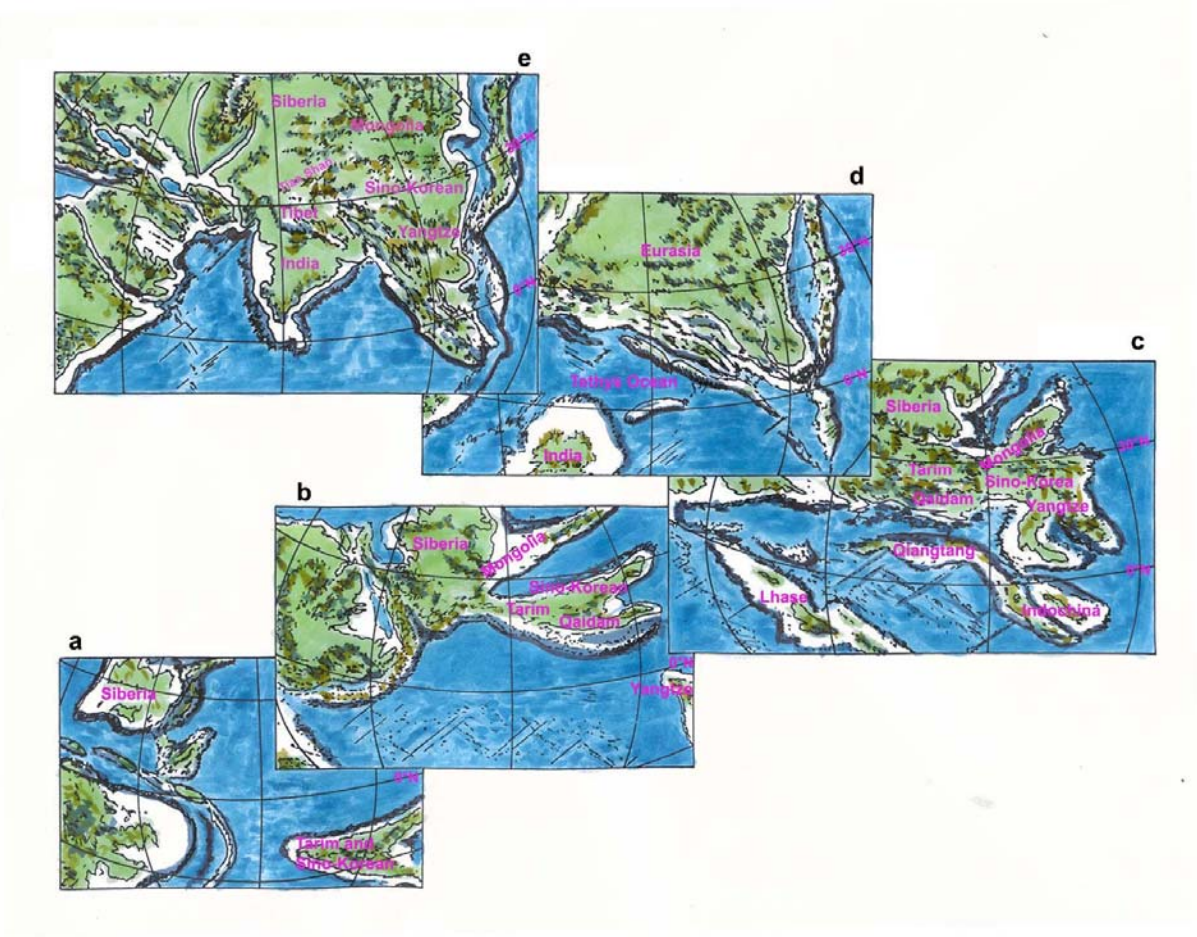

Figure 13. Evolution of the major tectonic blocks in Central Asia, beginning in the Proterozoic and continuing through the Cenozoic. Adapted from the website of *Northern Arizona University* (2001).

Chapter 3. Methods

3.1 Introduction

The surface faults of a continent are often unrelated to the lithospheric mantle in a simple manner on account of heterogeneities in the deformational properties of continental rocks (*Lyon-Caen and Molnar*, 1984; *Watts et al.*, 1980; *Zhao and Morgan*, 1987; *Burchfiel and Royden*, 1985; *Allen et al.,* 1991; *Willett and Beaumount*, 1994). The lithosphere of Tibet has two strong layers, the upper crust and the uppermost mantle, which are decoupled from each other by a weak lower crust with a lower seismic velocity (*Jin et al.*, 1994; *Herquel et al.*, 1995; *Zeng and Gao*, 1995). Therefore, crustal structures derived from surficial geologic and geodetic information may not correspond to the deep lithospheric deformations. In such a case, we must rely on geophysical observations to deduce plate interactions at depth. Reflection and refraction seismic profiles that reveal the locations of prominent reflectors and lateral variations in seismic velocities often provide the most straightforward constraints on the lithospheric structure. Thus, our knowledge on the deep structure of the lithosphere is primarily derived from seismic data. The INDEPTH (International Deep Profiling of Tibet and the Himalayas) project, for example, improved significantly our knowledge on the geological structures and evolution of the Tibetan Plateau. Since 1992, two profiles have been obtained in the framework of this project: the main INDEPTH profiles extending from the crest of the High Himalayas to the central Qiangtang Terrane, covering a distance of about 800 km, along which seismic reflection and broadband earthquake data have been collected, and the INDEPTH magnetotelluric (MT) profile crossing northern Tibet and extending into the Qaidam Basin (*Nelson et al.,* 1996; *Brown et al.,* 1996; *Kind et al.,* 1996; *Chen et al.,* 1996).

Seismic data are expensive and time-consuming to acquire, particularly in a mountainous setting. Applying the elastic plate theory of the lithosphere to the interpretation of gravity and topographic data has also been successful in deducing lithospheric structure in the oceans and on the continents at a fraction of the cost of a seismic survey (*Watts et al.,* 1980; *McNutt and Menard*, 1982; *Sheffels and McNutt*, 1986; *Jin et al.*, 1996). Plate tectonics is based on the assumption that the Earth's outermost layer, the lithosphere, behaves rigidly on large geological time scales. The main evidence for this rigidity has come from studies of the way the lithosphere responds to surface loads such as ice sheets, sediments, and volcanoes. By comparing observations of flexure to calculations based on

elastic plate models, it is possible to constrain the long-term elastic strength of the lithosphere.

The lithosphere is the rheologically strong portion of the crust and upper mantle that does not undergo significant viscous relaxation on the geological time scale and deforms elastically up to the point when it fails in a brittle or ductile fashion. The thickness of the mechanical lithosphere is constrained by the depth of faulting and the vertical deflection of the lithosphere in response to loads (*Forsyth,* 1985). The mechanical stiffness of a plate is often described by its flexural rigidity *D*, which is controlled by the effective elastic thickness *Te* of the plate. In response to the weight of a load (topographic or otherwise), the lithosphere flexures until the deflection of density interfaces and the bending stress within the plate balance the load.

Application of the elastic plate theory to geological problems are well known and dates back to *Vening Meinesz* (1941). Modelling the ocean lithosphere as an elastic plate is particularly common since the advent of plate tectonics. In most cases, the flexural response of an oceanic plate takes the form of deformation of its crust. Modelling results show that the elastic thickness (which is determined by the flexural rigidity) increases with the age of the lithosphere at the time of loading. Therefore, as the oceanic lithosphere ages and cools, it becomes more rigid in its response to surface loads. Some of the notable applications have been loading of the lithosphere by islands, seamounts and bending of downgoing plates in subduction zones (*Judge and McNutt,* 1991; *McNutt and Menard,* 1978; *Turcotte et al.,* 1978; *Walcott,* 1970; *Watts and Cochran,* 1974; *Watts and Brink,* 1989). For the continental lithosphere, crustal deformation may not be a response to its deep flexure.

The traditional three dimensional method to calibrate the mechanical strength of the continental lithosphere is based on the coherence theory of *Forsyth* (1985), and the method has been applied to a variety of continents such as Africa (*Bechtel et al*., 1987), Australia (*Zuber et al.,* 1989), North America (*Bechtel et al.,* 1990), the Tibetan portion of Asia (*Jin et al.,* 1994), and western North America (*Armstrong and Watts,* 2001; *Lowry and Smith,* 1994). In order to calculate the mechanical strengths of different tectonic blocks within a continental plate with the coherence method, the study area has to be divided into rectangular regions of various sizes to approximate the sizes of the tectonic blocks. The necessity of a rectangular region is a consequence of the coherence theory which uses the spectral approach and requires a homogeneous mechanical strength within the rectangle. The spectral approach has its deficiencies. Firstly, a tectonic block is obviously seldom

rectangular in shape due to its geological nature. Secondly, the coherence calculation requires a constant mechanical strength for a block. Unfortunately, a tectonic block is usually deformed and weakened at its boundary because of interaction with neighbouring blocks. A good example is the Tarim block. It has a strong core, but is weakened on its northern and southern edges because boundary crust is skinned during underthrusting beneath Tibet and the Tien Shan. Thirdly, the spectral calculation requires a proper rectangle sizes, otherwise the edge effect of Fourier transforms will deteriorate the modelling result (*Lowry and Smith,* 1994). *Wees* (1994) *and Jin* (1997) developed a 3D finite difference method in the space domain which takes the natural geometry and inhomogeneity of tectonic blocks into account.

3.2 Flexure of an elastic lithosphere: theory and model

The topography of the Earth is very varied, from rolling hills to jagged mountain peaks and deeply-incised river valleys. This topography is often strongly influenced by the underlying geology. Many events during the Earth's geologic history leave characteristic topographic imprints. For example, undeformed sedimentary layers have a different topographic expression compared with folded strata, and igneous rocks can have a distinct relief. Mountain belts are the result of plate collisions, with accompanying folding and faulting of rocks, igneous intrusive and extrusive activity, and metamorphism.

Physical and geophysical properties measured on the surface of the Earth reflect the state of the Earth's interior, rock composition and geological evolution. The Earth’s gravity field for example yields information on lithospheric deformations. The wavelength of gravity features depends on the dimension of the corresponding surface deformations as well as on the subsurface structure. High-resolution gravity and topographic anomalies combined with forward and "inverse" modelling techniques have often been used to estimate the geophysical characteristics of the continental elastic lithosphere. Complex near-surface geological events can be extremely difficult to unravel, even with the aid of borehole samples. Modern geophysical techniques can help to make a more accurate geologic interpretation and a better comprehensive site evaluation possible.

The bending of the lithosphere, approximated as an elastic thin plate, can be quantified using the conservation of angular momentum. Thus, the fundamental equation for the flexure of a plate considered as a continuous medium is (*Turcotte et al.,* 1978):

$$\frac{\partial}{\partial t}\iiint \vec{r} \times \rho \frac{\partial \vec{u}}{\partial t} dv = \iint \vec{r} \times \vec{T} ds + \iiint \vec{r} \times \vec{f} dv \qquad (1)$$

where $\vec{r}$ is the location vector, $\vec{u}$ the displacement of a particle in a plate, $\vec{T}$ the tractional force on a unit area (which is independent of coordinates), $\vec{f}$ the body force on a unit volume, ρ the density, *s* the surface area, *v* the volume, and *t* the time.

Because plate movements are slow, a plate can be considered to be in a steady state so that the left-hand side of equation (1) can be neglected:

$$0 = \iint \vec{r} \times \vec{T} ds + \iiint \vec{r} \times \vec{f} dv \qquad (2)$$

Introducing the *Levi-Civita* symbols ε_{ijk}, for which

$$\varepsilon_{ijk} = \begin{cases} 1 & ijk = 123, 231, 312 \\ -1 & ijk = 132, 213, 321 \\ 0 & otherwise, \end{cases}$$

equation (2) becomes:

$$\iint \varepsilon_{ijk} x_j T_k ds + \iiint \varepsilon_{ijk} x_j f_k dv = 0 \qquad i = 1, 2, 3 \qquad (3)$$

Equation (3) describes flexural bending around the *x*-axis (*i* = 1), the *y*-axis (*i* = 2), and the *z*-axis (*i* = 3). Rotation around the vertical *z*-axis is negligible if we do not consider any rotation between and within tectonic blocks. Then, equation (3) only has terms for which *i* = 1 and *j* = 2. Using the *Cauchy formula*, the traction $\vec{T}$ is related to the stress τ_{ij} by:

$$T_i = \tau_{ij} n_j = \tau_{ji} n_j$$

where τ_{ij} is stress tensor, and n_j the direction cosine of the stress surface. Thus, equation (3) becomes:

$$\begin{cases} \iint \varepsilon_{1jk} x_j \tau_{lk} n_l ds + \iiint \varepsilon_{1jk} x_j f_k dv = 0 \\ \iint \varepsilon_{2jk} x_j \tau_{lk} n_l ds + \iiint \varepsilon_{2jk} x_j f_k dv = 0 \end{cases} \qquad (4)$$

The lithosphere is a thin plate, its lateral dimension being much larger than its thickness. So, one may assume that the compression perpendicular to the plate and shearing parallel to the plate can be ignored:

$$\tau_{3k} = \tau_{k3} = 0 \qquad k = 1, 2, 3$$

This gives:

$$\begin{aligned}&\iint -x_3(\tau_{12}n_1+\tau_{22}n_2)ds+\iiint \varepsilon_{1jk}x_j f_k dv=0\\&\iint x_3(\tau_{11}n_1+\tau_{21}n_2)ds+\iiint \varepsilon_{2jk}x_j f_k dv=0\end{aligned} \quad (5)$$

Because

$$n_1 ds = dydz, \qquad n_2 ds = dxdz, \qquad n_3 ds = dxdy$$

$$(x_1, x_2, x_3) \Leftrightarrow (x, y, z)$$

$$n_1 ds = dx_2 dx_3, \quad n_2 ds = dx_1 dx_3, \quad n_3 ds = dx_1 dx_2,$$

equation (5) becomes:

$$\begin{cases}\iint -x_3(\tau_{12}dx_2dx_3+\tau_{22}dx_1dx_3)+\iiint \varepsilon_{1jk}x_j f_k dv=0\\ \iint x_3(\tau_{11}dx_2dx_3+\tau_{21}dx_1dx_3)+\iiint \varepsilon_{2jk}x_j f_k dv=0\end{cases} \quad (6)$$

If the thickness of the plate is *h*, and the coordinate of the neutral surface is 0, then:

$$\begin{cases}\int\left(\int_{-\frac{h}{2}}^{\frac{h}{2}} -x_3\tau_{12}dx_3\right)dx_2+\int\left(\int_{-\frac{h}{2}}^{\frac{h}{2}} -x_3\tau_{22}dx_3\right)dx_1+\iiint \varepsilon_{1jk}x_j f_k dv=0\\ \int\left(\int_{-\frac{h}{2}}^{\frac{h}{2}} x_3\tau_{11}dx_3\right)dx_2+\int\left(\int_{-\frac{h}{2}}^{\frac{h}{2}} x_3\tau_{21}dx_3\right)dx_1+\iiint \varepsilon_{2jk}x_j f_k dv=0\end{cases} \quad (7)$$

The bending moments can be defined by (*Wang,* 1984):

$$\begin{cases}M_{11}=\int_{-\frac{h}{2}}^{\frac{h}{2}} \tau_{11}x_3dx_3\\ M_{22}=\int_{-\frac{h}{2}}^{\frac{h}{2}} \tau_{22}x_3dx_3\\ M_{12}=\int_{-\frac{h}{2}}^{\frac{h}{2}} \tau_{12}x_3dx_3\\ M_{21}=\int_{-\frac{h}{2}}^{\frac{h}{2}} \tau_{21}x_3dx_3\end{cases} \quad (8)$$

Here M_{11} and M_{22} describe normal bending of the flexural plate around the *y*- and *x*-axes respectively. Similarly, M_{12} and M_{21} describe shear bending of the flexural plate around the *y*- and *x*-axes.

Substituting equation (8) into equation (7), we obtain:

$$\begin{aligned}&-\int M_{12}dx_2-\int M_{22}dx_1+\iiint \varepsilon_{1jk}x_j f_k dv=0\\&\int M_{11}dx_2+\int M_{12}dx_1+\iiint \varepsilon_{2jk}x_j f_k dv=0\end{aligned} \quad (9)$$

$$\begin{cases} -\dfrac{\partial M_{12}}{\partial x_1} - \dfrac{\partial M_{22}}{\partial x_2} + \int_{-\frac{h}{2}}^{\frac{h}{2}} \varepsilon_{1jk} x_j f_k dx_3 = 0 \\ \dfrac{\partial M_{11}}{\partial x_1} + \dfrac{\partial M_{12}}{\partial x_2} + \int_{-\frac{h}{2}}^{\frac{h}{2}} \varepsilon_{2jk} x_j f_k dx_3 = 0 \end{cases} \tag{10}$$

Taking $\dfrac{\partial}{\partial x_2}$ and $\dfrac{\partial}{\partial x_1}$ respectively in the above equations, and subtracting one from the other, we have:

$$\frac{\partial^2 M_{11}}{\partial x_1^2} + 2\frac{\partial^2 M_{12}}{\partial x_1 \partial x_2} + \frac{\partial^2 M_{22}}{\partial x_2^2} + A - B = 0 \tag{11}$$

where A and B are defined by:

$$A \equiv \frac{\partial}{\partial x_1}\left(\int_{-\frac{h}{2}}^{\frac{h}{2}} \varepsilon_{2jk} x_j f_k dx_3 \right)$$

$$B \equiv \frac{\partial}{\partial x_2}\left(\int_{-\frac{h}{2}}^{\frac{h}{2}} \varepsilon_{1jk} x_j f_k dx_3 \right)$$

It is obvious that

$$A = \frac{\partial}{\partial x_1}\left(\int_{-\frac{h}{2}}^{\frac{h}{2}} \varepsilon_{2jk} x_j f_k dx_3 \right)$$

$$= \frac{\partial}{\partial x_1}\left[\int_{-\frac{h}{2}}^{\frac{h}{2}} \left(\varepsilon_{213} x_1 f_3 + \varepsilon_{231} x_3 f_1 \right) dx_3 \right]$$

$$= \frac{\partial}{\partial x_1}\left[\int_{-\frac{h}{2}}^{\frac{h}{2}} \left(-x_1 f_3 + x_3 f_1 \right) dx_3 \right]$$

$$B = \frac{\partial}{\partial x_2}\left[\int_{-\frac{h}{2}}^{\frac{h}{2}} \left(x_2 f_3 - x_3 f_2 \right) dx_3 \right]$$

By defining the flexure of the lithosphere as:

$$w \equiv x_3(x_1, x_2),$$

we have

$$\begin{cases} A = \int_{-\frac{h}{2}}^{\frac{h}{2}} \left[-f_3 - x_1 \dfrac{\partial f_3}{\partial x_1} + \dfrac{\partial}{\partial x_1}(w f_1) \right] dx_3 \\ B = \int_{-\frac{h}{2}}^{\frac{h}{2}} \left[f_3 + x_2 \dfrac{\partial f_3}{\partial x_2} - \dfrac{\partial}{\partial x_2}(w f_2) \right] dx_3. \end{cases}$$

By assuming that the change in body force f can be neglected, *i.e.*,

$$\frac{\partial f_3}{\partial x_2} = \frac{\partial f_3}{\partial x_1} = \frac{\partial f_2}{\partial x_2} = \frac{\partial f_1}{\partial x_1} = 0,$$

we have

$$\begin{cases} A = \int_{-\frac{h}{2}}^{\frac{h}{2}} (-f_3) dx_3 + \dfrac{\partial^2 w}{\partial x_1^2} \int_{-\frac{h}{2}}^{\frac{h}{2}} \int_{x_1} f_1 dx_1 dx_3 \\ B = \int_{-\frac{h}{2}}^{\frac{h}{2}} f_3 dx_3 - \dfrac{\partial^2 w}{\partial x_2^2} \int_{-\frac{h}{2}}^{\frac{h}{2}} \int_{x_2} f_2 dx_2 dx_3 \end{cases}$$

We define horizontal loading as:

$$\begin{cases} N_{11} \equiv \int_{-\frac{h}{2}}^{\frac{h}{2}} \int_{x_1} f_1 dx_1 dx_3 \\ N_{22} \equiv \int_{-\frac{h}{2}}^{\frac{h}{2}} \int_{x_2} f_2 dx_2 dx_3 . \end{cases}$$

This gives:

$$\begin{cases} A = \int_{-\frac{h}{2}}^{\frac{h}{2}} (-f_3) dx_3 + N_{11} \dfrac{\partial^2 w}{\partial x_1^2} \\ B = \int_{-\frac{h}{2}}^{\frac{h}{2}} f_3 dx_3 - N_{22} \dfrac{\partial^2 w}{\partial x_2^2} \end{cases}$$

where N_{11} and N_{22} describe normal tectonic compression or extension of the thin plate in force per unit length. On substituting A and B into equation (11), we obtain:

$$\frac{\partial^2 M_{11}}{\partial x_1^2} + 2\frac{\partial^2 M_{12}}{\partial x_1 \partial x_2} + \frac{\partial^2 M_{22}}{\partial x_2^2} + N_{11}\frac{\partial^2 w}{\partial x_1^2} + N_{22}\frac{\partial^2 w}{\partial x_2^2} = 2\int_{-\frac{h}{2}}^{\frac{h}{2}} f_3 dx_3 \qquad (12)$$

Airy isostasy requires that:

$$wg(\rho_m - \rho_c) = \rho_c g h_t,$$

where h_t is topography, ρ_m is mantle density, ρ_c is crustal density, w is plate flexure, and g is gravitational acceleration. Airy isostasy holds when there is no horizontal support to the loading on a plate. Thus, the vertical compensation is:

$$2\int_{-\frac{h}{2}}^{\frac{h}{2}} f_3 dx_3 = -wg(\rho_m - \rho_c) + \rho_c g h_t \qquad (13)$$

On substituting equation (13) into (12) and converting coordinates (x_1, x_2, x_3) to (x, y, z), we have (*Turcotte and Schubert,* 1982):

$$\frac{\partial^2 M_{xx}}{\partial x^2} + \frac{\partial^2 M_{yy}}{\partial y^2} + 2\frac{\partial^2 M_{xy}}{\partial x \partial y} + N_{xx}\frac{\partial^2 w(x,y)}{\partial x^2} + N_{yy}\frac{\partial^2 w(x,y)}{\partial y^2} + \Delta\rho g w(x,y) = \rho_c g h_t \qquad (14)$$

If we consider that the lithosphere is purely elastic and isotropic, then, using the *Generalized Hook*'s *Law*, we have:

$$\tau_{ij} = \frac{E}{1+\nu}\left(\varepsilon_{ij} + \frac{\nu}{1-\nu}\varepsilon_{kk}\delta_{ij} \right), \qquad (15)$$

where E is Young's modulus, ν Poisson's ratio, ε_{ij} the strain tensor, and δ_{ij} the Dirac delta function. With the thin plate assumption, compression and extension perpendicular to the plate can be neglected, *i.e.*,

$\varepsilon_{33} = 0$.

We obtain:

$$\tau_{11} = \left[\frac{E}{1+\nu}\left(\varepsilon_{11} + \frac{\nu}{1-\nu}\varepsilon_{kk} \right) \right]$$

$$\tau_{22} = \left[\frac{E}{1+\nu}\left(\varepsilon_{22} + \frac{\nu}{1-\nu}\varepsilon_{kk} \right) \right]$$

$$\tau_{12} = \left[\frac{E}{1+\nu}\varepsilon_{12} \right]$$

where $\varepsilon_{kk} = \varepsilon_{11} + \varepsilon_{22}$.

The strain and displacement of a particle are related by:

$$\varepsilon_{ij} = \frac{1}{2}\left(u_{i,j} + u_{j,i} \right)$$

$$u_{i,j} = \frac{\partial u_i}{\partial x_j}$$

Therefore,

$$\tau_{11} = \frac{E}{1-\nu^2}\left(u_{1,1} + \nu u_{2,2} \right)$$

$$\tau_{22} = \frac{E}{1-\nu^2}\left(u_{2,2} + \nu u_{1,1} \right) \qquad (16)$$

$$\tau_{12} = \frac{E}{1+\nu}\frac{1}{2}\left(u_{1.2} + u_{2,1} \right).$$

We assume there is no shear strain parallel to the thin plate. Thus,

$$\begin{cases} \varepsilon_{31} = \frac{1}{2}\left(u_{3,1} + u_{1,3} \right) = 0 \\ \varepsilon_{32} = \frac{1}{2}\left(u_{3,2} + u_{2,3} \right) = 0 . \end{cases}$$

From the above two equations, we can derive the following :

$$\begin{cases} u_{1,1} = -u_{3,11} x_3 \\ u_{2,2} = -u_{3,22} x_3 \\ u_{1,2} = -u_{3,12} x_3 \\ u_{2,1} = -u_{3,21} x_3 \end{cases} \qquad u_{i,jk} = \frac{\partial^2 u_i}{\partial x_j \partial x_k} . \tag{17}$$

On substituting equation (17) into (16) and (8), we have:

$$M_{11} = -\frac{E}{1-\nu^2}\left(u_{3,11} + \nu u_{3,22}\right)\int_{-\frac{h}{2}}^{\frac{h}{2}} x_3^2 dx_3$$

$$M_{22} = -\frac{E}{1-\nu^2}\left(u_{3,22} + \nu u_{3,11}\right)\int_{-\frac{h}{2}}^{\frac{h}{2}} x_3^2 dx_3$$

$$M_{12} = -\frac{E}{1+\nu}\frac{1}{2}\left(u_{3,12} + u_{3,21}\right)\int_{-\frac{h}{2}}^{\frac{h}{2}} x_3^2 dx_3 .$$

This gives:

$$\begin{aligned} M_{11} &= -\frac{Eh^3}{12\left(1-\nu^2\right)}\left(u_{3,11} + \nu u_{3,22}\right) \\ M_{22} &= -\frac{Eh^3}{12\left(1-\nu^2\right)}\left(u_{3,22} + \nu u_{3,11}\right) \\ M_{12} &= -\frac{E}{1+\nu} u_{3.12}\frac{h^3}{12} . \end{aligned} \tag{18}$$

We define the flexural rigidity D of the lithosphere as:

$$D \equiv \frac{Eh^3}{12\left(1-\nu^2\right)} \tag{19}$$

Putting the equation (19) into (18), we have:

$$\begin{cases} M_{11} = -D\left(u_{3,11} + \nu u_{3,22}\right) \\ M_{22} = -D\left(u_{3,22} + \nu u_{3,11}\right) \\ M_{12} = -D(1-\nu) u_{3,12} \end{cases} \tag{20}$$

with $u_3 = w = w(x, y)$. On substituting equation (20) into (14), converting coordinates (x_1, x_2, x_3) into (x, y, z), and making the symbols consistent, we obtain the fundamental equation for flexure of the elastic lithosphere (*Wees and Cloetingh*, 1994; *Jin,* 1997).

$$\frac{\partial^2}{\partial x^2}\left\{D\ (x,y)\left[\frac{\partial^2 w}{\partial x^2} + \nu\frac{\partial^2 w}{\partial y^2}\right]\right\} + \frac{\partial^2}{\partial y^2}\left\{D\ (x,y)\left[\frac{\partial^2 w}{\partial y^2} + \nu\frac{\partial^2 w}{\partial x^2}\right]\right\}$$

$$+ 2\frac{\partial^2}{\partial x\ \partial y}\left[D\ (x,y)(1-\nu)\frac{\partial^2 w}{\partial x\ \partial y}\right] + N_{11}\frac{\partial^2 w}{\partial x^2} + N_{22}\frac{\partial^2 w}{\partial y^2} + \Delta\rho g w(x,y) = \rho_c g h_t \tag{21}$$

3.3 Finite difference solution to the equation for flexure of an elastic lithosphere

3.3.1 The two-dimensional equation

For the case of a profile, the equation for the flexure of an elastic plate (21) becomes:

$$\frac{d^2}{dx^2}\left[D(x)\frac{d^2w}{dx^2}\right] + N_{11}\frac{d^2w}{dx^2} + \Delta\rho g w(x) = \rho_c g h_t \,. \qquad (22)$$

We define the finite differences:

$$w'_n = (w_{n+1} - w_{n-1})/2dx$$

$$w''_n = (w_{n+1} - 2w_n + w_{n-1})/dx^2$$

$$w'''_n = (w_{n+2} - 3w_{n+1} + 3w_{n-1} - w_{n-2})/dx^3$$

$$w_n^{(4)} = (w_{n+2} - 4w_{n+1} + 6w_n - 4w_{n-1} + w_{n-2})/dx^4$$

where n defines a finite node point, n = 1, 2, 3, 4, ……N, and dx is sample interval along the x-axis. On substituting the above finite difference formulas into equation (22), we obtain:

$$D_n(w_{n+2} - 4w_{n+1} + 6w_n - 4w_{n-1} + w_{n-2})$$
$$+ (D_{n+1} - D_{n-1})(w_{n+2} - 3w_{n+1} + 3w_{n-1} - w_{n-2})$$
$$+ (D_{n+1} - 2D_n + D_{n-1} + dx^2 \cdot P_n)(w_{n+1} - 2w_n + w_{n-1})$$
$$+ \Delta\rho g dx^4 w_n = q_n dx^4$$

where $p_n \equiv N_{11_n}$. By combining the terms that are similar, we obtain:

$$w_{n+2}[D_n + D_{n+1} - D_{n-1}]$$
$$+ w_{n+1}[-2D_{n+1} - 6D_n + 4D_{n-1} + P_n dx^2]$$
$$+ w_n[10D_n - 2D_{n+1} - 2D_{n-1} - 2P_n dx^2 + \Delta\rho g dx^4]$$
$$+ w_{n-1}[-6D_n + 4D_{n+1} - 2D_{n-1} + P_n dx^2]$$
$$+ w_{n-2}[D_n - D_{n+1} + D_{n-1}] = q_n dx^4 \,. \qquad (23)$$

This leads to a linear equation for w (*Sheffels and McNutt* 1986):

$$a_{n,n-2}w_{n-2} + a_{n,n-1}w_{n-1} + a_{n,n}w_n + a_{n,n+1}w_{n+1} + a_{n,n+2}w_{n+2} = q_n dx^4$$

$$A\vec{w} = \vec{q} \qquad (24)$$

where

$$\vec{w}=\begin{bmatrix} w_{-2} \\ w_{-1} \\ w_0 \\ \vdots \\ w_n \\ w_{n+1} \\ w_{n+2} \end{bmatrix} \qquad \vec{q}=\begin{bmatrix} q_0 \\ q_1 \\ \vdots \\ q_{n-1} \\ q_n \end{bmatrix} \qquad n=0,1,2,\cdots N$$

$$A=\begin{bmatrix} a_{0-2} & a_{0-1} & a_{00} & a_{01} & a_{02} & & & & \\ & a_{1-1} & a_{10} & a_{11} & a_{12} & a_{13} & & & \\ & & a_{20} & a_{21} & a_{22} & a_{23} & a_{24} & & \\ & & & & \ddots & & & & \\ & & & & a_{Nn-2} & a_{Nn-1} & a_{Nn} & a_{Nn+1} & a_{Nn+2} \end{bmatrix}$$

There are N+1 equations and N+5 unknowns, so that w_{-2}, w_{-1}, w_{N+1}, w_{N+2} can be obtained using the boundary conditions.

3.3.2 The three-dimensional equation

We translate the three dimensional equation for the flexure of an elastic plate (21) into a finite difference equation (*Wees and Cloetingh* 1994; *Jin* 1997):

$$\begin{aligned} &\left\lfloor D_{\mathbf{ij}}\left(w_{\mathbf{ij},\mathbf{jj}}+\nu w_{\mathbf{ij},\mathbf{ii}}\right)\right\rfloor_{\mathbf{jj}}+\left\lfloor D_{\mathbf{ij}}\left(\nu w_{\mathbf{ij},\mathbf{jj}}+w_{\mathbf{ij},\mathbf{ii}}\right)\right\rfloor_{\mathbf{ii}} \\ &+2\left\lfloor D_{ij}(1-\nu)w_{ij,ij}\right\rfloor_{,ij}+N_{\mathbf{jj}}w_{\mathbf{ij},\mathbf{jj}}+N_{\mathbf{ii}}w_{\mathbf{ij},\mathbf{ii}}+w_{ij}\left[\Delta\rho g\right]=\rho_c g h_{\mathbf{ij}} \end{aligned} \qquad (25)$$

where $_{,jj}$ and $_{,ii}$ are second order derivatives,

$$\begin{cases} w_{ij,jj}=\dfrac{w_{i(j+1)}-2w_{ij}+w_{i(j-1)}}{dx^2} \\ w_{ij,ii}=\dfrac{w_{(i+1)j}-2w_{ij}+w_{(i-1)j}}{dy^2} \\ w_{ij,jj}=\left[\dfrac{w_{(i+1)j}-w_{(i-1)j}}{2dy}\right]_{,j}=\left[\dfrac{w_{(i+1)(j+1)}-w_{(i-1)(j+1)}}{2dy}-\dfrac{w_{(i+1)(j-1)}-w_{(i-1)(j-1)}}{2dy}\right]\Big/2dx \end{cases}$$

The first term on the left-hand side of equation (25) is:

$$\left\lfloor D_{\mathbf{ij}}\left(w_{\mathbf{ij},\mathbf{jj}}+\nu w_{\mathbf{ij},\mathbf{ii}}\right)\right\rfloor_{\mathbf{jj}}$$

$$=\left[D_{ij}\left(\frac{w_{i(j+1)}-2w_{ij}+w_{i(j-1)}}{dx^2}+\frac{w_{(i+1)j}-2w_{ij}+w_{(i-1)j}}{dy^2}\right)\right]$$

$$=\frac{1}{dx^2}\left\{D_{i(j+1)}\left[\frac{w_{i(j+2)}-2w_{i(j+1)}+w_{ij}}{dx^2}+\nu\frac{w_{(i+1)(j+1)}-2w_{i(j+1)}+w_{(i-1)(j+1)}}{dy^2}\right]\right.$$

$$-2D_{ij}\left[\frac{w_{i(j+1)}-2w_{ij}+w_{i(j-1)}}{dx^2}+v\frac{w_{(i+1)j}-2w_{ij}+w_{(i-1)j}}{dy^2}\right]$$

$$+D_{i(j-1)}\left[\frac{w_{ij}-2w_{i(j-1)}+w_{i(j-2)}}{dx^2}+v\frac{w_{(i+1)(j-1)}-2w_{i(j-1)}+w_{(i-1)(j-1)}}{dy^2}\right]$$

The second term on the left-hand side of equation (25) is:

$$\left\lfloor D_{ij}\left(vw_{ij,jj}+w_{ij,ii}\right)\right\rfloor_{,ii}$$

$$=\left[D_{ij}\left(v\frac{w_{i(j+1)}-2w_{ij}+w_{i(j-1)}}{dx^2}+\frac{w_{(i+1)j}-2w_{ij}+w_{(i-1)j}}{dy^2}\right)\right]_{,ii}$$

$$=\frac{1}{dy^2}\left\{D_{(i+1)j}\left[v\frac{w_{(i+1)(j+1)}-2w_{(i+1)j}+w_{(i+1)(j-1)}}{dx^2}+\frac{w_{(i+2)j}-2w_{(i+1)j}+w_{ij}}{dy^2}\right]\right.$$

$$-2D_{ij}\left[v\frac{w_{i(j+1)}-2w_{ij}+w_{i(j-1)}}{dx^2}+\frac{w_{(i+1)j}-2w_{ij}+w_{(i-1)j}}{dy^2}\right]$$

$$\left.+D_{(i-1)j}\left[v\frac{w_{(i-1)(j+1)}-2w_{(i-1)j}+w_{(i-1)(j-1)}}{dx^2}+\frac{w_{ij}-2w_{(i-1)j}+w_{(i-2)j}}{dy^2}\right]\right\}$$

The third term on the left-hand side of equation (25) is:

$$2\left\lfloor D_{ij}\left(1-v\right)w_{ij,ij}\right\rfloor_{,ij}$$

$$=2\left[D_{ij}\left(1-v\right)\left(\frac{w_{(i+1)j}-w_{(i-1)j}}{2dy}\right)_{,j}\right]_{,ij}$$

$$=2\left\{D_{ij}\left(1-v\right)\frac{1}{2dx}\left[\frac{w_{(i+1)(j+1)}-w_{(i-1)(j+1)}}{2dy}-\frac{w_{(i+1)(j-1)}-w_{(i-1)(j-1)}}{2dy}\right]\right\}_{,ij}$$

$$=\frac{2}{2dy}\left\{D_{(i+1)j}\left(1-v\right)\frac{1}{2dx}\left[\frac{w_{(i+2)(j+1)}-w_{i(j+1)}}{2dy}-\frac{w_{(i+2)(j-1)}-w_{i(j-1)}}{2dy}\right]\right.$$

$$\left.-D_{(i-1)j}\left(1-v\right)\frac{1}{2dx}\left[\frac{w_{i(j+1)}-w_{(i-2)(j+1)}}{2dy}-\frac{w_{i(j-1)}-w_{(i-2)(j-1)}}{2dy}\right]\right\}_{,j}$$

$$=\frac{2}{2dy2dx}\left\{D_{(i+1)(j+1)}\left(1-v\right)\frac{1}{2dx}\left[\frac{w_{(i+2)(j+2)}-w_{i(j+1)}}{2dy}-\frac{w_{(i+2)j}-w_{ij}}{2dy}\right]\right.$$

$$\left.-D_{(i-1)(j+1)}\left(1-v\right)\frac{1}{2dx}\left[\frac{w_{i(j+2)}-w_{(i-2)(j+2)}}{2dy}-\frac{w_{ij}-w_{(i-2)j}}{2dy}\right]\right\}$$

$$-\frac{2}{2dy2dx}\left\{D_{(i+1)(j-1)}\left(1-v\right)\frac{1}{2dx}\left[\frac{w_{(i+2)j}-w_{ij}}{2dy}-\frac{w_{(i+2)(j-2)}-w_{i(j-2)}}{2dy}\right]\right.$$

$$- D_{(i-1)(j-1)}(1-v)\frac{1}{2dx}\left[\frac{w_{ij}-w_{(i-2)j}}{2dy}-\frac{w_{i(j-2)}-w_{(i-2)(j-2)}}{2dy}\right]\Bigg\}$$

The fourth term on the left-hand side of equation (25) is:

$$N_{\boldsymbol{jj}}w_{\boldsymbol{ij},\boldsymbol{jj}} = N_{\boldsymbol{jj}}\frac{w_{\boldsymbol{i}(\boldsymbol{j}+1)}-2w_{\boldsymbol{ij}}+w_{\boldsymbol{i}(\boldsymbol{j}-1)}}{dx^2}$$

$$= w_{i(j-1)}\left[\frac{N_{jj}}{dx^2}\right]+w_{ij}\left[\frac{-2N_{jj}}{dx^2}\right]+w_{i(j+1)}\left[\frac{N_{jj}}{dx^2}\right]$$

The fifth term on the left-hand side of equation (25) is:

$$N_{\boldsymbol{ii}}w_{\boldsymbol{ij},\boldsymbol{ii}} = N_{\boldsymbol{ii}}\frac{w_{(\boldsymbol{i}+1)\boldsymbol{j}}-2w_{\boldsymbol{ij}}+w_{(\boldsymbol{i}-1)\boldsymbol{j}}}{dy^2}$$

$$= w_{(i-1)j}\left[\frac{N_{ii}}{dy^2}\right]+w_{ij}\left[\frac{-2N_{ii}}{dy^2}\right]+w_{(i+1)j}\left[\frac{N_{ii}}{dy^2}\right]$$

The sixth term on the left-hand side of equation (25) is:

$$w_{ij}\left[\Delta\rho g\right]$$

We combine terms with similar subscripts. There are 25 finite difference terms for each spatial point (i , j) (*Jin and Jiang,* 2002):

$$A\vec{w}=\vec{q}$$

$$a_{(\boldsymbol{i}-2)(\boldsymbol{j}-2)} = \frac{1-v}{8dx^2dy^2}D_{(i-1)(j-1)}$$

$$a_{(\boldsymbol{i}-2)\boldsymbol{j}} = \frac{1}{dy^4}D_{(i-1)j}+\frac{1-v}{8dx^2dy^2}\left(-D_{(i-1)(j+1)}-D_{(i-1)(j-1)}\right)$$

$$a_{(\boldsymbol{i}-2)(\boldsymbol{j}+2)} = \frac{1-v}{8dx^2dy^2}D_{(i-1)(j+1)}$$

$$a_{(\boldsymbol{i}-1)(\boldsymbol{j}-1)} = \frac{v}{dx^2dy^2}D_{i(j-1)}+\frac{v}{dx^2dy^2}D_{(i-1)j}$$

$$a_{(\boldsymbol{i}-1)\boldsymbol{j}} = -\frac{2v}{dx^2dy^2}D_{ij}-\frac{2v}{dy^4}D_{ij}-\frac{2v}{dx^2dy^2}D_{(i-1)j}-\frac{2}{dy^4}D_{(i-1)j}+\frac{N_{ii}}{dy^2}$$

$$a_{(\boldsymbol{i}-1)(\boldsymbol{j}+1)} = \frac{v}{dx^2dy^2}D_{i(j+1)}+\frac{v}{dx^2dy^2}D_{(i-1)j}$$

$$a_{\boldsymbol{i}(\boldsymbol{j}-2)} = \frac{1}{dx^4}D_{i(j-1)}+\frac{1-v}{8dx^2dy^2}\left(-D_{(i+1)(j-1)}-D_{(i-1)(j-1)}\right)$$

$$a_{i(j-1)} = -\frac{2}{dx^4}D_{ij} - \frac{2}{dx^4}D_{i(j-1)} - \frac{2v}{dx^2dy^2}D_{i(j-1)} - \frac{2v}{dx^2dy^2}D_{ij} + \frac{N_{jj}}{dx^2}$$

$$a_{ij} = \frac{1}{dx^4}D_{i(j+1)} + \frac{4}{dx^4}D_{ij} + \frac{4v}{dx^2dy^2}D_{ij} + \frac{1}{dx^4}D_{i(j-1)} + \frac{1}{dy^4}D_{(i+1)j} + \frac{4v}{dx^2dy^2}D_{ij}$$

$$+\frac{4}{dy^4}D_{ij} + \frac{1}{dy^4}D_{(i-1)j} + \frac{1-v}{8dx^2dy^2}\Big(D_{(i+1)(j+1)} + D_{(i-1)(j+1)} +$$

$$D_{(i+1)(j-1)} + D_{(i-1)(j-1)}\Big) - \frac{2N_{jj}}{dx^2} - \frac{2N_{ii}}{dy^2} + \Delta\rho g$$

$$a_{i(j+1)} = -\frac{2}{dx^4}D_{i(j+1)} - \frac{2v}{dx^2dy^2}D_{i(j+1)} - \frac{2}{dx^4}D_{ij} - \frac{2v}{dx^2dy^2}D_{ij} + \frac{N_{jj}}{dx^2}$$

$$a_{i(j+2)} = \frac{1}{dx^4}D_{i(j+1)} + \frac{1-v}{8dx^2dy^2}\Big(-D_{(i+1)(j+1)} - D_{(i-1)(j+1)}\Big)$$

$$a_{(i+1)(j-1)} = \frac{v}{dx^2dy^2}D_{i(j-1)} + \frac{v}{dx^2dy^2}D_{(i+1)j}$$

$$a_{(i+1)j} = -\frac{2v}{dx^2dy^2}D_{ij} - \frac{2v}{dx^2dy_2}D_{(i+1)j} - \frac{2v}{dy^4}D_{(i+1)j} - \frac{2v}{dy^4}D_{ij} + \frac{N_{ii}}{dy^2}$$

$$a_{(i+1)(j+1)} = \frac{v}{dx^2dy^2}D_{i(j+1)} + \frac{v}{dx^2dy^2}D_{(i+1)j}$$

$$a_{(i+2)(j-2)} = \frac{1-v}{8dx^2dy^2}D_{(i+1)(j-1)}$$

$$a_{(i+2)j} = \frac{1}{dy^4}D_{(i+1)j} + \frac{1-v}{8dx^2dy^2}\Big(-D_{(i+1)(j+1)} - D_{(i+1)(j-1)}\Big)$$

$$a_{(i+2)(j+2)} = \frac{1-v}{8dx^2dy^2}D_{(i+1)(j+1)}$$

The other items are zero.

$q_{\mathrm{ij}} = \rho_c g h_{ij}$

$i = 1, 2, 3, \cdots N_y;\ j = 1, 2, 3, \cdots N_x$

Thus, there are $(N_x + 4)(N_y + 4)$ variables for $N_x \times N_y$ equations. Boundary conditions are therefore needed to solve these finite difference equations. Because the flexure of the plate at the boundary is unknown, the simplest assumption at the boundaries is Airy isostasy (*Jin,* 1997):

$\Delta\rho g w_{ij} = \rho_c g h_{ij}$

$$w_{ij} = \frac{\rho_c}{\Delta\rho} h_{ij}$$

We shall also assume that the boundaries are flat. That is,

$$\frac{\partial w}{\partial x} = 0 \rightarrow w_{ij,j} = \frac{w_{i(j+1)} - w_{i(j-1)}}{2dx} = 0$$

$$w_{i(j+1)} = w_{i(j-1)}$$

$$\frac{\partial w}{\partial y} = 0 \rightarrow w_{ij,i} = \frac{w_{(i+1)j} - w_{(i-1)j}}{2dy} = 0$$

$$w_{(i+1)j} = w_{(i-1)j}$$

This gives the boundary conditions for equation (25):

$$\begin{cases} w_{ij} = \dfrac{\rho_c}{\Delta\rho} h_{ij} \\ w_{i(j+1)} = w_{i(j-1)} \\ w_{(i+1)j} = w_{(i-1)j} \end{cases} \qquad \begin{matrix} i = -1, 0, N_y + 1, N_y \\ j = -1, 0, N_x + 1, N_x \end{matrix} \qquad (26)$$

The flexure equations (23) and (25) for a two- and three-dimensional elastic plate respectively are now complete.

We processed the gravity data from the Tien Shan and the northern and northwestern margins of Tibet, Altyn Tagh and West Kunlun using the 2D elastic plate equation (22) for pairs of variably-rigid elastic plates subjected to vertical and horizontal loads, shear forces, and terminal bending moments. Because of the lack of constraints on the structure of the upper mantle beneath this area, we had to allow for a considerable latitude in possible plate models. For example, we searched for the best fitting models by assuming either one continuous plate beneath our study area or two separate plates (a severed plate). The elastic thickness h of the plate or plates was allowed to vary laterally, and we had to consider the possibility of lateral compression on the system. The corresponding gravity was computed using the 2D *Okabe*'s (1979) formula. The crust and mantle densities assigned are 2670 kg/m^3 and 3300 kg/m^3 respectively.

In our 3D model, we allowed the mechanical strengths of the lithosphere to vary according to the geological nature of each tectonic block. Firstly, we assumed that the effective lithospheric elastic thickness is h (rigidity D), and calculated the flexure w based on the equation (25). Using the gravity formula of *Parker* (1972), the theoretical gravity

anomalies were computed. The miss-tie between the observed Bouguer gravity and the theoretical Bouguer gravity is used to adjust the flexural rigidity parameters of the model lithosphere. By computing iteratively, we obtained the best-fit D and w, for which the residual gravity anomaly is minimized. We extended our calculation area out of China to ensure that the boundaries are flat enough to approximate our boundary condition which is Airy isostasy or super-long-wavelength surface loading. The choice of compensation with very long wavelengths at the boundaries is due to the lack of knowledge on the actual deflection at the boundaries.

The main programs used in this dissertation were kindly provided by Professor Marcia McNutt and Dr. Yu Jin.

Chapter 4. Data

The data used in this dissertation are Bouguer gravity and topography which cover an area ranging from 75° E to 115° E in longitude and 25° N to 45° N in latitude (Figs. 1 and 14). The major part of the study area is located in the People's Republic of China, the southern part includes Nepal and part of India, and the northern portion belongs to Mongolia.

The gravity data in China were digitized from a 1:4,000,000 regional Bouguer gravity map of China (*Sun*, 1989). This gravity map was compiled by the Institute of Geophysical and Geochemical Exploration and the Technical Centre of Regional Gravity Survey, Ministry of Geology and Mineral Resources (MGMR) in the period 1987-1988. Gravity data measured since 1979 by geophysical prospecting under the supervision of MGMR have been integrated into this map. The gravity surveys were implemented according to the Technical Stipulation for Regional Gravity Survey Issued by the MGMR of China at scales of 1:100,000, 1:200,000 and 1:500,000 respectively. The dots in Fig. 14 give the original gravity stations in the study area. The original gravity measurements were made using the Potsdam Standard with the Beijing 54 coordinate system and the Yellow Sea elevation system as geographic reference. The gravity data were reduced using the Helmert Normal Gravity Formula on the spheroid and converted to free air anomalies. The Bouguer gravity field was calculated using a topographic density of 2670 kg/m^3, and terrain corrections were applied out to a distance of 166.7 km using digitized topographic data from a 1:50,000 topographic map (*Sun*, 1989). The cumulative error in the Bouguer gravity is estimated to be less than ±3 mgal (*Sun*, 1989), including errors in elevation.

As shown in Fig. 14, the gravity survey points used in this regional Bouguer gravity map of China were not evenly distributed. There is a large unsurveyed region in northern Tibet. To close this gap, two gravity surveys were conducted in October 1997 and June 1998 across the Altyn Tagh at the northern edge of Tibet and the West Kunlun Mountains at the northwestern edge of Tibet (Fig. 14). This project was supported by the Geophysics Program of the U.S. National Science Foundation. For the Altyn Tagh area, the first transect was the Alagan-Mangya profile starting in the Tarim Basin and ending in the Qaidam Basin. It is about 700 km long and includes 237 new observations. The second transect is the Qiemo-Tula profile which does not cross the mountain range completely for the lack of a passable route. It is about 300 km long and consists of 109 new observations. The survey in the West Kunlun area was unprecedented because of the frigid temperatures and thin air

(average oxygen content is 30%~50% of that at sea level). We departed from Yecheng and surveyed along National Route 219 across the Xinjiang-Tibet border, with oxygen bottles for each person. We ascended the Kunlun Mountains with difficulty and stopped at the end of the highway in Songxi, Tibet. This West Kunlun gravity transect is about 730 km long with 122 observations at a spacing of about 5 km.

We used a LaCoste-Romberg LCR-G gravimeter for the survey. Prior to this survey, the only Chinese national base points where absolute gravity have been measured were in the Tarim Basin. We introduced several new base points across the faults into Tibet by closing loops (to control drift) with our relative gravimeter, returning later for additional measurements between these new base points. Each survey started from one base point and ended at another to correct for gravimeter drift. The altitude was determined with a Trimble 4600 GPS receiver. The control points for the elevation were observed for 20 minutes, while other points were surveyed for 10 minutes. The observation error for topography is ± 2 m.

The gravity measurements were reduced to the Potsdam standard with the geographical reference of the Beijing-54 Coordinate System and the Yellow Sea Elevation System. Data were reduced using the Helmert normal gravity, the usual practice for the survey team, with a flattening of 1/298.3. Terrain corrections were applied to zones of 0-2 km and 2-166.7 km using digital topographic data from a 1:50,000 topographic map. The total RMS error for gravity measurements is ±0.043 mGal. These gravity data plotted as a function of distance along the survey lines are shown in Fig. 15.

The gravity data in India and Nepal are from the Lamont Geobase, which includes land gravity measurements assembled from various sources by Garry Karner and others at the Lamont-Doherty Earth Observatory of Columbia University (*Watts et al.,* 1985). These data were interpolated into a 5′ x 5′ grid (*Jin et al.*, 1996).

The gravity data in Mongolia are from Professor M. K. McNutt. They were averaged over a grid of 5′ x 7′ (*Kogan and McNutt*, 1993).

The topographic data are from the latest DEM database, Topo30, which can be easily accessed through Internet. These data were gridded at 5′ x 5′ by interpolation for our calculations.

It is instructive to compare the gravity data with the best global gravity database from the Scripps Institution of Oceanography, UCSD. The marine gravity data in this database are from satellite altimetry.

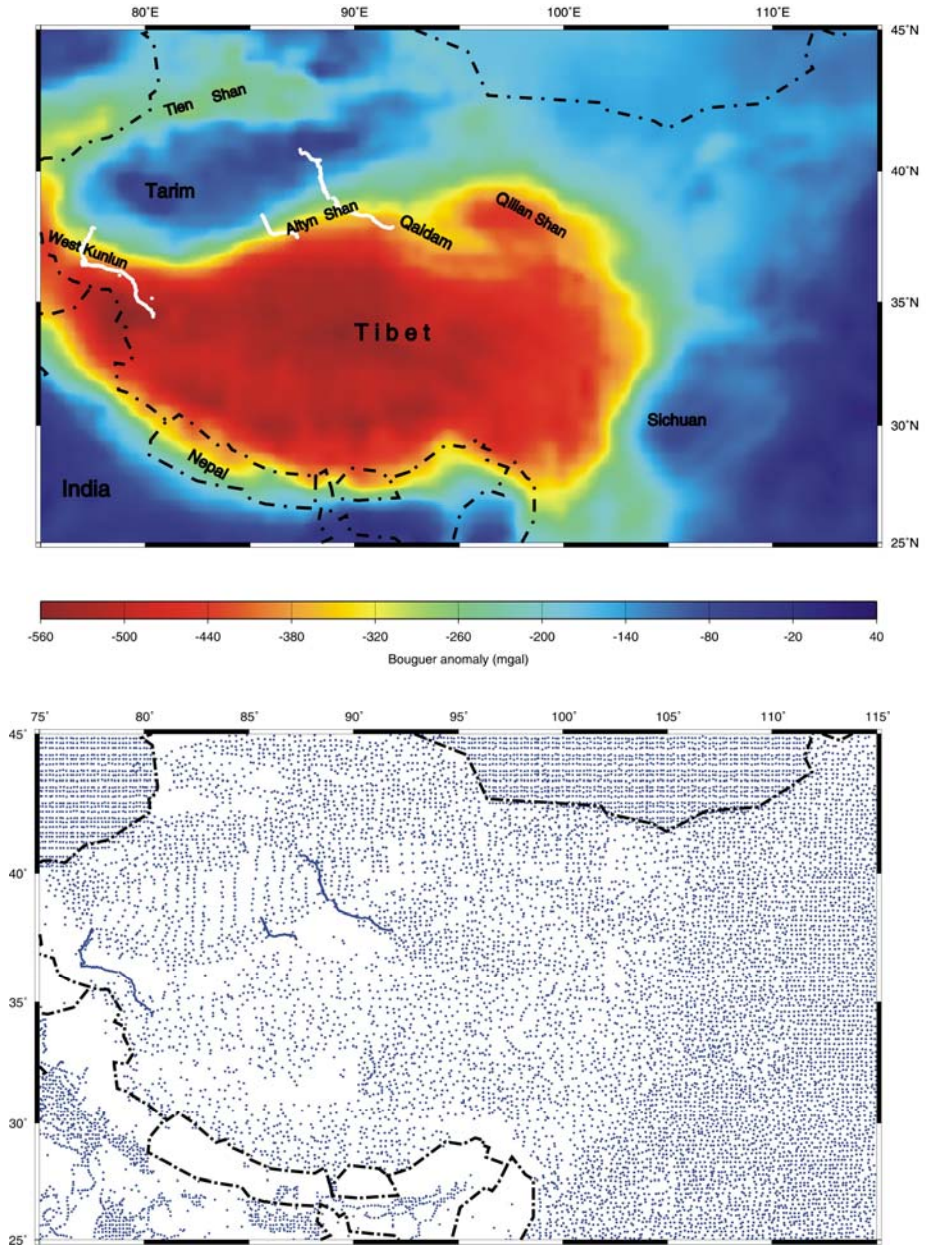

Figure 14. Top: Bouguer gravity map of the study area. The data coverage in China is digitized from a 1:4,000,000 regional gravity map. The coverage in India is from the Lamont Database, and the coverage in Mongolia is from *Kogan and McNutt* (1993). The latter two are in the public domain. The three white lines from Tarim to Northern Tibet are our new gravity transects surveyed in 1997 and 1998. The black dash-dotted lines are national boundaries. The colour bar is elevation in meters. Bottom: Dots give original survey points inside China, but represent grid data in Mongolia and the former Soviet Union. National boundaries are dash-dotted.

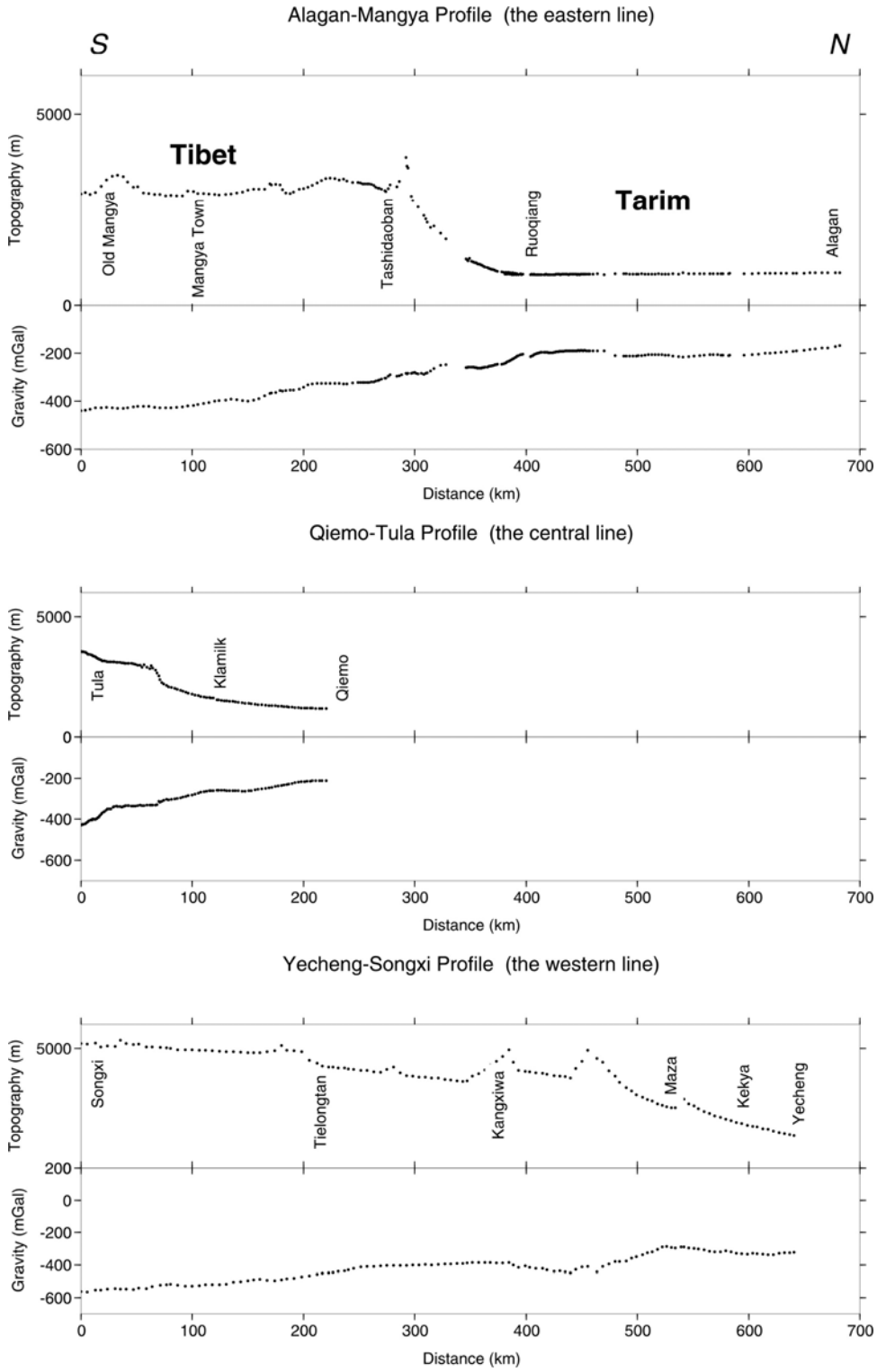

Figure 15. The observed topography and Bouguer gravity anomalies as a function of linear distance along the survey routes of the three profiles shown in Fig. 14.

If waves, winds, tides and currents are ignored, the surface of the ocean is an "equi-potential surface" of the Earth's gravity field. This equi-potential surface of the earth is approximately an ellipsoid of revolution. While this ellipsoidal shape fits the earth remarkably well, the actual ocean surface deviates from this ideal ellipsoid. The bumps and dips in the ocean surface are caused by minute variations in the Earth's gravitational field. Using a very accurate radar mounted on a satellite, these tiny bumps and dips in the geoid height can be measured. The height of the satellite above the ellipsoid h^* is measured by tracking the satellite from a globally-distributed network of laser stations, and the height of the satellite above the closest ocean surface h is measured with a microwave radar. The geoid height H is approximately equal to $h^* - h$. These raw geoid heights are converted into grids of gravity anomaly (*Sandwell and Smith,* 1997), which can then be compared with shipboard gravity measurements.

Land gravity cannot be measured yet by satellite altimetry, though ideally this can be done by measuring variations in the Doppler wave velocity from a satellite. The grid gravity data in the Scripps Global Gravity Database is an integration of existing land gravity and satellite gravity (*Sandwell and Smith,* 1997). This database shows that the average gravity anomaly over the Tibetan Plateau is –300 mgal; our land gravity anomalies on the plateau however average at –500 mgal. CMP seismic reflection results of the Tibet INDEPTH project and earthquake focal depths indicate that the average crustal thickness is about 70 km (*Makovsky et al.,* 1996*; Nelson et al.,* 1996), suggesting that our gravity anomaly average of –500 mgal is probably more reliable.

Commercial gravity databases such as that from the company GEOTECH are available but very expensive. It is not known whether Chinese gravity data are incorporated into these commercial databases. Apart from commercial gravity databases, the price and resolution of which are unknown to us, our gravity data are currently the best data available

Chapter 5. Results

5.1 Flexural modelling of the laterally varying elastic strength of the lithosphere in Central Asia

Estimation of the mechanical strength of the Earth's lithosphere helps earth scientists to better understand the processes of global tectonics as well as inter- and intra-plate deformations. The average mechanical strengths of plates vary from one plate to another. Within a plate, the mechanical strength can also change from one tectonic block to another due to variations in tectonic evolution and accretion history from block to block. Plate interactions may reactivate zones of weakness between tectonic blocks in a plate, and induce significant earthquakes and faulting. Brittle failure associated with faulting together with a weak middle/lower crust may decouple upper crustal deformations from deformations of the upper mantle, or a new plate boundary may form if deformations are coupled throughout the lithosphere. The elastic thickness of the lithosphere (*Te*) is an excellent physical parameter to measure the extent of deformation of different tectonic blocks. Weak blocks (or weak zones) with low *Te* values tend to deform first under the same background tectonic stress field (in this case the compressional stress field caused by the convergence between India and Eurasia).

One of the important scientific questions tackled in this dissertation is: To what extent do the upper crustal deformations in Central Asia resulting from the convergence between India and Eurasia weaken the underlying lithosphere? To try to answer this question, the elastic strengths of each tectonic unit is calculated using numerical 3D modelling of the gravity and topographic data (see Chapter 3).

Because flexure of the plate at its boundary is unknown, we assumed Airy isostasy at the boundaries for the 3D flexural equation (25). The geometry of our study area was chosen in such a way that our boundary condition, namely that Airy isostasy is established or the wavelengths of the surface loads are extremely long, is approximately valid. Results for the test of Airy isostasy at the boundaries of our study area are shown in Fig. 16.

The 3D flexural model allows the mechanical strength of the lithosphere to be varied according to the geological nature of each tectonic block in the study area. Topographic data are used as an input loading force to calculate the flexure of the elastic lithosphere, and the flexure is converted to flexural stress field and elastic rigidity of the plate. The initial model in our calculations assumed that Central Asia has an average elastic thickness of 40

km (*Lyon-Caen and Molnar,* 1984*; Jin et al.,* 1994, 1996), and that the corresponding value for India is 80 km (*Karner and Watts,* 1983*; Lyon-Caen and Molnar,* 1983) (Fig. 17). The stress was calculated iteratively by adjusting the flexural rigidity parameters of the model lithosphere until the observed gravity and topography are well approximated. The best fit was reached after six iterations, and the corresponding effective elastic thickness (*Te*) distribution is shown in Fig. 18. This figure shows significant variations in the strength of the lithosphere in Central Asia. There are five weak belts where the elastic thickness is less than 15 km. They correspond to the following five tectonic belts from south to north: Indus-Zhangbo suture, West Kunlun Fault, Altyn Tagh Fault, Qilian suture and Tien Shan suture. A moderately rigid (*Te* = 40-50 km) lithosphere characterizes the tectonic units Mongolia, Sino-Korea, Yangtze, Tarim and Qaidam blocks, Zungar Basin, East Tien Shan, and eastern Tibetan Plateau. Thus, the old, stable Chinese continent does not have a higher lithospheric rigidity. *Te* remains within the range of 40-50 km even when we increase the initial average elastic thickness of 40 km to 50 km and then to 60 km, suggesting that the moderate rigidity is not an artefact.

The miss-tie between the observed Bouguer gravity and the calculated Bouguer gravity was used as a measure of the goodness of fit of the model. We calculated the Bouguer gravity from lithospheric flexure with the best-fit *Te* (Fig. 19). Figure 20 shows the residual anomalies of this model (the difference between the observed and the calculated Bouguer anomalies at the best fit). For comparison, the initial residuals between the observed Bouguer anomalies and the values calculated with the initial elastic thickness distribution are shown in Fig. 21. The best-fit RMS residual is 24.54 mgal, which is significantly lower than the initial RMS residual of 34.84 mgal. Fig. 20 shows that, over large parts of the study area, the best-fit gravity residuals are close to zero. Exceptions include the large positive residuals in southwestern Tibet north of the Indian subcontinent, which may be artefacts since here, gravity survey stations are lacking (Fig. 22). In addition, large negative residuals are found in the Tarim, Zungar, Qaidam, Sichuan and Gangetic basins and a large positive linear residual anomaly occurs at the southern boundary of Tibet (Fig. 23). The negative residuals in the basins are probably a result of lateral lithospheric density variations. Structural maps of the basement of the Tarim, Qaidam, Zungar and Sichuan basins based on oil exploration seismic data suggest that the maximum sediment thicknesses reach 12 km (*Teng et al.,* 1991; Figs. 24-27). Contributions to the Bouguer gravity by these thick, lower-density sediments in the four basins are estimated to be over 100 mgal

(Figs. 28-31). Although sediment thickness data in the Gangetic Basin are unavailable, we believe that the situation there is similar.

The initial model we used is one of a continuous plate. Any significant linear feature in Fig. 20 implies that this assumption is not satisfied. Thus, we ascribe the positive linear residual anomaly in the southern Himalayas along the eastern axis of the Indo-Eurasian collision to breakdown of the continuous plate assumption. Therefore, two 2D profiles (A and B in Fig. 23) are calculated using a severed plate model (*i.e.*, a model with two plates). The results show that the Indian continent is underlain by an elastic rigid lithosphere with a *Te* = 95-105 km. Beneath the Himalayas, the severed plate model suggests that the lithosphere is weaker than what is indicated by our 3D results (*Te* = 10–20 km) (Figs. 32 and 33).

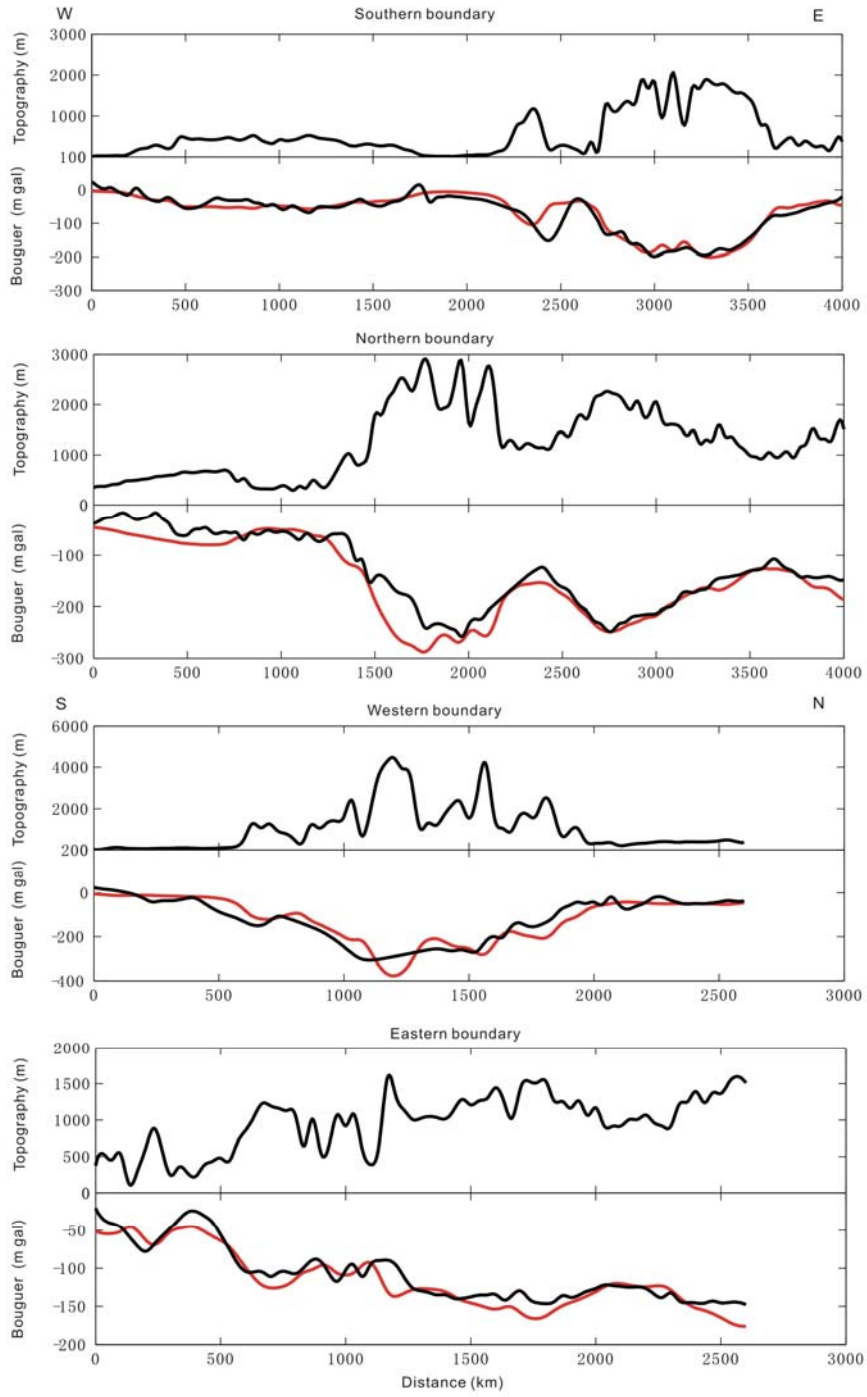

Figure 16. Gravity modelling along the southern, northern, western and eastern boundaries of the study area. Top panel is topography, bottom panel is observed Bouguer gravity anomalies (black) and predicted gravity from the Airy assumption (red) for every boundary.

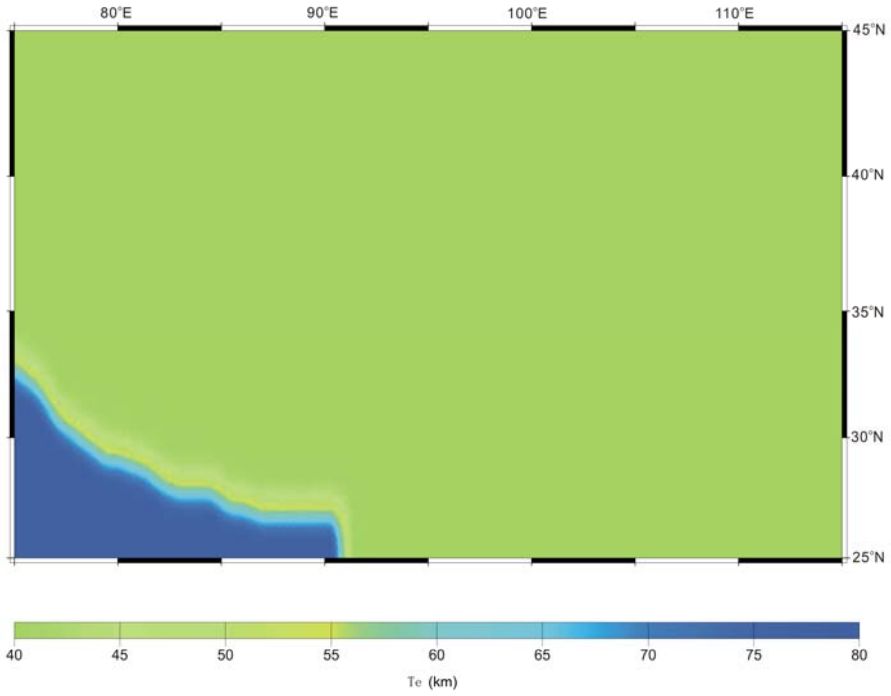

Figure 17. Initial elastic thickness distribution (*Te*) for flexural modelling.

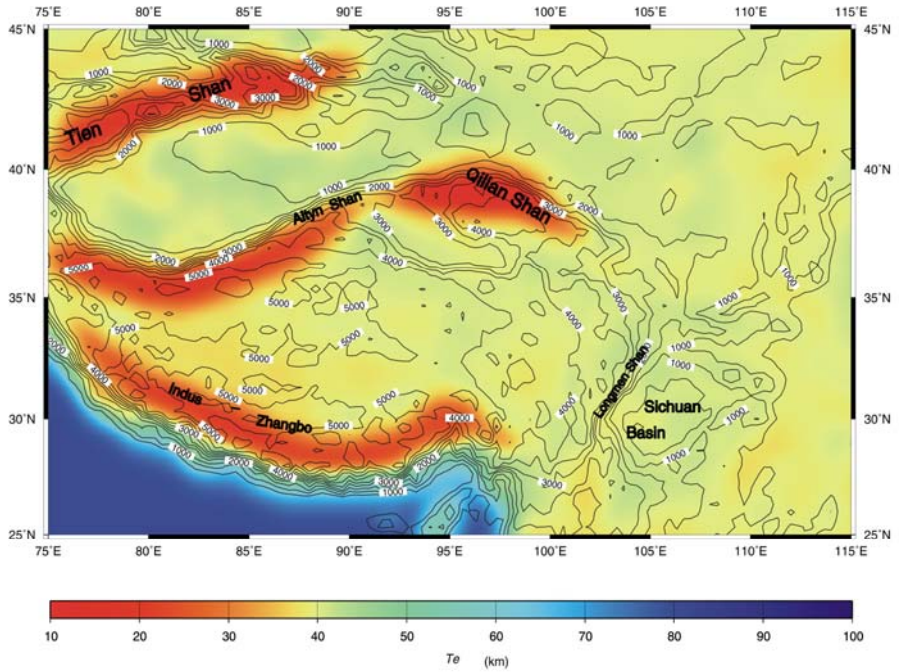

Figure 18. Calculated elastic thickness (*Te*) of the Central Asian lithosphere. The colour bar is *Te* in km. Contours give the elevation in meters.

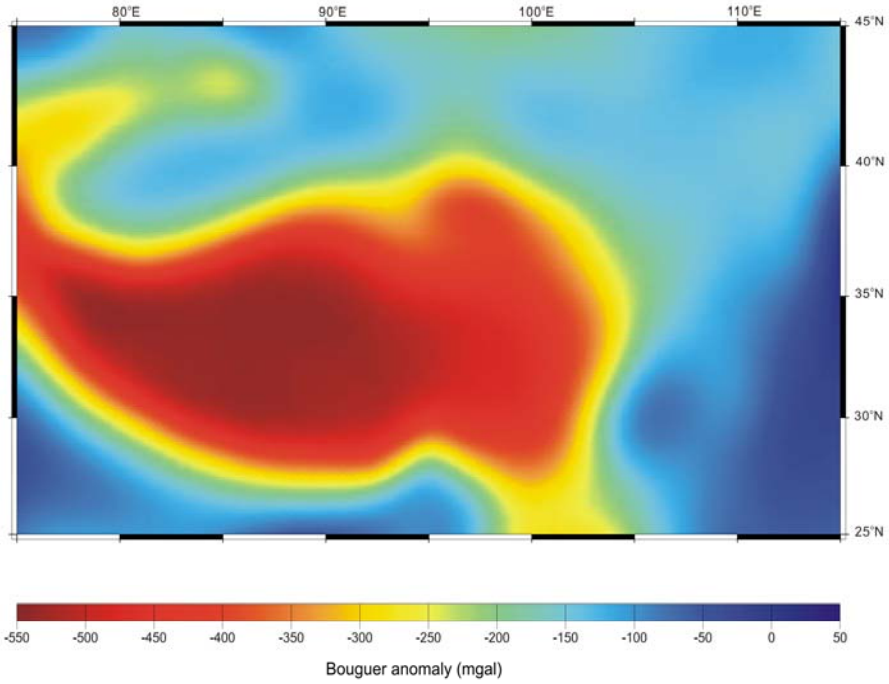

Figure 19. Calculated theoretical Bouguer gravity from the flexural model with the *Te* distribution of Fig. 18.

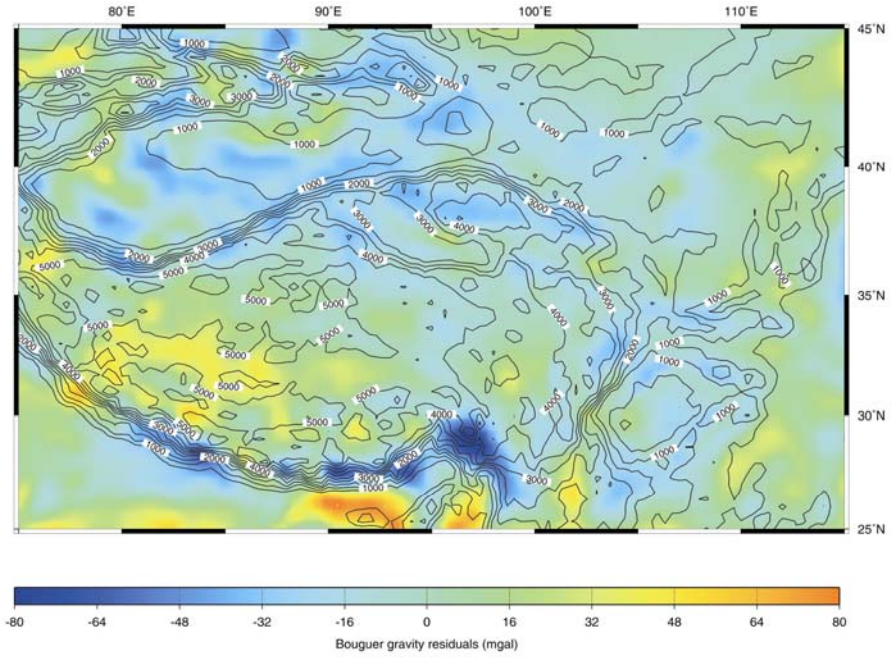

Figure 20. Final gravity residuals between the observed Bouguer gravity (Fig. 14) and the calculated theoretical gravity (Fig. 19). The colour bar gives residual anomalies in mgal and contours give the topography in meters.

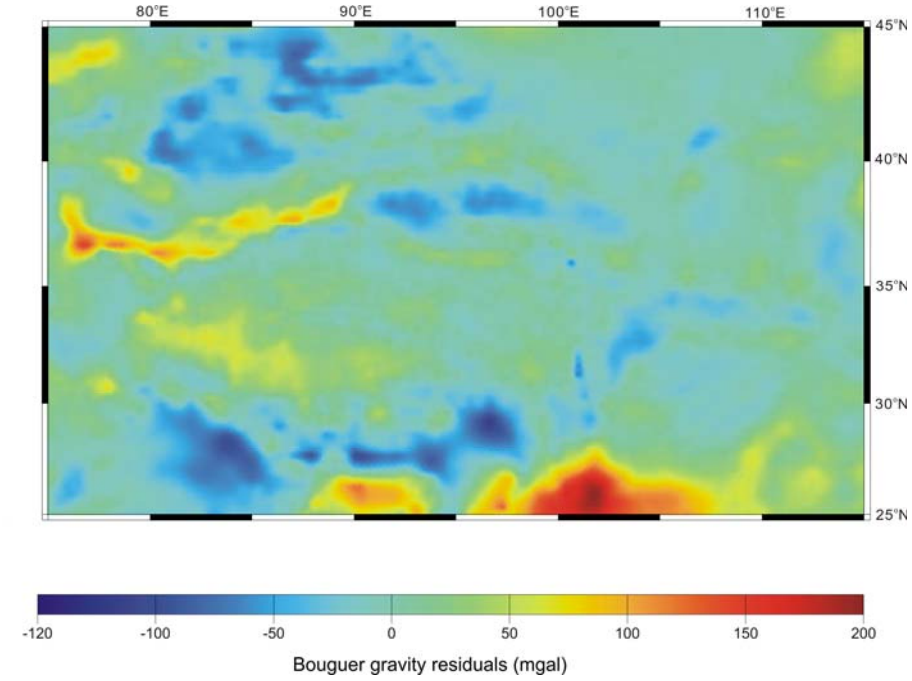

Figure 21. Initial gravity residuals between the observed Bouguer gravity (Fig. 14) and that calculated from the initial elastic thickness (*Te*) model of Fig. 17. The colour bar is residual anomalies in mgal.

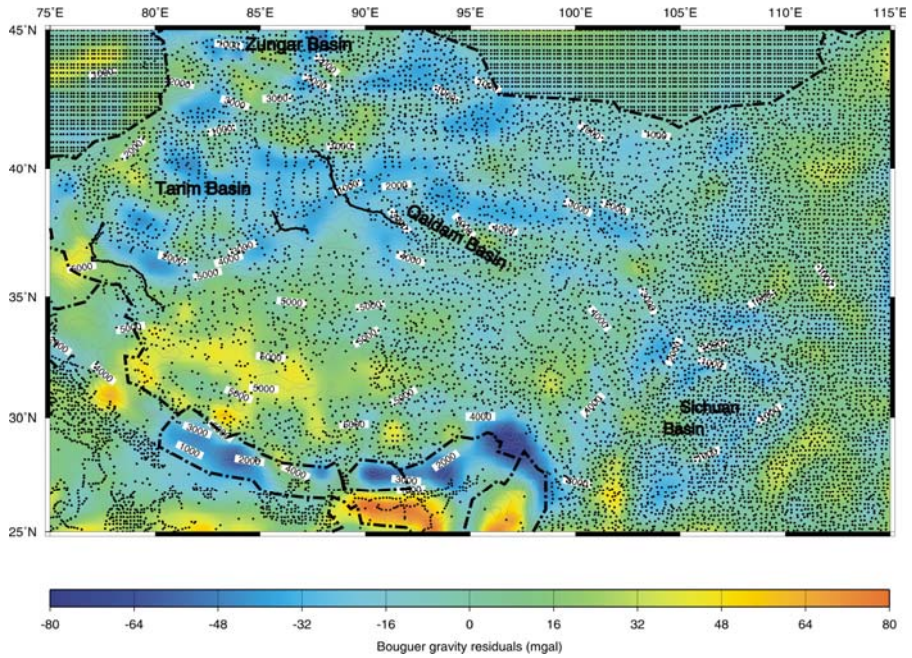

Figure 22. Location of gravity values in our gravity database. Values from the northern part of the study area, Mongolia is grid data. The Bouguer gravity residuals are shown in the background.

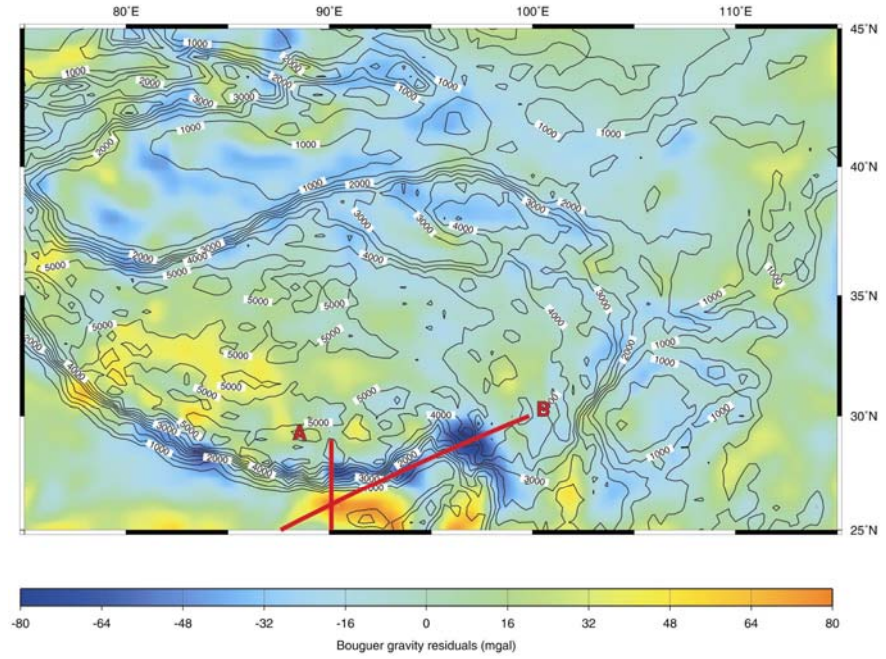

Figure 23. Gravity residuals between the observed Bouguer gravity and that calculated from the model of Fig. 18, with locations of basins and interpreted profiles. The colour bar is residual anomalies in mgal.

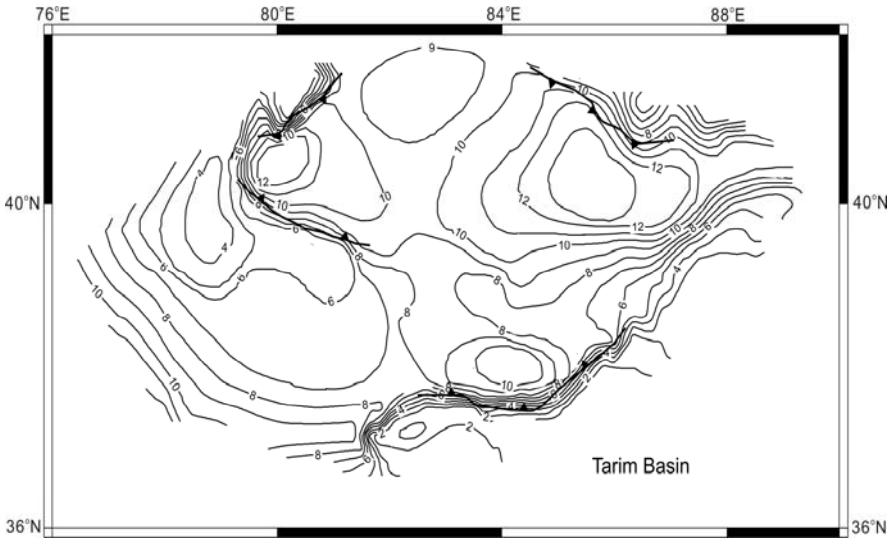

Figure 24. Sediment thickness in the Tarim Basin (km) at an isopach interval of 1 km. From *Li* (2002).

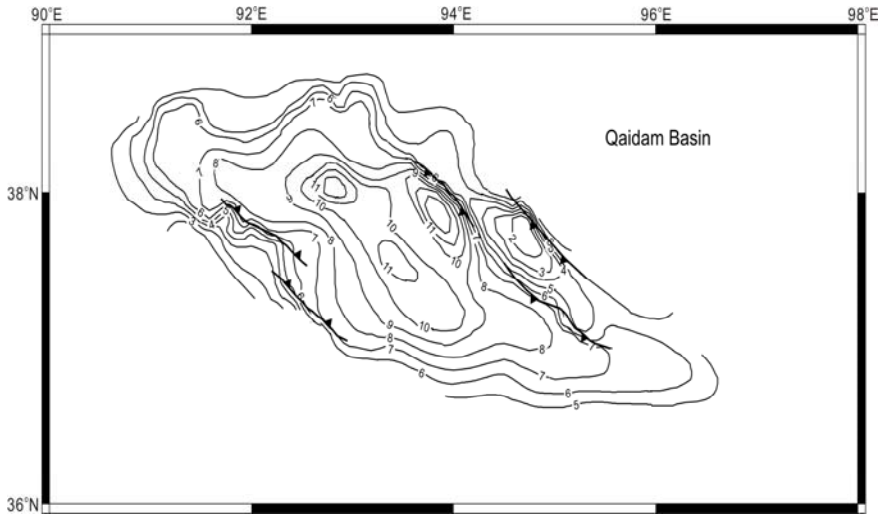

Figure 25. Sediment thickness in the Qaidam Basin (km) at an isopach interval of 1 km. From *Huang* (1996).

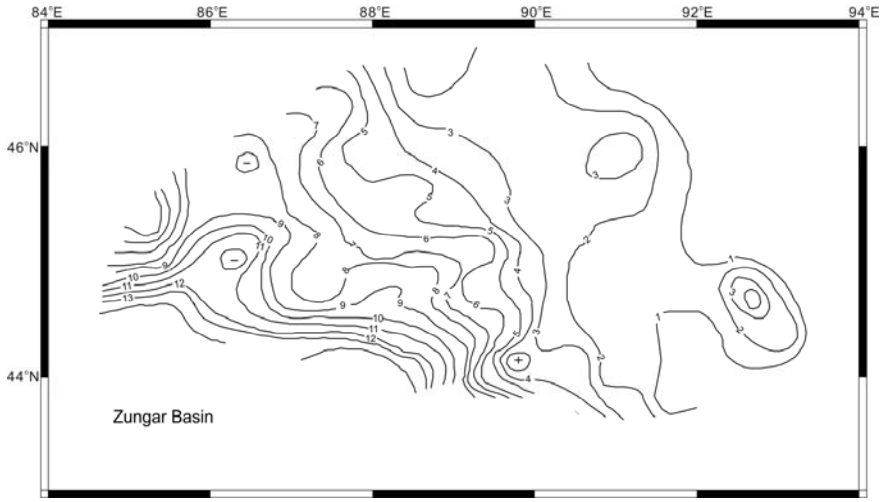

Figure 26. Sediment thickness in the Zungar Basin (km) at an isopach interval of 1 km. From *Li* (2002).

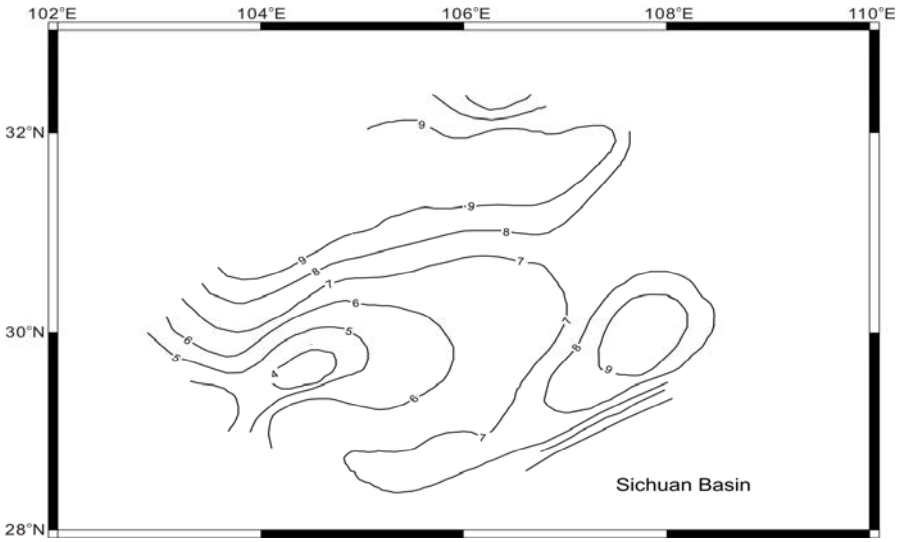

Figure 27. Sediment thickness in the Sichuan Basin (km) at an isopach interval of 1 km. From *Song and Lou* (1995).

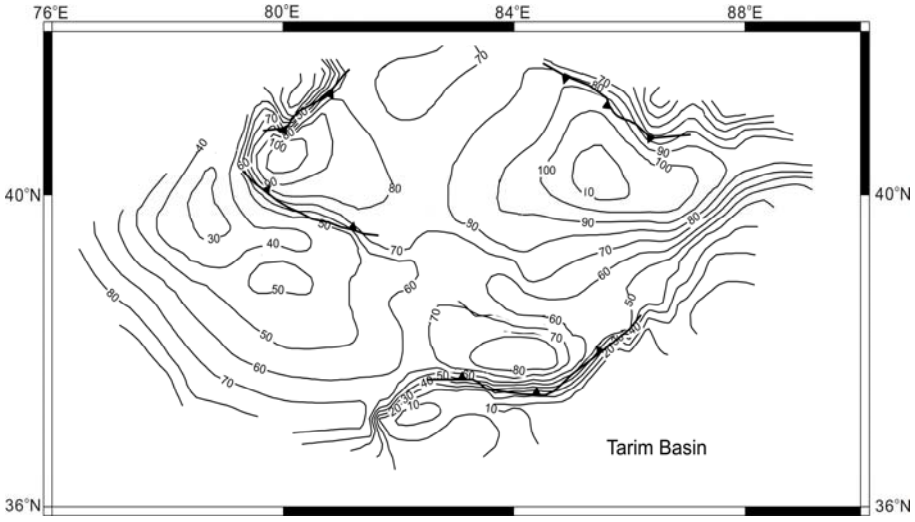

Figure 28. Predicted Bouguer gravity with sediment correction in the Tarim Basin in mgal at 10 mgal intervals.

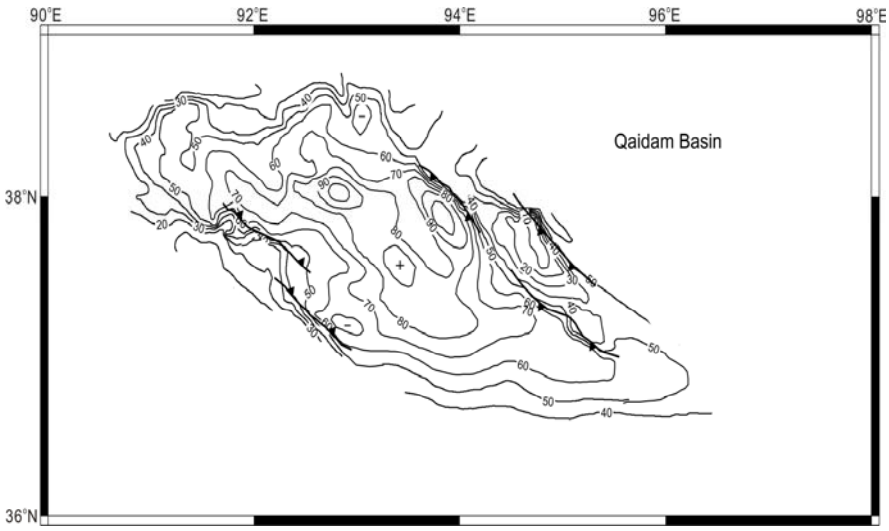

Figure 29. Predicted Bouguer gravity with sediment correction in the Qaidam Basin in mgal at 10 mgal intervals.

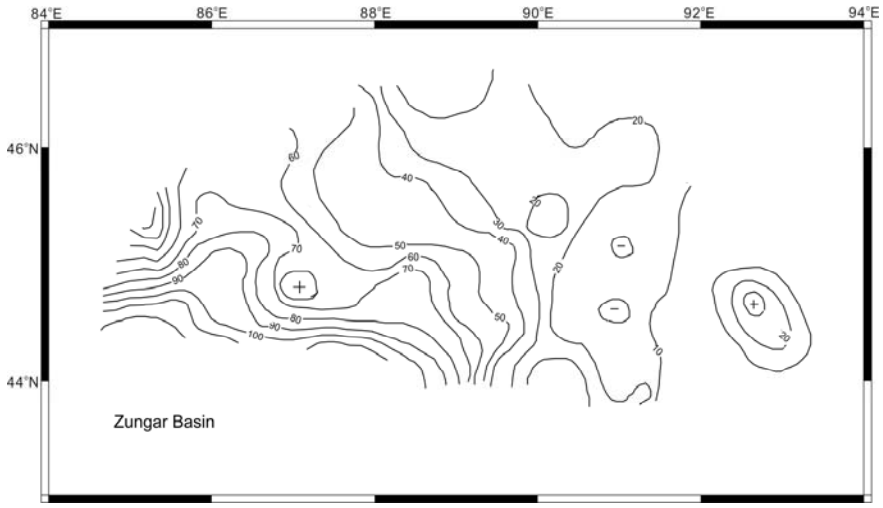

Figure 30 Predicted Bouguer gravity with sediment correction in the Zungar Basin in mgal at 10 mgal intervals.

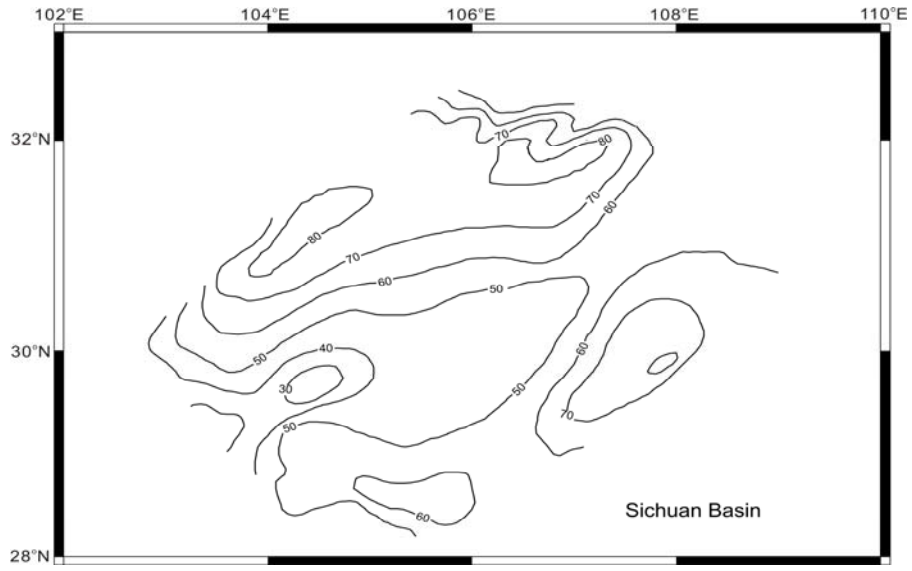

Figure 31. Predicted Bouguer gravity with sediment correction in the Sichuan Basin in mgal at 10 mgal intervals.

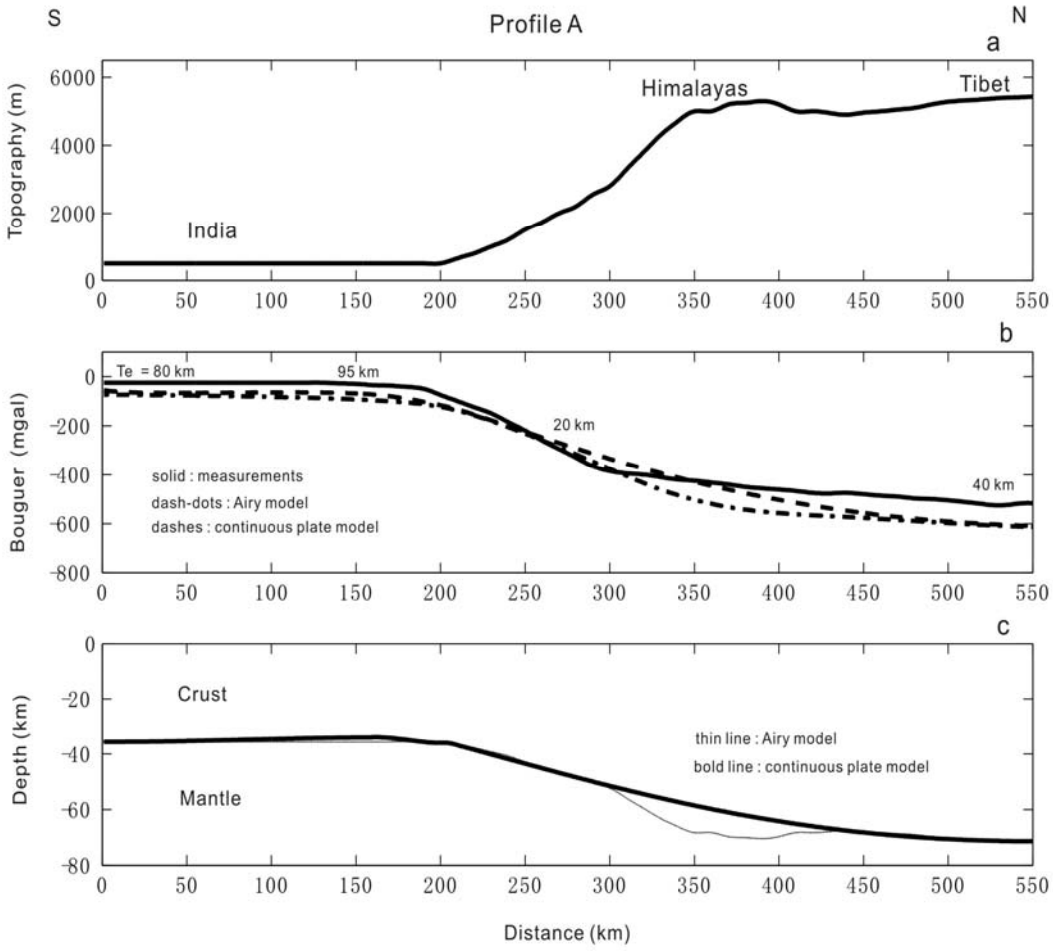

Figure 32. Gravity modelling along profile A (see Fig. 23 for location). (a) Topography. (b) Observed Bouguer gravity anomalies, gravity predicted using the Airy assumption, and predicted gravity for a continuous variable-rigidity plate model. *T*e is the elastic thickness of the plate. (c) Depth model showing deflection of the Moho from the Airy and continuous plate models.

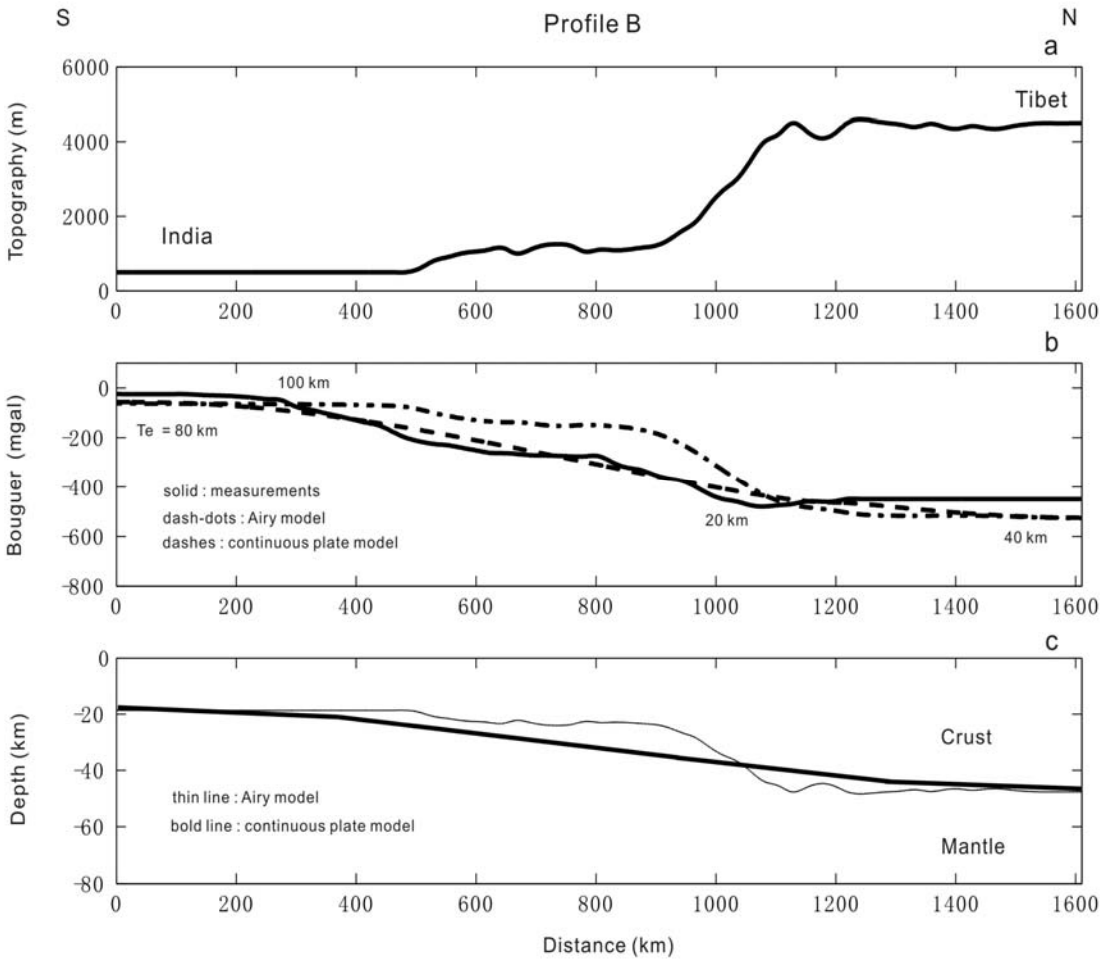

Figure 33 Gravity modelling along profile B (see Fig. 23 for location). (a) Topography. (b) Observed Bouguer gravity anomalies, gravity predicted using the Airy assumption, and predicted gravity for a continuous plate model. *Te* is the elastic thickness of the plate. (c) Depth model showing deflection of the Moho from the Airy and continuous plate models.

5.2 Lithospheric deformations beneath the Altyn Tagh and West Kunlun faults from new gravity survey data

Uplift of the Tibetan Plateau is due to the collision of the Indian plate with Eurasia beginning at about 50 Ma (*Boulin*, 1981; *Royden and Burchfiel*, 1995; *Kind et al.,* 2002; *Sinha-Roy*, 1982; *Tapponnier et al.,* 2001). Some of the north-south shortening in Central Asia in response to this collision was accommodated when the flexural foredeep of the West Kunlun developed along the southern edge of the Tarim Basin. East of the Kunlun foredeep is a spectacular left-lateral strike-slip fault, the Altyn Tagh Fault (Fig. 15), with an east-west extent of at least 1600 km along the northern edge of the Tibetan Plateau. Here, an attempt is made to place some constraints on the deep structure of this fault along the northern edge of Tibet using the 2D flexural model [formula (22)] of Chapter 3.

Our 2D flexural modelling results are presented starting from the western profile across the West Kunlun Fault to the two eastern profiles across the Altyn Tagh Fault.

We used the 468 new gravity and elevation stations along three survey lines in our model (Fig. 34). The data points were projected onto straight profiles trending roughly perpendicular to the trace of the Altyn Tagh and the West Kunlun faults. In addition, the western and central profiles were extended to cover both the highland and the lowland using digitized regional gravity data (black dots in Fig. 34). Digitized data, including those from a 1:2,500,000 regional gravity map, are added at the ends of our modelling profiles. Data coverage in the extended areas (especially in the Tarim Basin) was sufficient for this purpose, and our new surveys provided an important data source to fill the rough terrain gap between the basin and the highland of Tibet.

The surface load was assigned a density of 2670 kg/m^3 in the mountain areas, while a value of 2450 kg/m^3 was used for the Tarim and Qaidam basins. The latter value is derived from a density log located at 87°20 'E and 40°05 'N (red dot in the Tarim Basin in Fig. 34). Publication of this well log (Fig. 35) is made possible by an agreement between the Ocean University of China and the Shenli Oil Complex. The gravity contributions of the sediments in the Tarim and Qaidam basins have to be taken into account because they reach 100 mgal according to our estimates. The basement depths are taken from the contour maps of *Huang* (1996). The density log shows a density break at about 1105 m well depth. Above the break, the average density is about 2350 kg/m^3, and below the break, it is around 2500 kg/m^3. Because the sedimentary thickness is generally greater than 5 km, an average density of 2450 kg/m^3 was used in our modelling.

The Yecheng-Songxi profile across the Western Kunlun Fault

For the profile across the West Kunlun fault zone, a continuous plate with a varying rigidity can explain the observed gravity in the southern part of the profile only up to x = 270 km (Fig. 36). The Airy model fails to account for the observations in the transition zone from lowland to highland (dotted line in Fig. 36b), and neither model can explain the large gravity low from about x = 270 km to x = 450 km (Fig. 36b). It is unlikely that any mechanical model can reproduce this gravity depression without introducing lateral density variations or non-isostatic (*e.g.*, dynamic) mechanisms.

Lateral variations in density are indeed likely in this region. In response to the convergence between India and Eurasia, a foreland basin was formed in front of the West Kunlun Ranges. A basement structural map of the Tarim Basin based on exploration seismic data (*Teng et al.*, 1991) suggests that the foredeep sediments of the West Kunlun Mountains are over 12 km in thickness between 76º-80º E, and our western transect crosses the thickest part of the foredeep (Fig. 34). Fig. 36c shows the best-fit gravity model after introducing a foredeep basin with a density of 2450 kg/m^3. The crosses in Fig. 37c give basement depths (or sediment thicknesses) digitized from *Li* (2002). We smoothed these basement depths from x = 450 km to about x = 250 km, and recalculated the flexure that would result if the uppermost load on the plate consists of lower-density sediments. The model of a rigid plate with a Moho flexure and covered by lower-density sediments fits the observed gravity well (Fig. 37b). In general, for the western Kunlun transect, a continuous plate stronger in the north and weaker in the south fits the observed Bouguer gravity anomalies well except for some short wavelength anomalies. This proposed weakening of the Tarim block beneath the West Kunlun Ranges could be the consequence of stripping of the top of the Tarim crust as it is being underthrusted. Note that the inferred depth of the Moho based on flexure and gravity modelling also suggests that the Tarim crust is thinned as it approaches the thrust (Fig. 37c).

The Qiemo-Tula profile across the Altyn Tagh Fault

The fundamental difference between the western and this central transect is that the Airy model provides a superior fit to the data beneath the mountain belt south of x = 250 km as compared with the predictions of a continuous elastic plate model with significant rigidity (Fig. 38b). However, the existence of a weak plate (Airy isostasy) along the entire profile seems unlikely. From our modelling along the western transect and from other

studies (*Lyon-Caen and Molnar*, 1984; *Jin* 1994 *and* 1996; *Tapponnier et al*., 2001), the elastic thickness of the plates beneath Tibet and the Tarim Basin is 30 to 40 km. Furthermore, the small gravity low at about x = 270 km (Fig. 38b) suggests a small foredeep due to elastic loading of the highland between the Altyn Tagh Fault and the Tarim Basin. In general, foredeep basins along the Altyn Tagh Fault are not well developed (generally less than 5 km thick) due to the strike-slip nature of the fault (*Teng et al*., 1991). Therefore, we examined whether an elastic plate model that was weak only locally on account of the Altyn Tagh Fault penetrating the lithosphere could fit the data as well or better than Airy isostasy. Fig. 38b shows that the southern part of the Qiemo-Tula gravity profile can be well modelled if we assume flexure of a severed elastic plate (*i.e*., two independent plates) with their boundary located at the Altyn Tagh Fault. Fig. 39 shows an improved gravity fit for the northern portion of the same profile after the loading effect of the Tarim sediments on the northern subplate is account for. The density and depth constraints of the basin were derived in a manner similar to the approach taken for the western transect.

The Alagan-Mangya profile across the Altyn Tagh Fault

Both the Qaidam and Tarim basins contribute large sediment effects along the easternmost profile (Figs. 24 and 25). As is the case for the central profile, the Airy and severed plate models match the observed gravity better than the continuous plate model in the transition zone from lowland to highland. However, the predicted gravity from Airy isostasy is about 100 mgal above the observed Bouguer anomalies in both the Tarim and Qaidam basins (Fig. 40b), implying that the lithosphere is over-compensated. To create over-compensation by pulling the lithosphere downward, we need to assume either significant downwelling in the mantle or a large bending moment. There are no plausible geological or geophysical arguments to support either assumption, nor is it necessarily required by flexural modelling.

As with the modelling of the western and central profiles, the more plausible explanation for the apparent over-compensation is the effect of the basinal sediments. Multi-channel seismic profiling imaged thick sediments in the Qaidam Basin even though the foredeep basin on the Tarim side is not well developed (*Teng et al*., 1991). Fig. 41c shows that the digitized sediments thickness in both the Qaidam and Tarim basins can exceed 10 km along this profile. Data on this sediment thickness are, however, limited (crosses), although they include the areas of greatest gravity data misfit. Exactly how

sediment thickness is interpolated into the regions of poor coverage (solid lines in Fig. 41c) has negligible impact on the fit of the final models, as long as we assume that the sediments in the overthrust area are thin.

Analogous to the Qiemo-Tula profile, we fitted preferably the data with a severed plate model with the line of severance along the Altyn Tagh Fault. Fig. 41b shows our best-fit gravity derived from Moho flexure of the severed plate model and the effect of sediments.

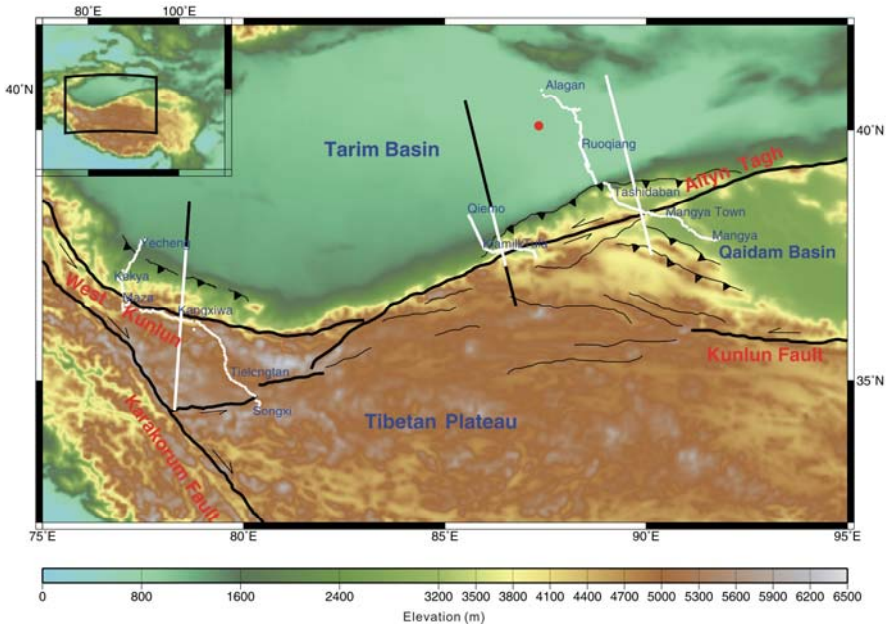

Figure 34. Gravity surveys conducted in 1997 and 1998. The location of the gravity stations across the Altyn Tagh and the West Kunlun are shown as white dots. The lines perpendicular to the trend of the Altyn Tagh and the West Kunlun are projections of the survey lines. The black dots at the ends of the white straight lines are additional data points complied from available gravity maps. The red dot gives the well location for the density log of Fig. 35.

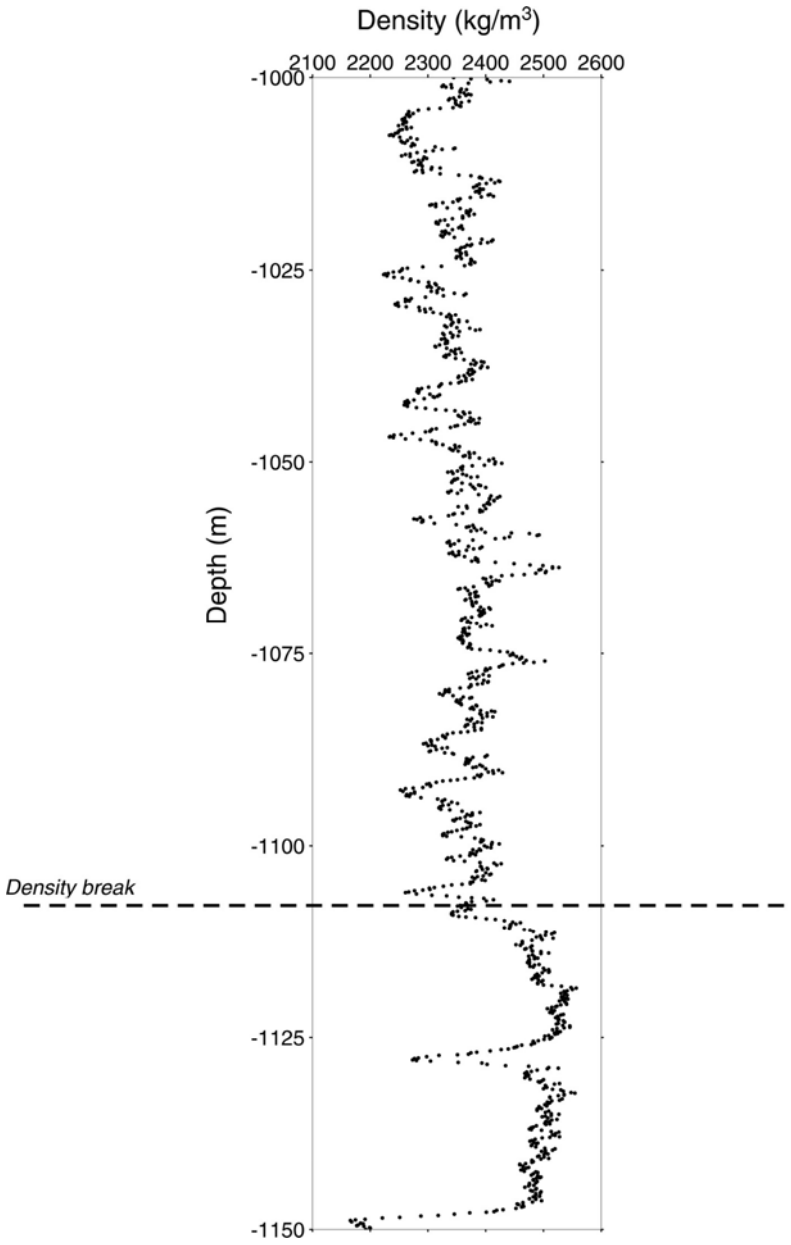

Figure 35. Density log from the well in the Tarim Basin. See red dot in Fig. 34 for location.

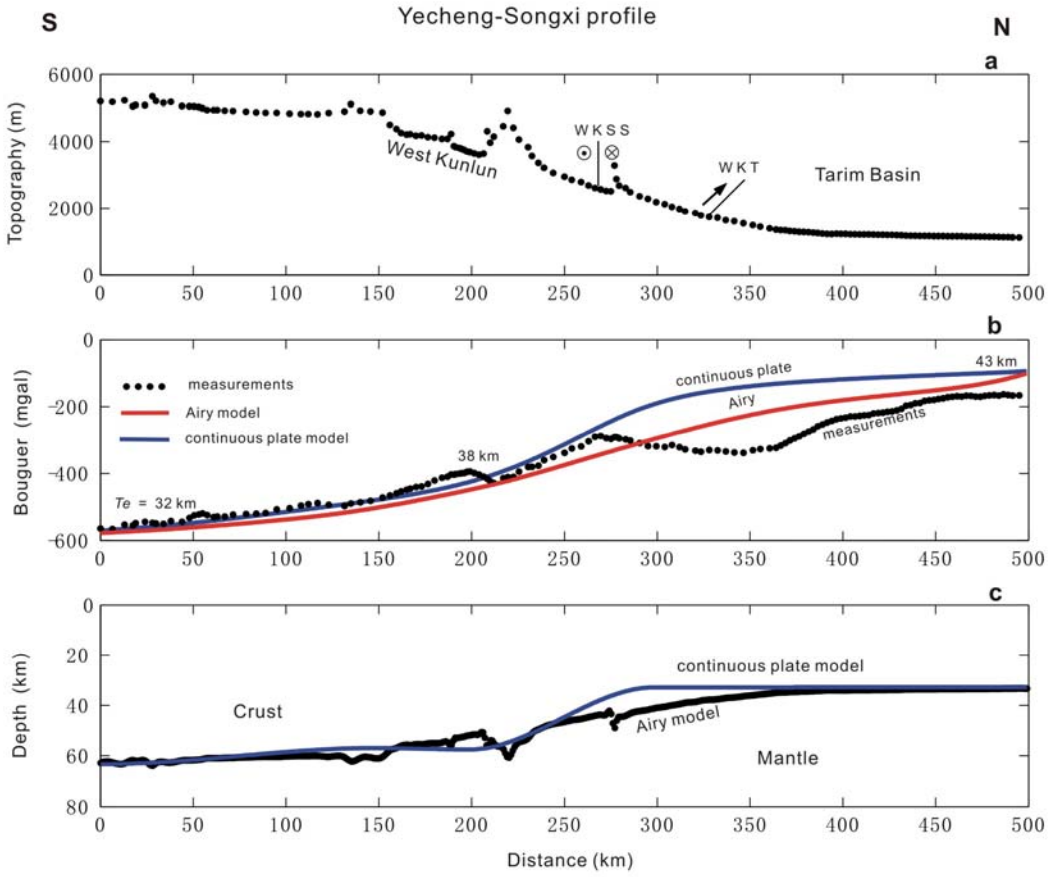

Figure 36. Gravity modelling along the Yecheng-Songxi profile (the western transect). (a) Topography. WKSS: West Kunlun strike-slip, WKT: West Kunlun Thrust. (b) Observed Bouguer gravity anomalies (black dotted), predicted gravity using the Airy assumption (red), and predicted gravity for a continuous plate model (blue). *Te* is the elastic thickness of the plate. (c) Depth model showing the location of the Moho from the Airy and continuous plate models.

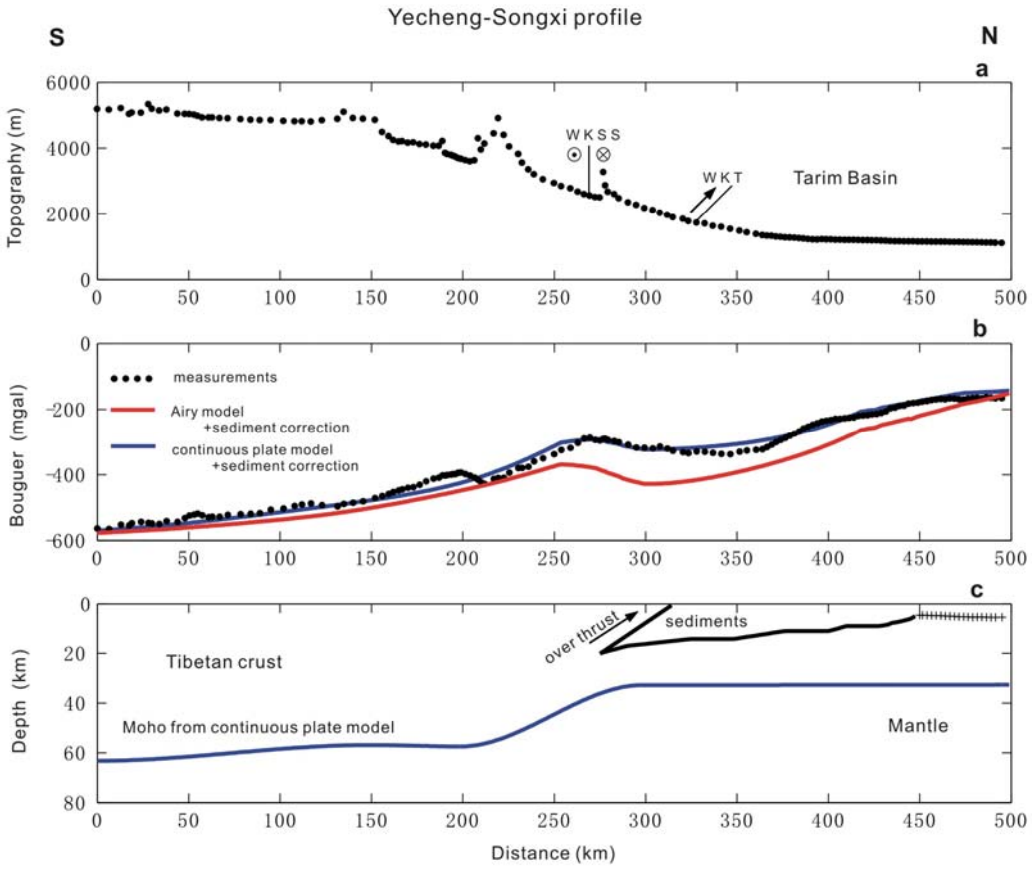

Figure 37. Gravity modelling along the Yecheng-Songxi profile as in Fig. 36, but with sediment corrections. The basement depths (crosses in panel **c**) used to deduce the sediment thickness are digitized from *Li* (2002). Solid lines in panel **c** are predicted basement depths. In accordance with the density log of Fig. 35, the average sediment density is chosen to be 2450 kg/m^3. Arrows in panels **a** and **c** denote overthrusting. WKSS: West Kunlun strike-slip, WKT: West Kunlun Thrust.

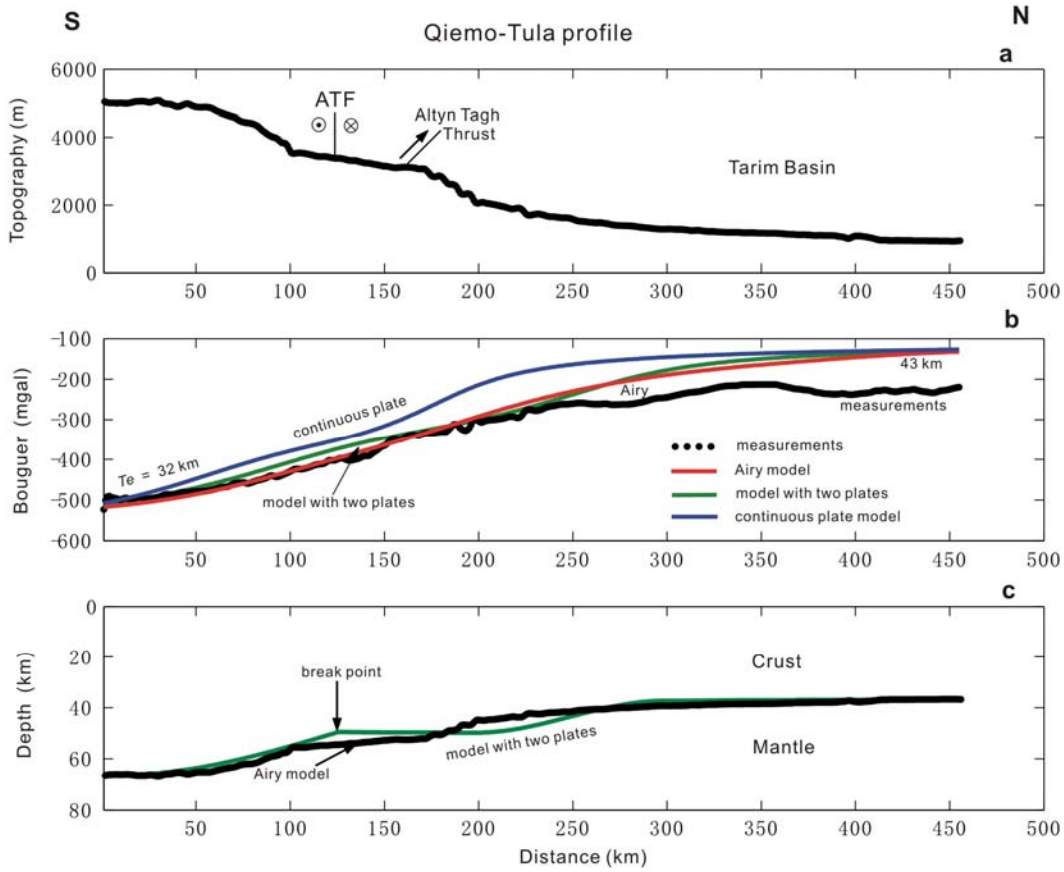

Figure 38. Gravity modelling along the Qiemo-Tula profile (the central transect). (a) Topography. ATF denotes Altyn Tagh strike-slip Fault. (b) Observed Bouguer gravity anomalies (black dotted) and predicted gravity of several plate models: Airy (red), continuous plate model (blue), and the model with two plates (green). *Te* is the elastic thickness of the plate. (c) Depth model showing the deflection of the Moho from the Airy (black dotted) and the model with two plates (green). The point where the two parts of the severed plate (or the two plates) meet is marked by the Altyn Tagh Fault.

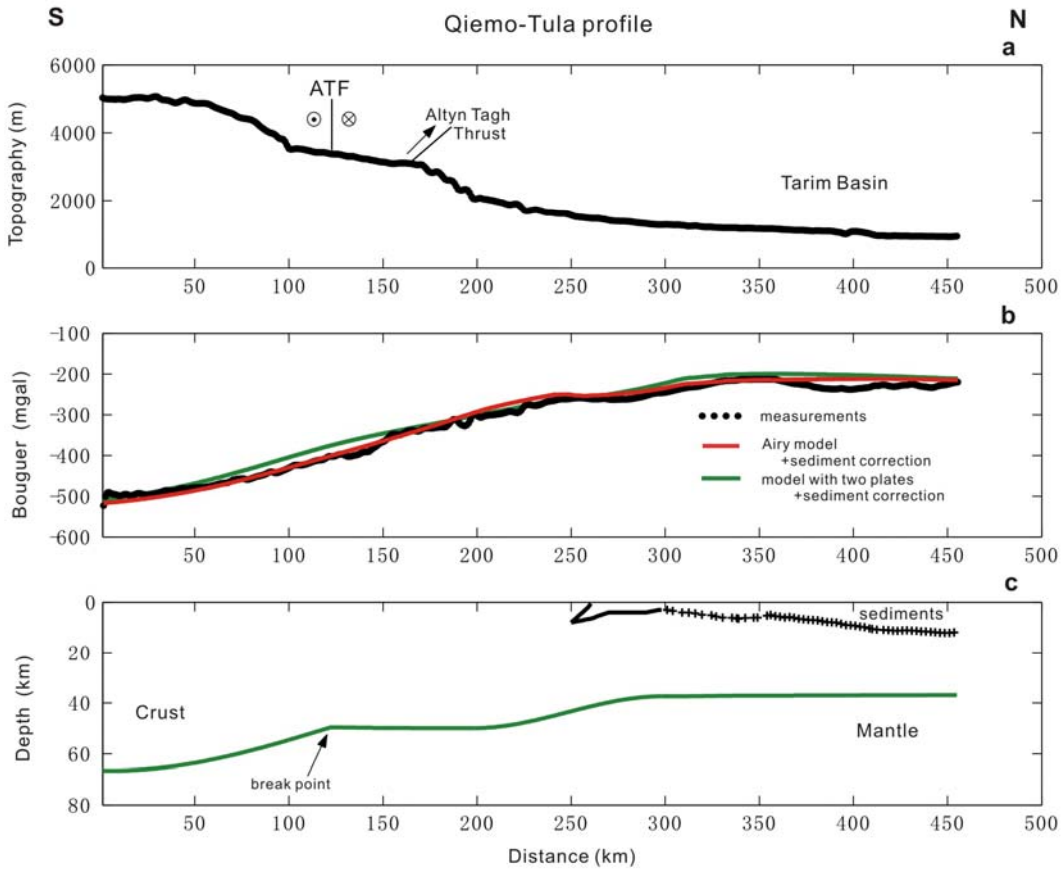

Figure 39. Gravity modelling along the Qiemo-Tula profile as in Fig. 38, but with sediment corrections. The basement depths (crosses in panel **c**) used to deduce the sediment thickness are digitized from *Huang* (1996). Dots are predicted basement depths. Based on the density log in Fig. 35, the average sediment density is chosen to be 2450 kg/m^3. ATF denotes Altyn Tagh strike-slip Fault.

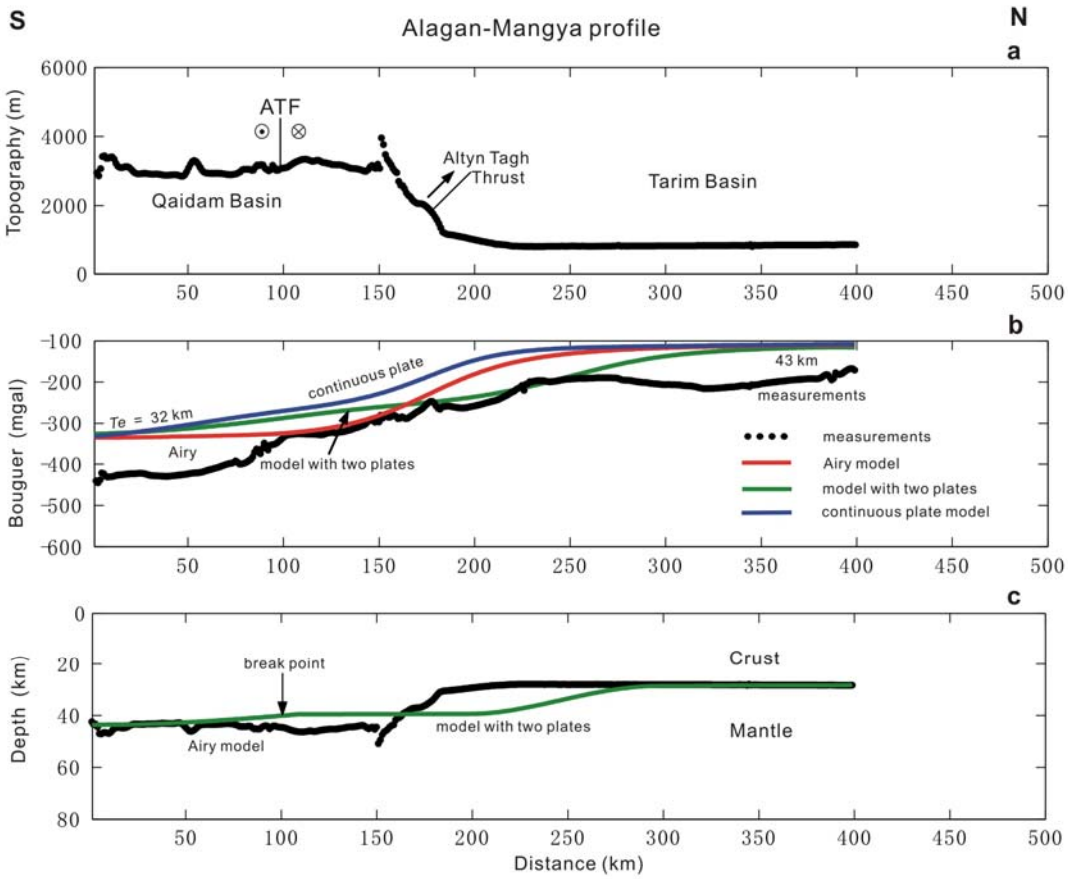

Figure 40. Gravity modelling along the Alagan-Mangya profile (the eastern transect). (a) Topography. ATF denotes Altyn Tagh strike-slip Fault. (b) Observed Bouguer gravity anomalies (black dotted) and predicted gravity from three models: Airy (red), continuous plate (blue) and the model with two plates (green). *Te* is the elastic thickness of the plate. (c) Depth model showing the deflection of the Moho from the Airy (red) and the model with two plates (green). The point where the two parts of the severed plate meet is marked by the Altyn Tagh Fault.

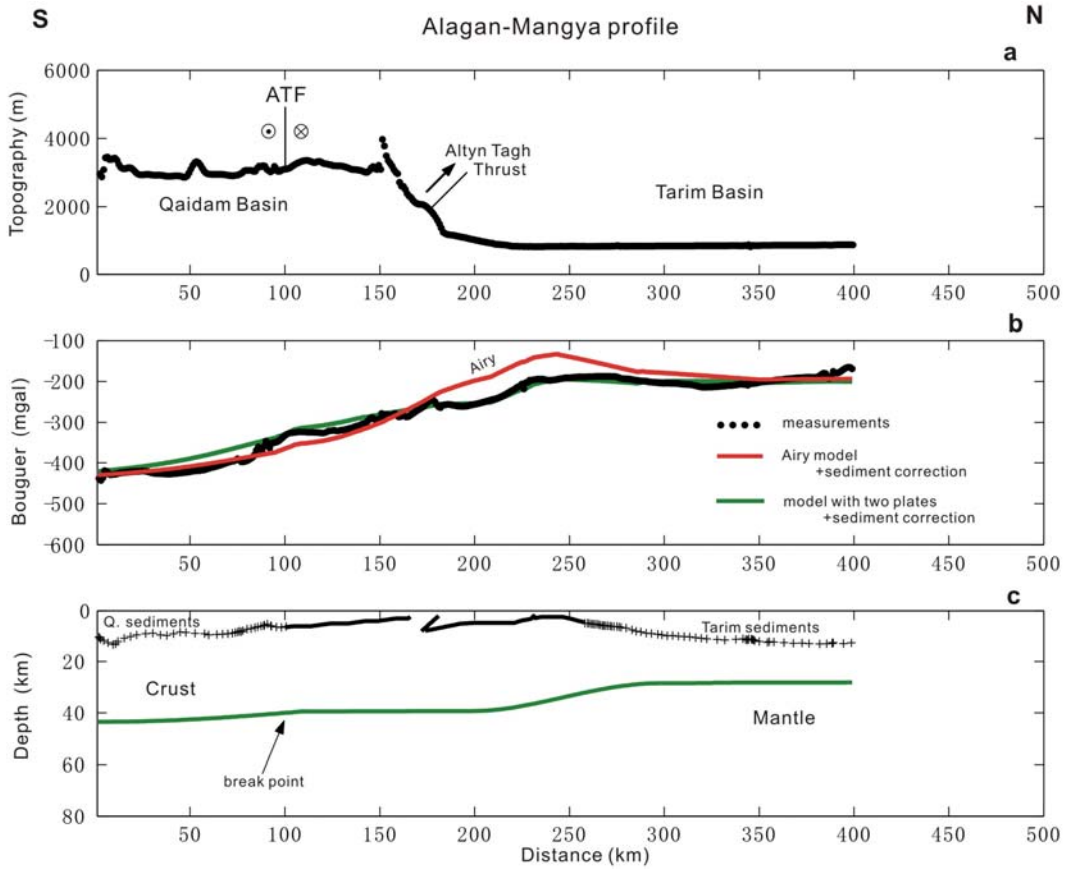

Figure 41. Gravity modelling along the Alagan-Mangya profile as in Fig. 40, but with sediment corrections. The basement depths (crosses in panel **c**) used to deduce the sediment thickness are digitized from *Huang* (1996) and *Li* (2002). Based on the density log of Fig. 35, the average sediment density is chosen to be 2450 kg/m^3. ATF denotes Altyn Tagh strike-slip Fault. Q. sediments denotes Qaidam sediments.

5.3 Lithospheric deformations in the Tien Shan

Many aspects of intra-continental deformations are still an enigma. This is true also of the Tien Shan in central Asia. It is one of the young and very active intra-continental ranges in the world and is bounded by the Kazakh Platform to the northwest, the Zungar Basin to the northeast and the Tarim Basin to the south (Fig. 42). Though over 1500 km north of the Indian-Eurasian collision zone, the Tien Shan presently absorbs about 30% of the total relative plate convergence of 45 mm/yr (*Abdrakhmatov et al.,* 1996*; DeMets et al.,* 1994*; Holt et al.,* 2000). Global Positioning System (GPS) measurements indicate that the 12–13 mm/yr north-south shortening is broadly distributed across the northern two thirds of the central Tien Shan (*Abdrakhmatov et al.,* 1996). Thus, the Tien Shan is an excellent location to study localized deformations in an intra-continental setting. Various aspects of active tectonics in the Tien Shan, including timing of the uplift, rates of slip on thrust systems that bound the margins, and Quaternary shortening in the interior of the fold belt have been investigated in detail (*Avouac et al.,* 1993; *Brown et al.,* 1998; *Burchfiel et al.,* 1999; *England and Molnar,* 1997; *Sun et al.,* 2004; *Thompson et al.,* 2002; *Yin et al.,* 1998). Lithospheric folding with wavelengths of 50 and 300-360 km has been reported using thin elastic plate modelling of gravity data (*Burov et al.,*1990; 1993), and dynamic processes are found to occur both in the crust and the mantle lithosphere beneath mountain ranges (*Kogan and McNutt* 1993; *Lyon-Caen and Molnar,* 1983). Here, we modelled lateral heterogeneities in high-resolution Bouguer gravity and topographic data to elucidate the dynamic processes in the crust and mantle responsible for them.

Areas adjacent to the Tien Shan, namely the Kazakh Platform and the Tarim and Zungar basins, are stable Precambrian structures that have suffered little deformation during the Cenozoic convergence of India and Asia (*Carroll et al.,* 1995; *Yin and Nie,* 1996). The Tien Shan itself consists mainly of a Lower Proterozoic gneissic basement (*Bukharin,* 1978). Its marine basins were closed in the Early Permian and the fold belt itself developed during the middle Permian as a consequence of final collision and suturing of the Tarim continent with the Kazakh continent (*Hendrix et al.,* 1994). The change from marine to continental sedimentation and the marked angular unconformity separating the Paleogene and Neogene strata (*Zhang*, 2003) are consistent with Cenozoic tectonic reactivation in the Tien Shan in response to the Indian-Asian collision (e.g. *Chen et al.,* 1999; *Me' tivier and Gaudemer*, 1998; *Sobel and Dumitru*, 1997). Recent tectonics in the Tien Shan appears to be dominated by thrusting on roughly E-W striking faults and by folding of Cenozoic

sediments (*Molnar and Tapponnier,* 1975; *Tapponnier and Molnar,* 1979; *Molnar et al.,* 1994; *Thompson et al.,* 2002). The maximum crustal thickness in the Tien Shan reaches 50 km and is larger than that of its adjacent areas (*Burbank et al.,* 1999; *Molnar and Tapponnier,* 1975). It is not clear whether the surface thrust faults here are related to the structure of the lithospheric mantle in any simple way since deformational properties of continental rocks are heterogeneous and the crustal thickness is extremely large. Therefore, we analysed geophysical data to better understand plate interactions at depth.

We begin by quantifying lateral heterogeneities of the deep structure using high-resolution Bouguer gravity and topographic data in order to elucidate the dynamic processes in the crust and mantle responsible for these lateral heterogeneities. Then we shall calculate the lithospheric stress to better understand the Tien Shan local stress field. At a late stage, we hope to better understand the dynamic processes responsible for intra-continental mountain building in general.

The locations of the four transects used in our two dimensional modelling are shown in Figs. 42 is numbered 1 to 4 from east to west across the Tien Shan.

The sediment layers imaged seismically in the foreland basins of the Tarim and Zungar basins along the four lines modelled two-dimensionally are shown in Fig. 43 (dotted lines in the lower panels of Fig. 43). These layers were extended from x = 440 to about 500 km on profile 1 (wedge marked by straight solid lines), from x = 490 to about 540 km on profile 2, and from x = 90 to about 190 km on profile 3 in a smooth fashion to simulate underthrusting. Figure 43 shows the calculated gravity effects for a sediment density of 2450 kg/m^3 along the four profiles. They amount to over 100 mgal, in agreement with *Braitenberg et al.* (2003) and our 3D results of section 5.1.

Our modelling suggests that there are large discrepancies between the calculated Bouguer anomalies of the Airy model and the observed data along each of the four profiles (see panel **b** of Figs. 44-46 and 48). This model, for which topographic relief is pointwise compensated by crustal thickening at the Moho, produces a theoretical Bouguer gravity anomaly that resembles an inverted, low-pass filtered version of the topography. The predicted gravity at the edge of the Tien Shan, and in the northern Tarim Basin (western profiles) and southern Zungar Basin (eastern profiles) are much greater than what is observed.

Regional compensation occurs by elastic lithospheric flexure, whereby the lithosphere is deflected by topographic and subsurface loads. The relationship between topography and gravity anomalies due to the compensating mass at depth provides an estimate of the flexural strength of the elastic lithosphere using our thin plate model in the space domain.

Figure 44 examines the fit to the gravity data along profile 1 for several models: Airy isostasy (T_e = 0 km), a continuous elastic plate with uniform rigidity (T_e = 40 km) and variable rigidity respectively, and a model of two separate plates. The constant rigidity model fails to explain the observations in the transition zone from low basins to high mountains. Assuming that the plate is broken at the Southern Tien Shan Thrust Fault results in a worse fit. The successful model consists of a continuous plate with an elastic thickness of 40 km in the Tarim Basin, decreasing to 25 km beneath the Tien Shan and increasing to 45 km in the Zungar Basin. The model with Moho flexure of a rigid plate, which is slightly stronger in the basins than in the ranges, fits the observed gravity well except for some short wavelength anomalies. Its RMS residual is 6.8 mgal. The lithosphere is weakened by about 10 km in elastic thickness, which is consistent with the missing crust of the thrusting lithosphere of the Tarim and Zungar basins.

Modelling along profile 2 provides results similar to those along profile 1. A continuous plate with a laterally varying elastic thickness (T_e = 45 km in the Tarim Basin, decreasing to 25 km beneath the Tien Shan and increasing to 45 km in the Zungar Basin) is required for a best fit of the observed Bouguer gravity (blue line in Fig. 45b). Its RMS residual is 7.5 mgal. The Airy and the uniform rigidity (T_e = 40 km) elastic plate models fail to fit the observed gravity (red and orange lines of Fig. 45b). Analogously, assuming that the plate is broken at the Southern Tien Shan Thrust Fault produces a worse fit (green line). Because a break point is not required along the two eastern profiles, the mantle lithosphere and the lowermost crust of the Tarim and Zungar basins here could be the same as the lithosphere beneath the Tien Shan ranges.

There are fundamental differences between the two eastern profiles and the western transect 3. As shown in Fig. 46, several models fail to explain the observed gravity. These are: Airy isostasy (red line, T_e = 0 km), uniform rigidity plate model (orange line, T_e = 40 km), and two variable-rigidity continuous elastic plate models, one having an elastic thickness of 40 km both in the Tarim and Zungar basins, decreasing to 25 km beneath the Tien Shan (light blue line) and the other with an elastic thickness of 40 km in the Tarim Basin, decreasing to 20 km beneath the Tien Shan and increasing to 45 in the Zungar Basin

(blue line). The RMS residual of the best-fit continuous plate model (blue line) is 22.1 mgal. We also examined the model of two independent elastic plates with their ends meeting at the Southern Tien Shan Thrust Fault. The best-fit model of two separated plates has T_e = 40 km at the southernmost Tarim plate, decreasing to 23 km at its northern end where it is subjected to a bending moment 0.5×10^{17} N, and T_e = 48 km at the northernmost Kazakh plate, decreasing to 25 km at the southern end where the bending moment is 0.2×10^{17} N (Fig. 47). The latter bending moment could be produced by about 20-40 MPa of shear stress on the fault surface between the underthrusting Tarim and the overriding Kazakh plates. The RMS residual of this model is 10.9 mgal and is smaller than any continuous model. It is clear that the model with a plate broken along the Southern Tien Shan Thrust Fault (green line in Fig. 47) is superior to the Airy isostasy (red line in Fig. 46) as well as the continuous plate models (light blue and blue lines in Fig. 46).

Analogous to profile 3, profiles 4 crossing the western Tien Shan is also characterized by obvious discrepancies between measurements and the predictions of either Airy isostasy (red line in Fig. 48, *Te* = 0 km), a uniform rigidity continuous plate (orange line in Fig. 48, T_e = 40 km), or two variable-rigidity continuous elastic plate models, one having an elastic thickness of 40 km both in the Tarim and Zungar basins, decreasing to 25 km beneath the Tien Shan (light blue line in Fig. 48) and the other with an elastic thickness of 40 km in the Tarim Basin, decreasing to 20 km beneath the Tien Shan and then increasing to 45 in the Zungar Basin (blue line in Fig. 48). The RMS residual of the best-fit continuous plate model (blue line in Fig. 48) is 12.3 mgal. As with profile 3, a better fit is provided by the model with two separated plates having T_e = 40 km at the southernmost Tarim plate, decreasing to 20 km at the northern end where it is subjected to a bending moment of 0.5×10^{17} N, and T_e = 48 km at the northernmost Kazakh plate, decreasing to 23 km at the southern end where the bending moment is 0.2×10^{17} N (Fig. 49). The corresponding RMS residual improved to 8.1 mgal.

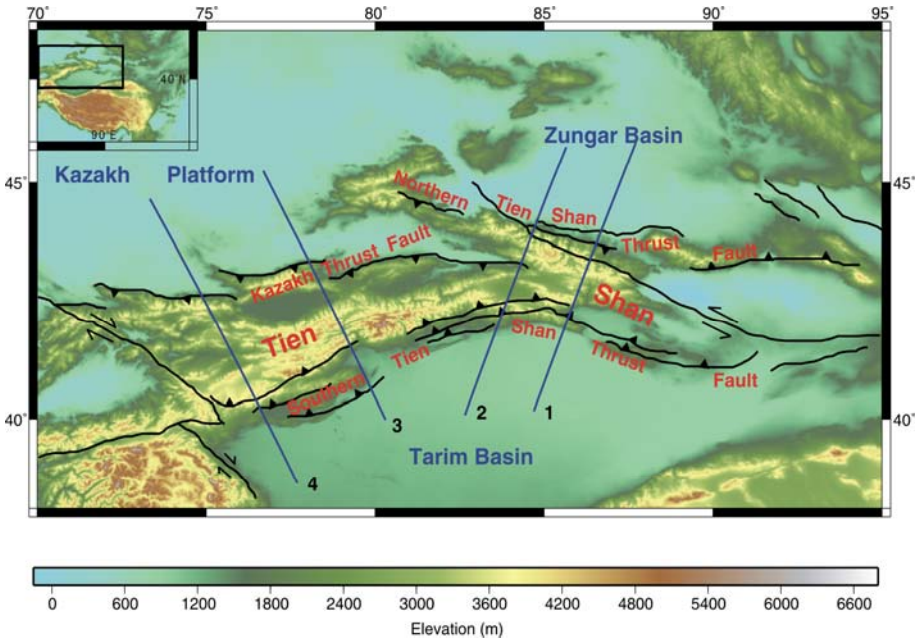

Figure 42. Topography of the Tien Shan area from TOPO30. Numbered lines are the locations of profiles modelled in this paper. Thick solid lines are major faults in the study area (*Ren et al.,* 1999).

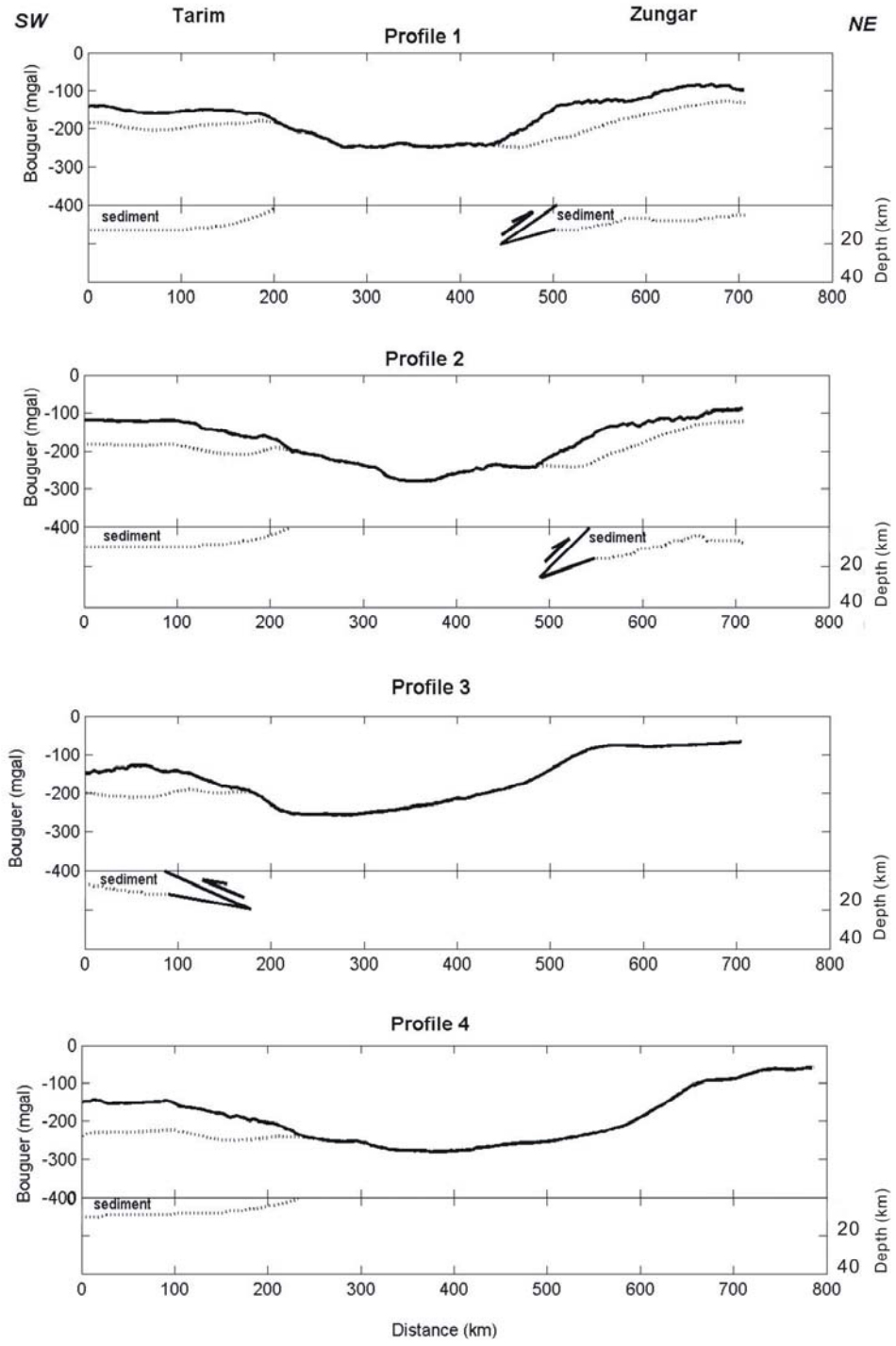

Figure 43. Observed, sediment-corrected Bouguer gravity anomalies along four 2D transects (solid lines in upper panels). Dots are uncorrected original data. The basement depths used for the sediment corrections (dots in lower panels) are digitized from *Li* (2002). The solid lines in the lower panels give predicted basement depths. The average sediment density is assumed to be 2450 kg/m^3 based on density logs of drill holes (see section 5.2).

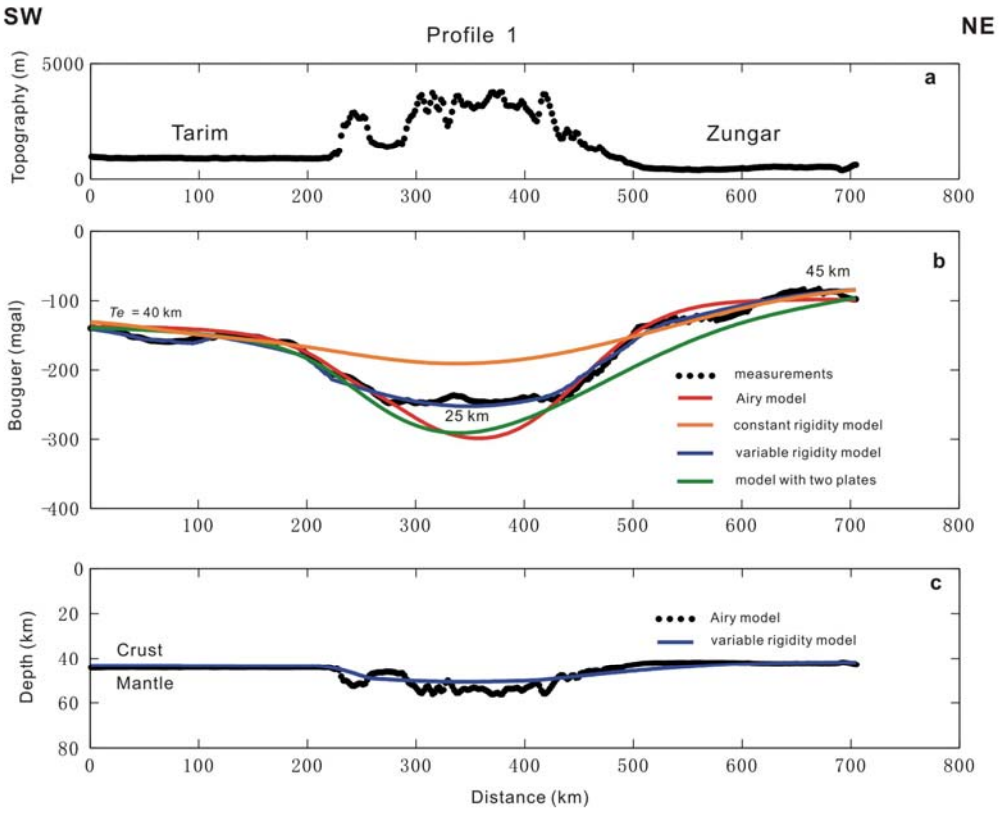

Figure 44. Gravity modelling along profile 1. (a) Topography. (b) Observed Bouguer gravity anomalies (black dotted), and predicted gravity for several models: Airy isostasy (red), continuous plate with a constant rigidity (elastic thickness of the plate T_e = 40 km, orange), continuous elastic plate with a varying rigidity (blue, T_e = 40 km in the Tarim Basin, decreasing to 25 km beneath the Tien Shan and increasing to 45 km in the Zungar Basin), and model with two separated plates (green, same parameters as the varying rigidity plate model with a bending moment of 0.2×10^{17} N applied to the ends of the plates). (c) Depth distribution of the Moho showing its deflection according to the Airy model (black dotted) and the model of a continuous elastic plate with varying rigidity (blue). The densities of the crust and mantle are taken as 2670 and 3300 kg/m^3, respectively.

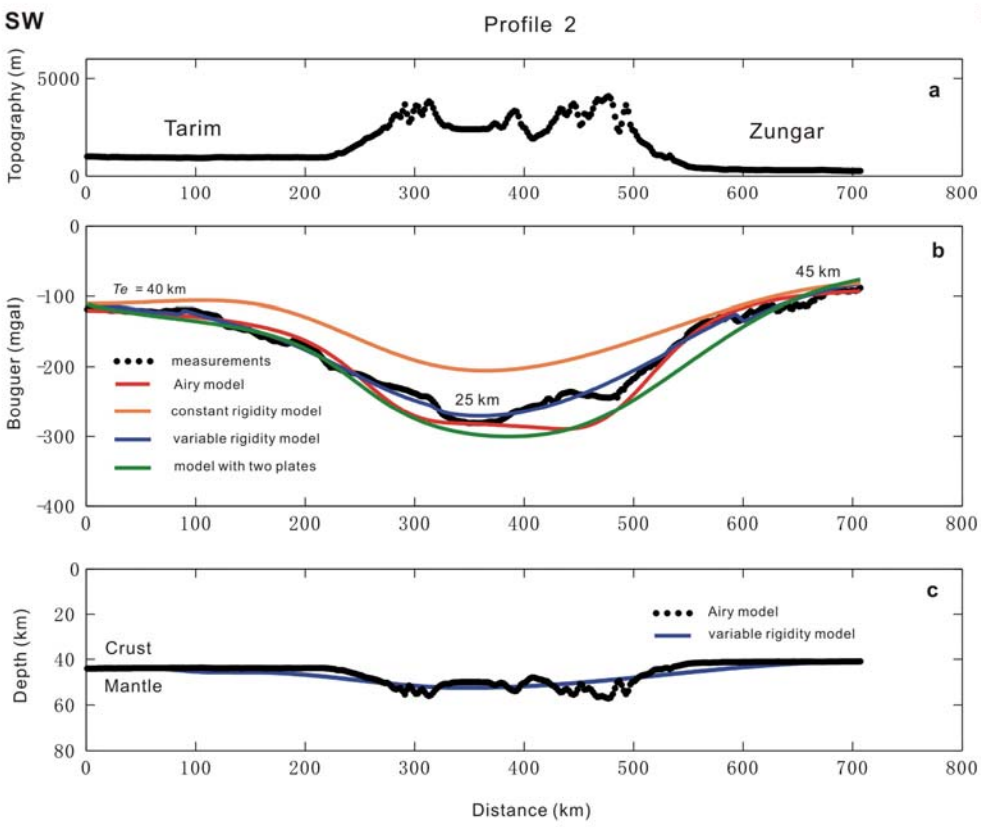

Figure 45. Gravity modelling along profile 2. Symbols same as in Fig. 44. The parameters of the continuous elastic plate model with varying rigidity are: T_e = 45 km in the Tarim Basin, decreasing to 25 km beneath the Tien Shan and increasing to 45 km in the Zungar Basin.

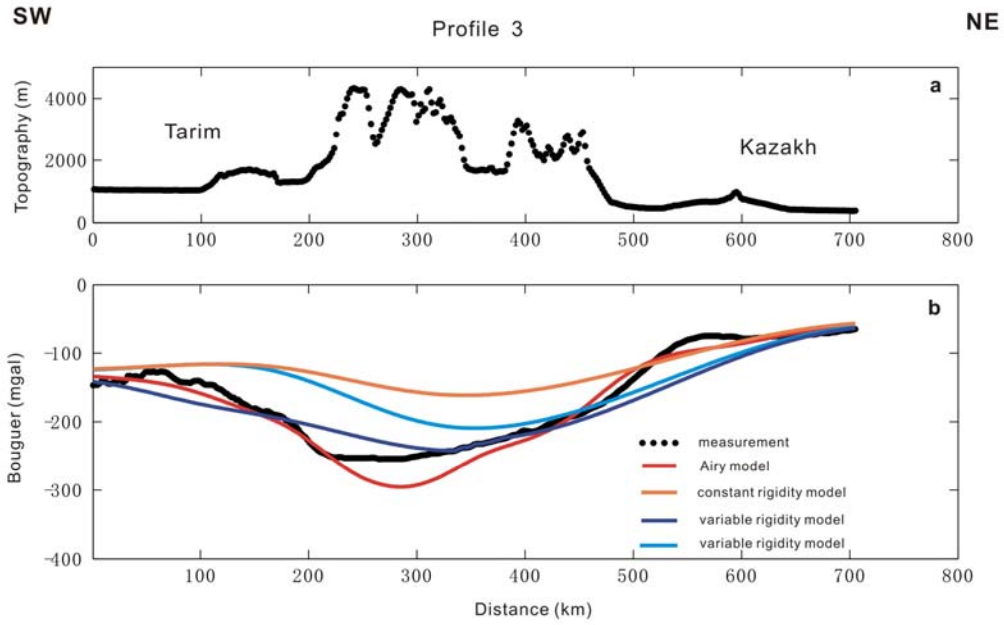

Figure 46. The fit of several continuous plate models to the observed Bouguer gravity data along profile 3. (a) Topography. (b) Observed Bouguer gravity anomalies (black dotted) and predicted gravity of the following models: Airy isostasy (red); constant rigidity elastic plate model with T_e = 40 km (orange); and two variable-rigidity continuous elastic plate models, one with T_e = 40 km in both the Tarim and Zungar basins and T_e = 25 km beneath the Tien Shan (light blue) and the other with T_e = 40 km in the Tarim Basin, decreasing to 20 km beneath the Tien Shan and increasing to 45 km in the Zungar Basin (blue).

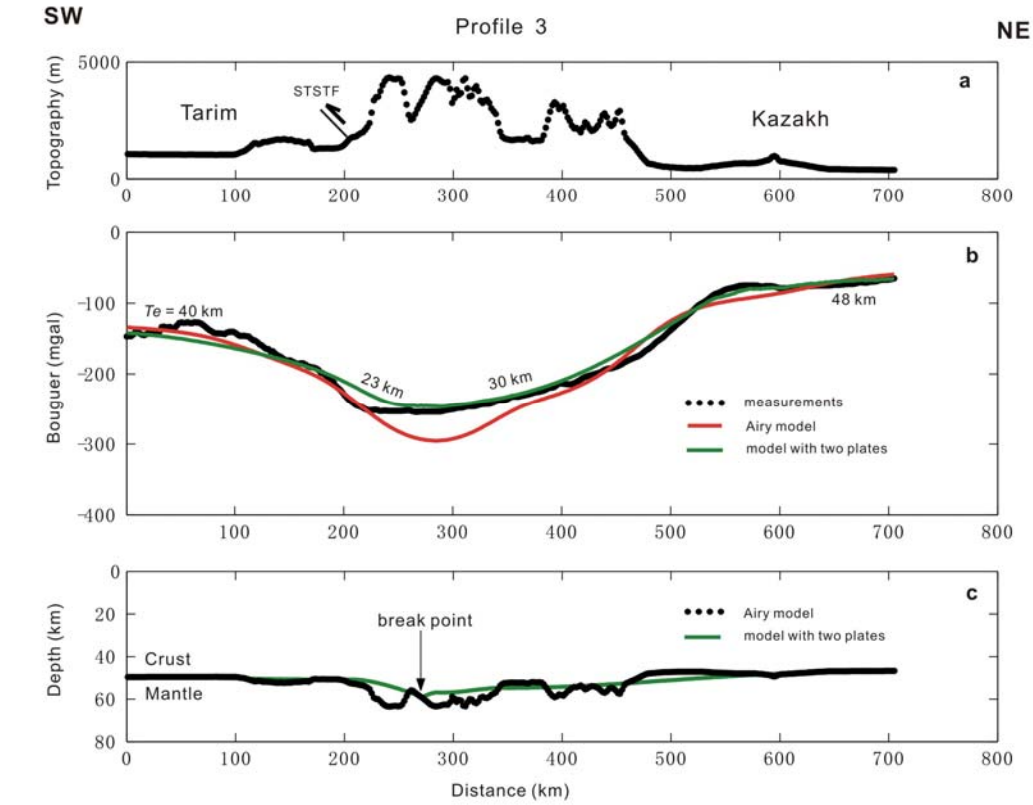

Figure 47. Gravity modelling along profile 3. (a) Topography. (b) Observed Bouguer gravity anomalies (black dotted), predicted gravity for a model with two separated plates with the break point at about x = 270 km (green). The Tarim plate has an initial elastic thickness T_e of 40 km (at southern end of the profile), decreasing to 20 km beneath the Tien Shan. It is subjected to a terminal bending moment of 0.5×10^{17}N. The Kazakh plate begins with T_e = 48 km at the northern end of the profile, decreasing to 25 km beneath the Tien Shan. A bending moment 0.2×10^{17}N is applied to its end. The calculated Bouguer gravity for Airy isostasy is shown for reference (red). (c) Depth distribution of the Moho showing its deflection according to the Airy model (black dotted) and a two plate model (green). The point where the two independent plates meet is indicated beneath the Southern Tien Shan Thrust Fault (STSTF). The crust and mantle densities are taken as 2670 and 3300 kg/m^3, respectively.

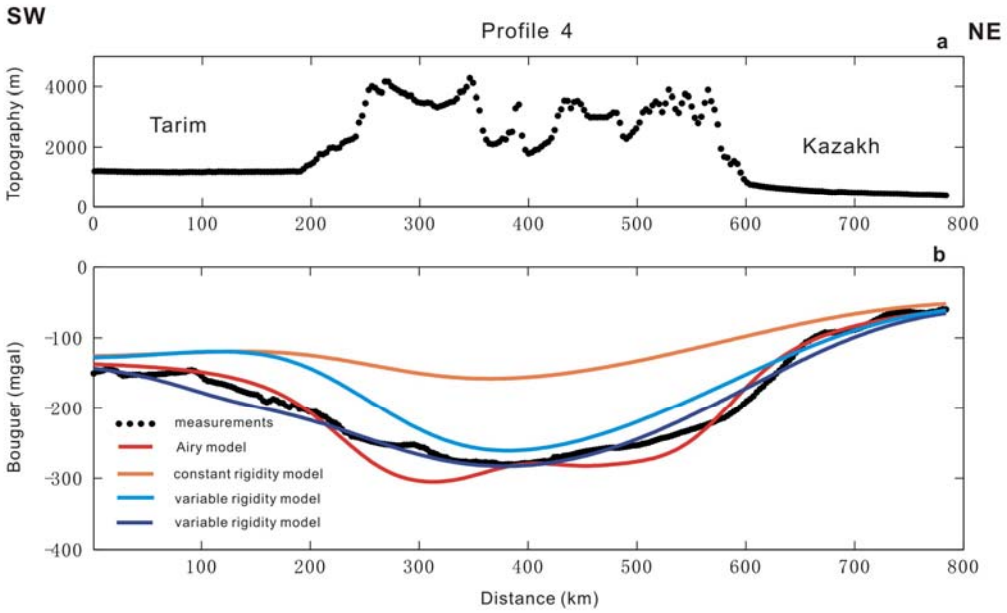

Figure 48. Same as Fig. 46, but for profile 4.

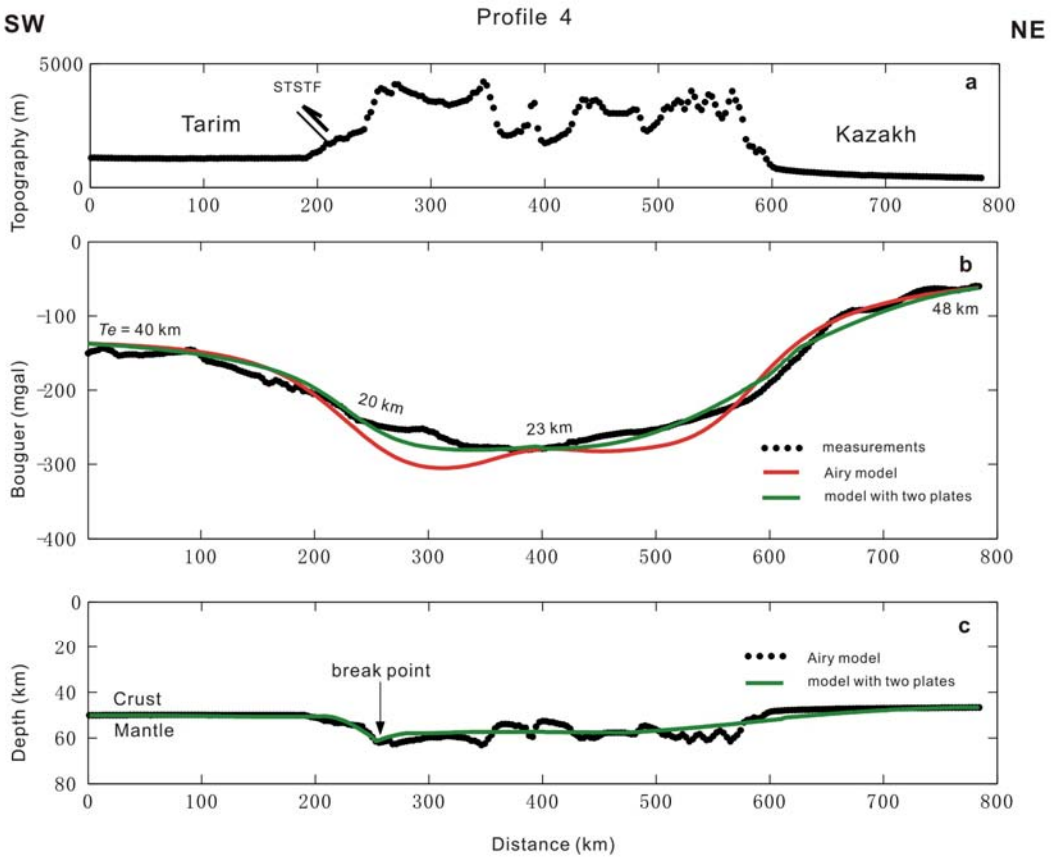

Figure 49. Same as Fig. 47, but for profile 4. The parameters for the two plate model are: the break point is at about x = 250 km. The Tarim plate has an initial T_e of 40 km (at southern end of profile), decreasing northward to 20 km beneath the Tien Shan. The Kazakh plate begins with T_e = 48 km at the northern end of the profile, decreasing southward to 23 km beneath the Tien Shan.

5.4 Tectonic stress field in the Tien Shan

As already stated, the convergence between India and Eurasia leads to a major compression in the direction of N 10° E in Central Asia (*e.g.*, *England and Molnar,* 1997; *Molnar and Tapponnier,* 1975; *Wang et al.,* 2001), for which the distribution of the averaged vertical stress has been calculated using a viscous model (Fig. 50) (*Flesch et al*., 2001). However, deformations observed in the Tien Shan are not consistent with the direction of convergence between India and Eurasia. Earthquake focal solutions, geodetic GPS measurements, geological evidence and viscous thin-shell modelling show that the direction of principal stress in the Tien Shan is roughly normal to the strike of the mountain belt (*Abdraknmatov et al.,* 1996; *England and Molnar* 1997a; *Holt et al.,* 2000; *Neil and Houseman,* 1997; *Reinecker et al.,* 2003; *Thompson et al.,* 2002; Fig. 50). It is very likely that there is a causal relationship between the Indian-Eurasian collision and the formation of this intraplate mountain belt. If the Tien Shan is an unusually weak region and stress is transmitted from the plate boundary to the plate interior and is concentrated at the zone of weakness, then the stress field of the Tien Shan should be oriented at about N 10° E rather than normal to its strike. Thus, we tested the hypothesis that the compressive stress is generated *locally* by the underlying mantle circulation induced by the collision.

Here, we consider three sources of lithospheric stress, each of which can be calibrated fairly reliably both in terms of magnitude and direction. These are: the boundary force caused by the collision between the Indian and Eurasian plates; the topographic stress field caused by elevated gravitational potential energy; and flexure of the elastic plate caused by bending of the lithosphere. We hope to thereby better understand the localized stress field in and the cause for deformation of the Tien Shan.

Stress from the boundary force

Observations from seismic focal mechanisms, well bore breakout, fault slip, neo-tectonic structure, Cenozoic volcanic alignments, hydraulic fracturing, and overcoring demonstrate that large regions within the interiors of plates have consistent stress orientations and are principally dominated by compression except for highly elevated areas (*Zoback,* 1992; *Coblentz and Richardson,* 1996). The global pattern of intraplate stress can be explained simply by forces, mainly ridge push and collisional forces at trenches, applied at the plate boundary (*Richardson,* 1976). Also, the orientation of the principal stress axes of the stress tensor can be constrained by specifying the direction of just one of the

horizontal principal stresses (*Zoback,* 1989). In Central Asia, the regional stress field is dominated by horizontal compression generated by the collision of India with the southern margin of Asia and its convergence direction is well constrained (N 10° E), although its magnitude is more difficult to estimate. *McAdoo and Sandwell* (1985) and *Zuber* (1987) estimated that it is several hundred MPa based on observations of folding of the oceanic lithosphere in the central Indian basin. *Flesch et al.* (2001), on the other hand, suggested using a viscous model that it may be an order of magnitude smaller. *Coblentz et al.* (1995) predicted that the stress fields in most regions of Australia due to ridge push force acting on the India-Australian plate approaches 20 MPa. To test our hypothesis, we shall choose 50, 300 and 46 MPa respectively for the components of the stress vector with a compressional principal stress direction of N 10° E and a magnitude of 308 MPa (*Jin,* 1997). Alternatively, we shall assume that the boundary stress field is given by the quantitative stress field of *Flesch et al*. (2001).

Stress from elevated topographic gravitational potential energy

Regions of high topography are exceptions to the rule that plate interiors are generally in a compressonal stress state. Highly uplifted topography has a high gravitational potential energy and is inherently unstable. It tends to spread laterally in order to return to its minimum energy state. This tendency to spread causes extension in the interior of highlands and compression in the surrounding lowlands (Fig. 51) (*McGarr,* 1988; *Savage and Morin,* 2002). For highly elevated regions, the extensional forces can exceed the regional compressional force, leading to the formation of normal faults (*Molnar and Lyon-Caen,* 1989). Normal faults of the Tibetan Plateau are typical examples.

We estimate the horizontal and vertical stresses S_h and S_v due to variations in gravitational potential energy by using *McGarr's* formula (1988):

$$S_h = S_v = -\ \rho_c \times g \times h_t$$

where h_t is topography, g is gravitational acceleration and ρ_c is crustal density. Extension is positive. In the Tien Shan area, the maximum magnitude of this (compressive) stress is 1.58 MPa and the minimum (extensional stress) is −126 MPa.

Flexural stress from lithospheric bending

In addition to the horizontal forces described above, topography also represents vertical loads on an elastic lithosphere (*e.g., Bank et al.,* 1977; *Watts et al.,* 1980; *McNutt,* 1983; *Forsyth,* 1985). As the plate flexures beneath the loads, the top of the elastic plate is placed under relative extension or compression, depending on whether the plate is curved concave upwards or downwards. The bottom of the plate would be subjected to the opposite stress state. The neutral surface is the boundary between compression and extension (Fig. 52).

To evaluate the flexural stress, we first solved the equation governing the flexure of an elastic lithosphere (equation 21, Chapter 3) to determine the lithospheric flexure of the Tien Shan (*Jin,* 1997*; Wees and Cloetingh,* 1994). The laterally inhomogeneous rigidities used (D) are based on the elastic thicknesses (Te) from gravity modelling (Fig. 18). N_{11}, N_{22} and N_{12} of equation 21 that are due to the convergence between India and Asia here are given by:

$$(N_{11}, N_{22}, N_{12}) = (S_{11}, S_{22}, S_{12}) \times h$$

where (S_{11}, S_{22}, S_{12}) = (50, 300, 46) MPa (*Jin,* 1997) or the quantitative stress field of *Flesch et al.* (2001).

The flexural equation is solved by the finite difference method (*Jin* 1997*; Wees and Cloetingh,* 1994). The region chosen for the calculations lies between 70 – 110° E and 25 – 50° N, and the boundaries are assumed flat enough that the boundary conditions can be approximated by Airy isostasy. The choice of Airy isostasy (compensation with very long wavelengths) at the boundaries is due to the lack of knowledge on the actual deflections at these locations. The topography and sediment columns in the Tarim and Zungar basins are considered to be vertical loads on the elastic lithosphere. The flexural stress is calculated using the following equations (*Jin,* 1997):

$$\begin{cases} \tau_{xx} = -\dfrac{Ez}{1+\nu}\left[\dfrac{1-\nu}{1-2\nu}\dfrac{\partial^2 w}{\partial x^2} + \dfrac{\nu}{1-2\nu}\dfrac{\partial^2 w}{\partial y^2}\right] \\ \tau_{yy} = -\dfrac{Ez}{1+\nu}\left[\dfrac{\nu}{1-2\nu}\dfrac{\partial^2 w}{\partial x^2} + \dfrac{1-\nu}{1-2\nu}\dfrac{\partial^2 w}{\partial y^2}\right] \\ \tau_{xy} = -\dfrac{Ez}{1+\nu}\dfrac{\partial^2 w}{\partial y \partial x} \end{cases}$$

where τ is flexural stress, z the depth coordinate (positive is down and zero is at the centre of the plate where the neutral surface of the bending lithosphere is located). Using this model, the flexural stress can be calculated at any depth in the lithosphere. It reaches a maximum at the top and bottom of the lithospheric plate.

Figure 53 shows the 3D flexure of the Central Asian lithosphere in the region between 70° – 110° E and 25° –50° N, for which the background stress components are assumed to be (50, 300, 46) MPa (*Jin,* 1997) (Fig. 53a) or identical to the quantitative stress field of *Flesch et al.* (2001) (Fig. 53b) respectively. Because of the large topographic loading in the area, the calculated lithosphere flexure *w* is large. After *w* is determined, the flexural stress distribution is estimated using the flexural stress equation. Figures 54a-c give the stress fields calculated from the deflections of the elastic lithosphere shown in Fig. 53a at depths of zero, 1/4 and 1/8 of the thickness of the lithosphere respectively. Analogously, stress fields when the deflections of the elastic lithosphere shown in Fig. 51b are used are given in Figs. 55a-c.

Figures 56a-b show the average flexural stress field in the Tien Shan and its adjoining areas calculated using a background stress of 308 MPa (*Jin,* 1997) (components of 50, 300 and 46 MPa) and that from *Flesch et al.* (2001) respectively (see Figs. 54 and 55). For the former case, the maximum magnitude (compression) of the average flexural stress is 169 MPa and the minimum magnitude (extension) is -99 MPa. For the latter case, the corresponding values are 114 MPa and -118 MPa respectively. We note that the maximum average flexural stress of the stress field applied is only 40 MPa (*Flesch et al.,* 2001). Thus, the magnitude and distribution of the local flexural stress field in the Tien Shan using the two different regional stress fields are similar, being characterized by a dominance of vertical loading. Figure 56 shows in addition that: (1) the greater the elastic bending of the plate in response to topographic loading, the larger a role the flexural stress field plays in our study area; (2) the Tien Shan mountain belt is under a large compression, while the Tarim and Zungar basins are under extension; (3) the stress field is oriented perpendicular to the strike of the load (*i.e.*, the mountain belt), rather than to the major collision direction between India and Eurasia; (4) the flexural stress comprises over 40 % of the total stress (Fig. 57); and (5) the principal stress direction is NW-SE in the western Tien Shan but rotates to N-S in the central part and NE-SW in the easternmost areas. The stress direction is NW-SE in the westernmost Tarim Basin and is

roughly N-S elsewhere, while the corresponding directions in the Zungar Basin are NE-SW in the easternmost areas and N-S elsewhere respectively.

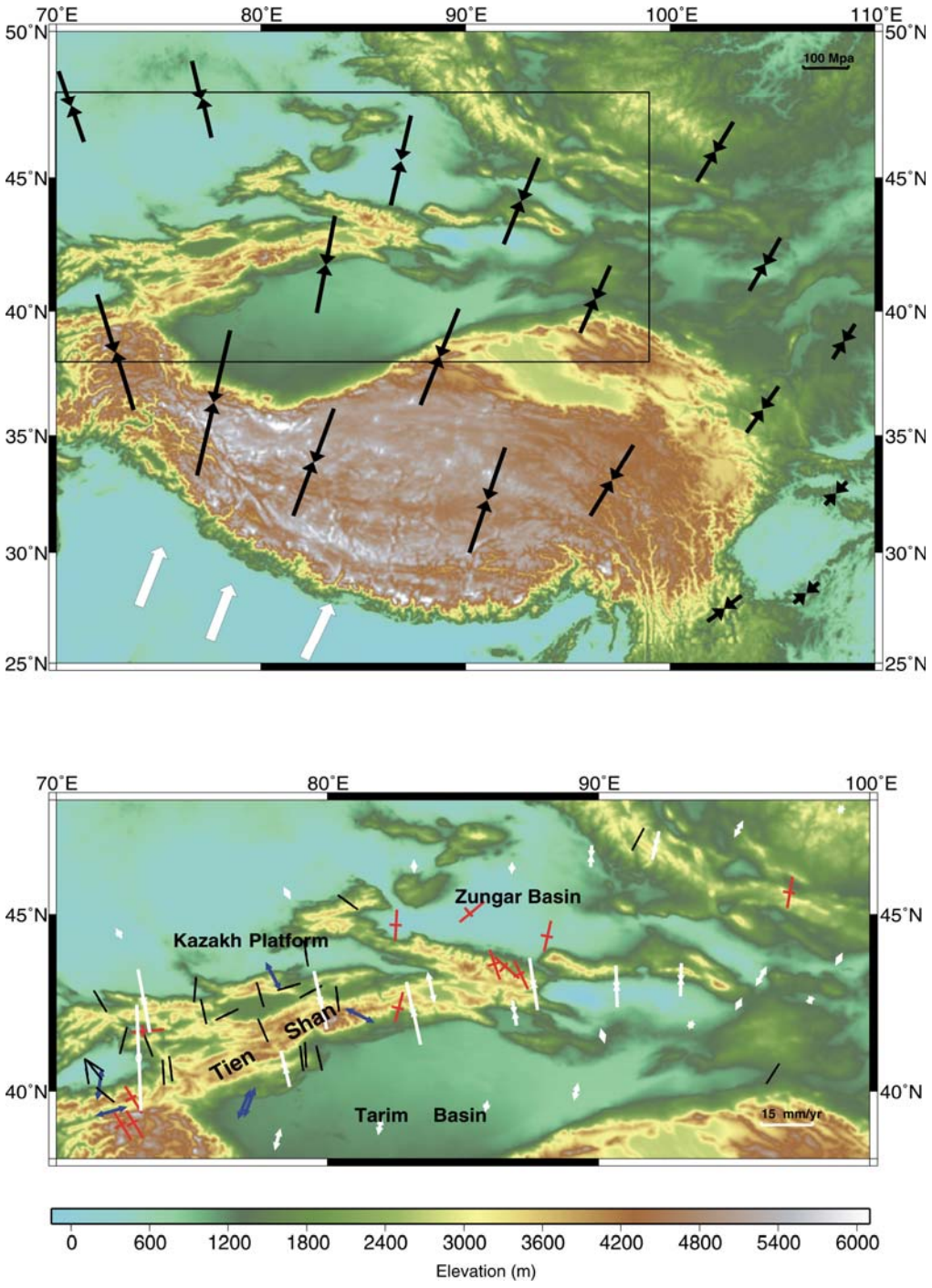

Figure 50. (a) Topography and regional horizontal compressional stress field caused by the collision of India with Eurasia (*Flesch et al.,* 2001). (b) Observed horizontal strain rate distribution (white) inferred from Quaternary fault slip rates and model strain rates from GPS velocities (*Abdrakhmatov et al.,* 1996*; England and Molnar,* 1997*; Holt et al.,* 2000). The compressional (black bars), extensional (blue open arrows) and strike-slip (red cross-bars) stress axis directions are derived from earthquake focal mechanism solutions (*Reinecker et al.,* 2003).

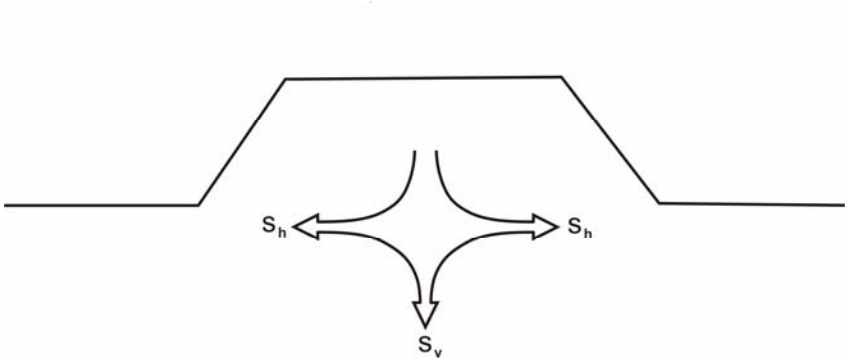

Figure 51. Cartoon showing the gravitational stress model due to elevated topography. See text for discussions

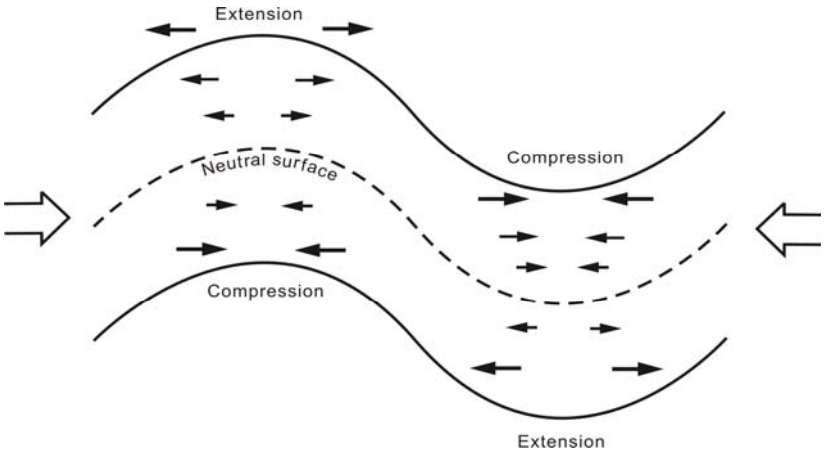

Figure 52. Cartoon showing the flexural response of a plate to topographic loading.

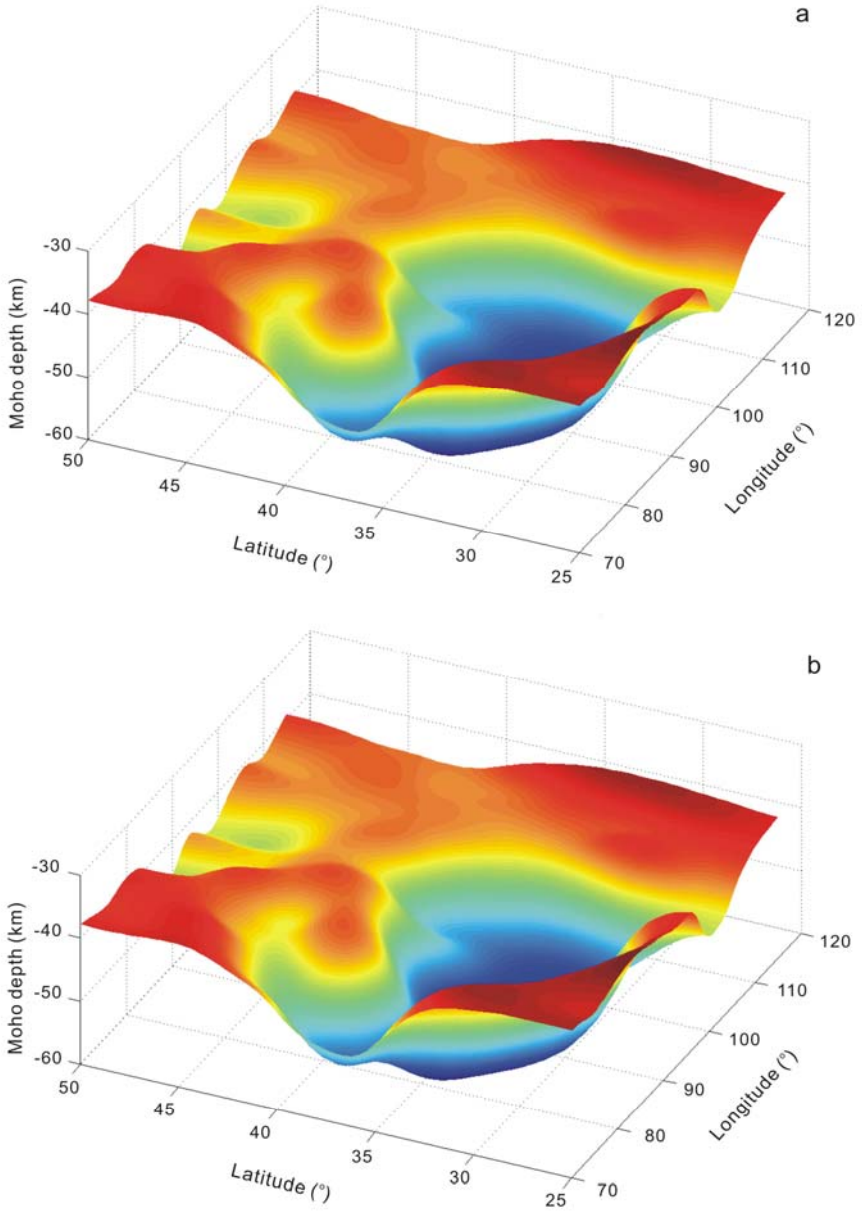

Figure 53. Deflections of the Central Asian lithosphere calculated from the elastic thickness distribution of Fig. 18. The background regional stress field is 308 MPa (*Jin,* 1997) in (a) and is taken from *Flesch et al.* (2001) in (b).

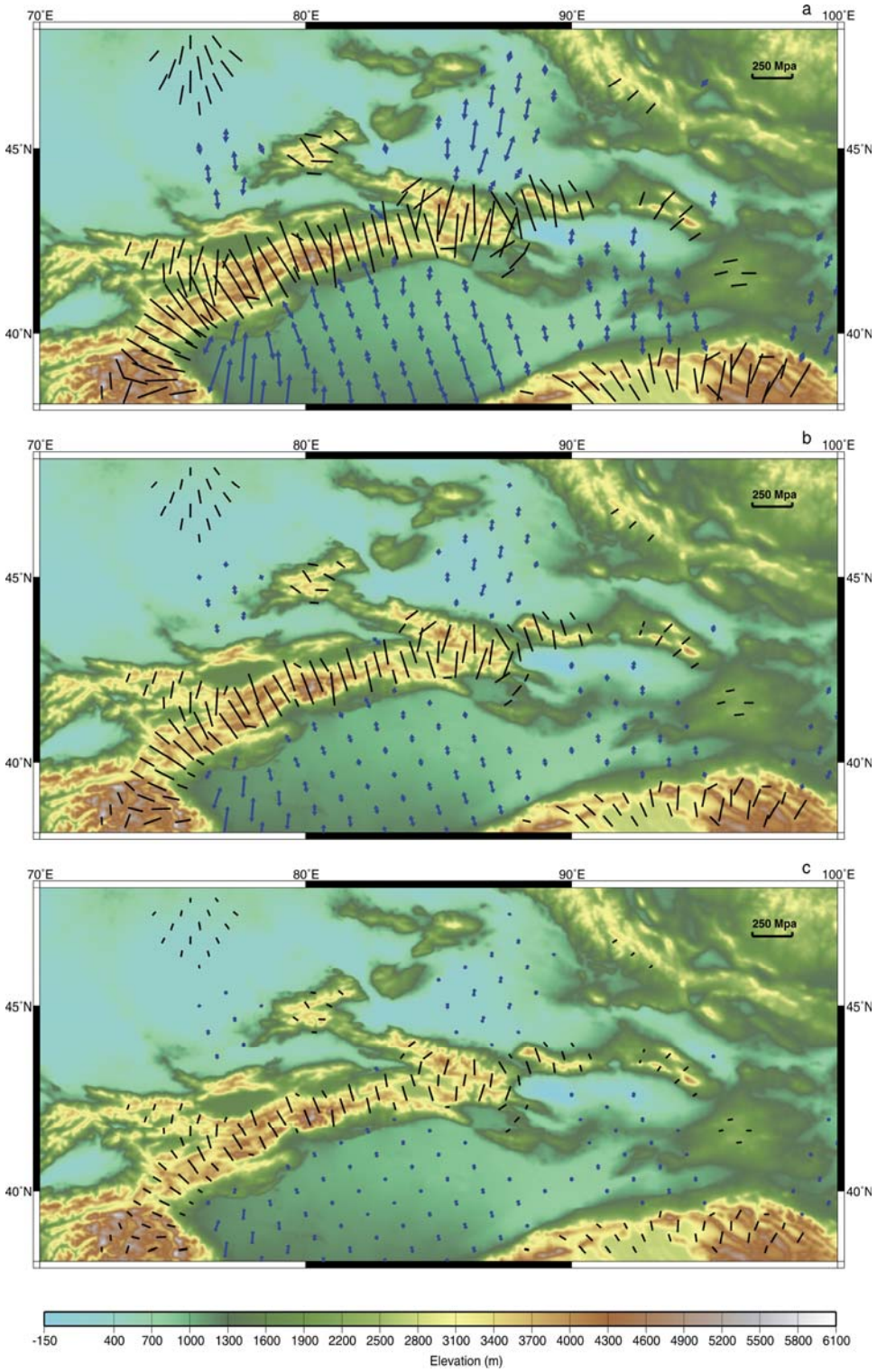

Figure 54. Flexural stress field at several depths calculated from the lithospheric deflections of Fig. 53a. Black lines give the compressional stress field ($\sigma_{Hmax} > \sigma_v > \sigma_{Hmin}$; σ_{Hmax} = maximum horizontal principal stress; σ_{Hmin} = minimum horizontal principal stress; σ_v = vertical principal stress), blue arrows represent extensional stresses. (a) The flexural stress field on the surface, (b) at a depth equal to 1/4 of the lithospheric thickness, and (c) at a depth equal to 1/8 of the lithospheric thickness.

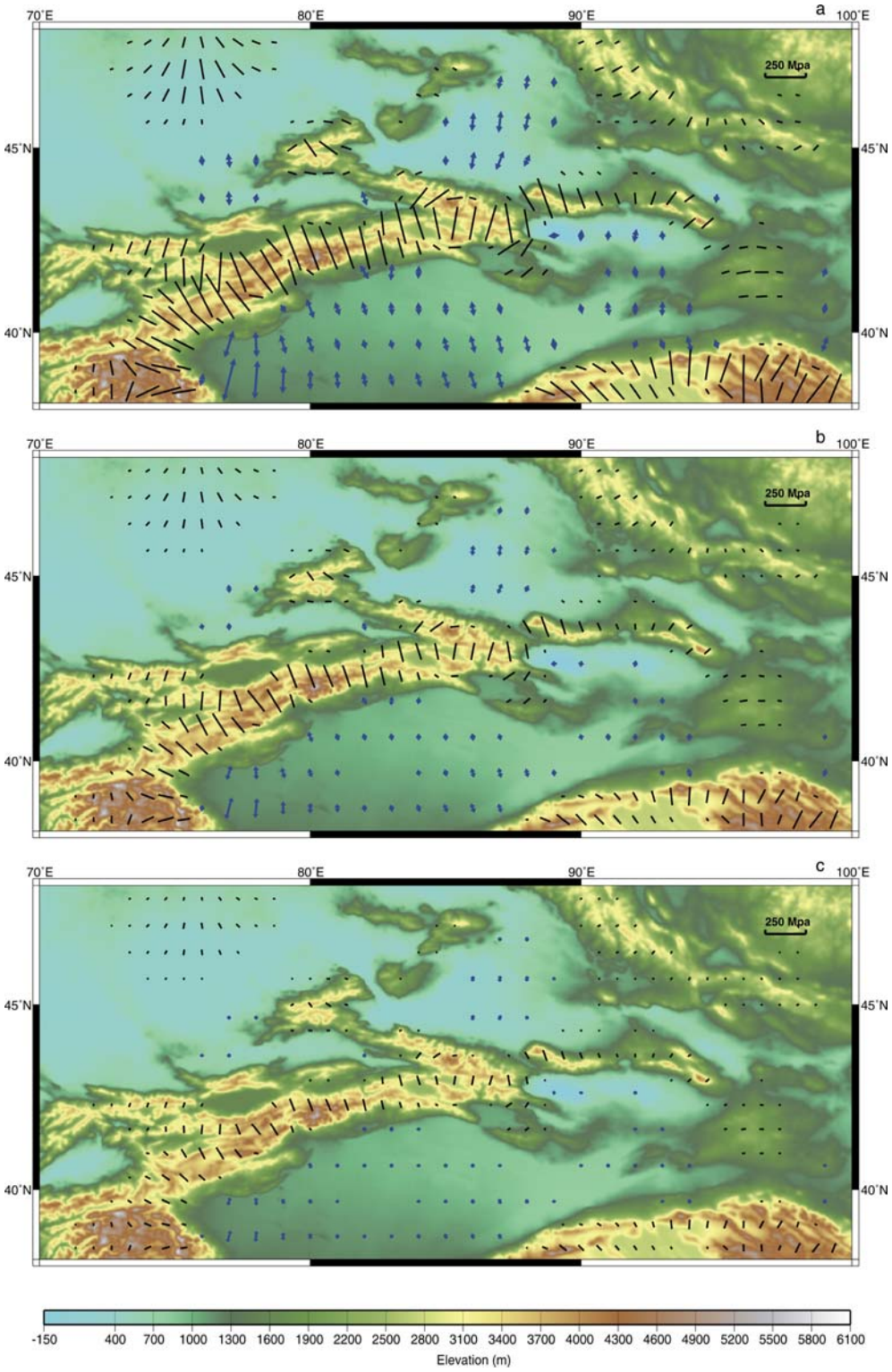

Figure 55. Flexural stress field at several depths calculated from the lithospheric deflections of Fig. 53b. Black lines give the compressional stress field ($\sigma_{Hmax} > \sigma_v > \sigma_{Hmin}$; σ_{Hmax} = maximum horizontal principal stress; σ_{Hmin} = minimum horizontal principal stress; σ_v = vertical principal stress), blue arrows represent extensional stresses. (a) The flexural stress field on the surface, (b) at a depth equal to 1/4 of the lithospheric thickness, and (c) at a depth equal to 1/8 of the lithospheric thickness.

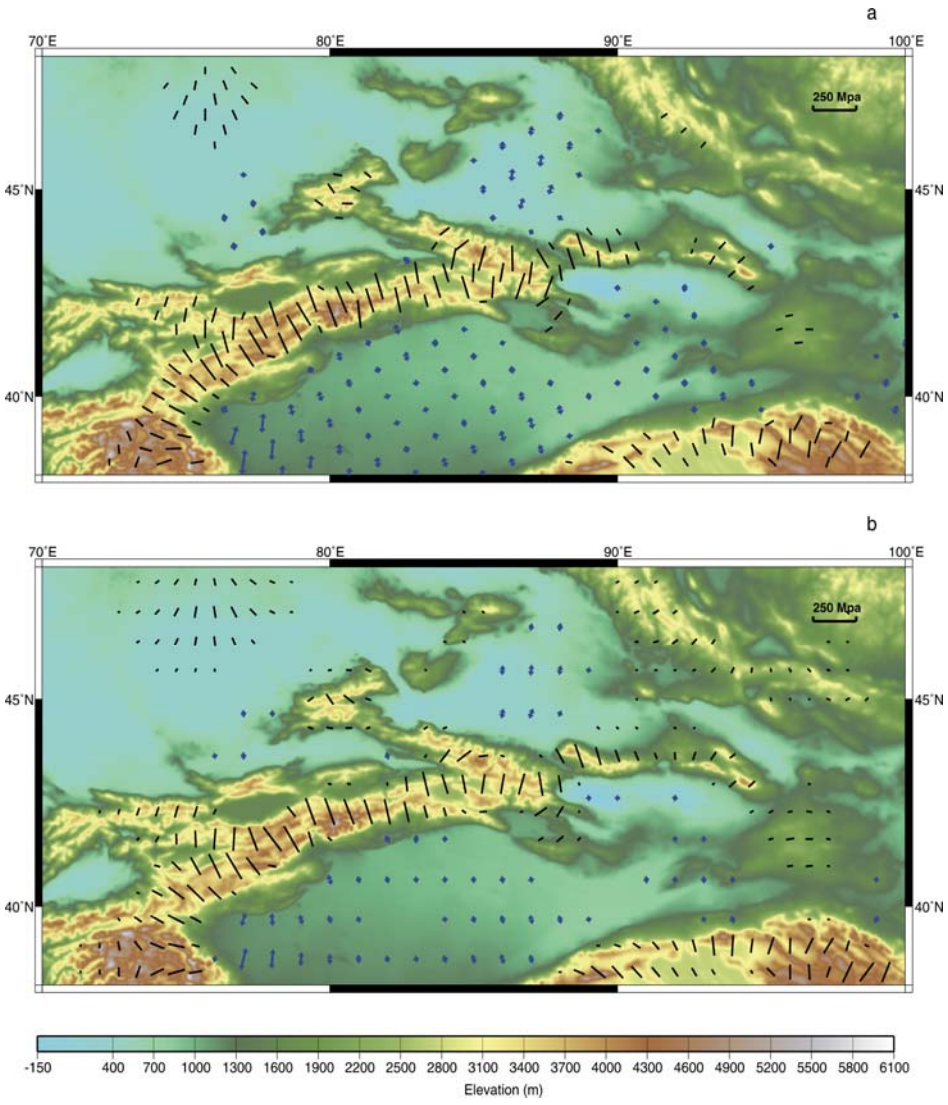

Figure 56. Average flexural stress field in the Tien Shan area. The background regional stress is 308 MPa (*Jin,* 1997) in (a) and the stress field is taken from *Flesch et al.* (2001) in (b). Black bars: compressional stress; blue arrows: extensional stress.

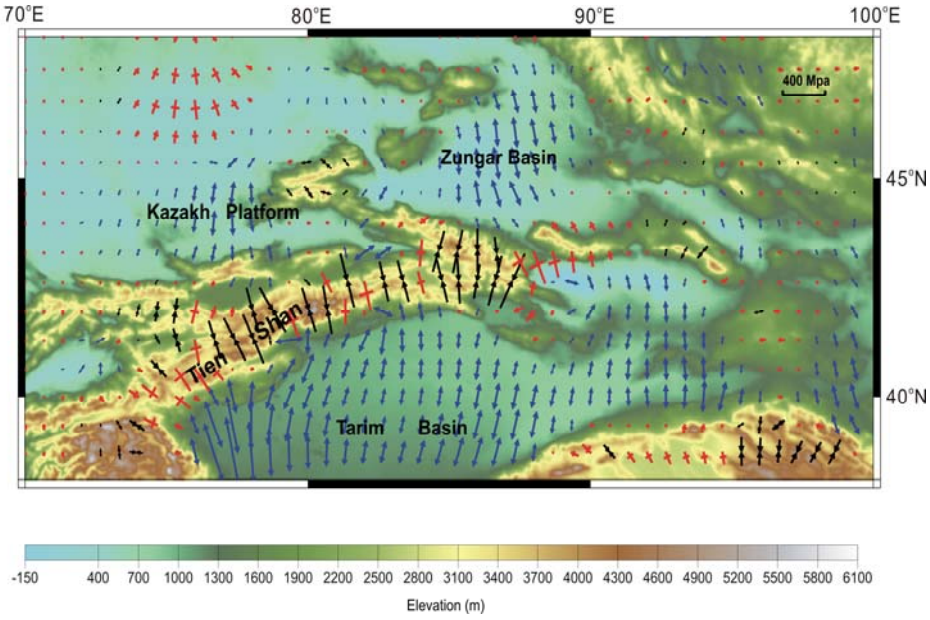

Figure 57. Total stress field in the Tien Shan area obtained by summing the stress fields derived from plate boundary force (the quantitative stress field of *Flesch et al.* (2001)), elevated topography, and flexural stress (Fig. 56b). The black convergent arrows denote compression, blue divergent arrows extension, and red cross-bars strike-slip.

Chapter 6. Discussion

Our modelling shows that the 3D flexure of the Central Asian lithosphere is characterized by a large downward deflection where topographic loading is high (Fig. 53). The largest lithospheric bending (65–70 km) occurs on the northern and southern Tibetan Plateau; bending over the central plateau is in comparison moderate (60-63 km). (A plate flex upwards or downwards depending on whether it is under relative extension or compression. Plate bending is always downwards in our study area, and 'bending' means 'bending downwards' in this dissertation). In contrast, flexure in northeastern Tibet between the Altyn Tagh Fault and the Kunlun Fault is low, the lowest values being reached in the Qaidam Basin (58 km). The Tarim Basin and the Yangtze and Sino-Korean blocks have suffered very low lithospheric flexure (45–50 km). Seismic reflection imaging of the Moho in the Tarim Basin shows that it dips southward from a depth of 42 km to a depth of 50 km (*Kao et al.,* 2001), and teleseismic tomography across Altyn Tagh give a mean crustal thickness of 54 km for the Qaidam Basin (*Wittlinger,* 1998). Our modelling results on lithospheric bending are therefore compatible with these measurements.

Our gravity modelling of the strength of the lithosphere in Central Asia suggests that the strong Indian plate weakens the Eurasia plate in the course of collision (Fig. 18). However, the degree of weakening varies from place to place within Eurasia. Firstly, the lithosphere at the collision zone on both sides of the Zhangbo suture zone suffers a large weakening with low *Te* values of 10-20 km or less. Secondly, although the Tien Shan is far from the collision zone, it is currently a very active thrust belt. Brittle failure caused by this thrusting weakens the lithosphere of the Tien Shan with *Te* value similar to that of the Zhangbo suture zone. Thirdly, the rigid Tarim block with a Precambrian or Lower Palaeozoic basement (*Avouac et al.,* 1993*; Yin* 1993*; Zhou and Chen,* 1990) functions as a barrier to the northward motion of India. Fourthly, the lithosphere beneath Qilian Shan is another highly weakened area. The mechanism of its weakening is similar to that of the Tien Shan. Fifthly, the Yangtze and Sino-Korean blocks as well as the eastern boundary of the Tibetan Plateau where the elevation drops from >4 km on the plateau to <1 km in the Sichuan Basin via Longmen Shan have high elastic strengths. The sharp decrease in *Te* along the eastern boundary of the Tibetan Plateau indicates that large changes in mantle structure are restricted to major crustal boundaries. Beneath the central Altyn Tagh Fault, teleseismic tomography reveals a steep, low-P-wave velocity anomaly (relative to the

adjacent regions) aligned with the surface trace of the fault (*Wittlinger et al.,* 1998). These observations argue for localized shear in the continental lithospheric mantle along the Tien Shan and Altyn Tagh, Qilian and Zhangbo faults, rather than for uniform, widespread anisotropic flow beneath Tibet (*Holt,* 2000). Along major tectonic block boundaries, lithosphere deformation is partitioned between steep strike-slip shear zones.

It is well accepted that the lithosphere may exhibit non-zero mechanical strength over geological time. The parameter that characterizes the apparent strength of the lithosphere is the flexural rigidity, which is characterized by the effective elastic thickness. Because the effective elastic thickness of the continental lithosphere is controlled primarily by its thermal structure and by the degree of coupling between the crust and the mantle (*e.g., Burov and Diament,* 1995), the lateral inhomogeneity of the elastic strength of the lithosphere in Central Asia should have some correlation with surface geology and tectonic activity.

The Yangtze (Sichuan Basin) and Sino-Korean (Ordos Basin) blocks are characterized by a large effective elastic rigidity of the lithosphere, implying that they have acted as stable units for a prolonged geological time. Surface geological studies and recent GPS observations show that these two blocks have suffered relatively little internal deformations until the Mesozoic (*Gilder and Courtillot,* 1997*; Hacker et al.,* 1998, 2000). They were sutured in the Late Triassic along the Dabie-Qinling-Qilian suture zone (*Mattauer et al.,* 1985*; Meng and Zhang,* 1999*; Oberhänsli et al.,* 2002). That the lithospheric rigidity of the Dabie-Qinling section of this fault is not lower than its surroundings suggests that the associated deformations are crustal. The mechanical models of *Chemenda* (2000) support our results. The longstanding suture and a minimum in tectonic activity for over 200 m.y. in this area makes this portion of the Eurasian plate a unique block with a consistent intermediate mechanical strength. However, the lithosphere underneath Qilian Shan (west of the Dabie-Qinling-Qilian suture zone) is a highly weakened area. Although this weakening on the lithospheric scale is poorly understood, its surface geology suggests that the mechanism responsible for it is crustal thrusting (*Tapponnier et al.,* 2001). The strong lithosphere of the Longmen Shan may be considered an extension of the strong South China plate into the Tibetan lithosphere.

Our gravity modelling yields an elastic thickness for the Tarim block of 40-45 km, a value which is consistent with published results (*Jin,* 1996*; Lyon-Caen and Molnar,* 1984) and is typical for stable, moderately rigid continental micro-plates. Despite the fact that the

basement of the Tarim Basin is Precambrian in age based on well analysis and surface geological studies (*Hua*, 1992; *Liu, et al*., 1997*; Li and Mooney*, 1998), the Tarim lithosphere does not have an elastic strength typical of that for an old continental lithosphere. It is well known that the Tarim Basin is filled with >12 km of sediments overlying an old, stable continental core (Fig. 24). These sediments have a low density, so that the elastic rigidity of the lithosphere is reduced (*Zhou and Chen,* 1990). Space geodetic studies also show that the Tarim Basin has suffered little internal deformations and has rotated as a rigid block (*Reigber et al.,* 2001). The lack of earthquake activity from January 1980 to May 2003 suggests that the Tarim Basin is not tectonically active today (*NEIC,* 2003). Seismic profiles from hydrocarbon exploration in the basin show that the center of the Tarim Basin is hardly deformed (Fig. 58, see Fig. 59 for location). Based on the known stratigraphy and the seismic faces of sequences in the Tarim Basin (*Zhao et al.,* 1997), three unconformities (T_g, T_8 and T_3 from old to young) have been interpreted on this section. T_g, the base of the sedimentary column, is characterized by high amplitudes, low frequencies and continuous phases. The basement below T_g consists of strata of Sinian age or older, including Archean high-grade metamorphic rocks and Proterozoic intermediate-low grade metamorphic rocks (*Zhou and Chen,* 1990). T_8, the lower boundary of the Paleogene, is a high amplitude, lower frequency, continuous to intermittent reflector. It is underlain by Mesozoic terrestrial and fluvial sediments (dominantly sandstones) and Palaeozoic marine carbonates and sandstones (*Carroll et al.,* 1995; *Zhao et al.,* 1997; *Zhou and Chen*, 1990). T_3, the Oligo-Miocene boundary, is marked by a reflector with intermediate amplitudes and frequencies, and continuous phases. The depositional environment changed from littoral and shelf to fan alluvium at the Paleogene-Neogene boundary (*Zhao et al.,* 1997*)*. Because reflectors in the central Tarim Basin are flat-lying, deformations must have been almost absent here since the Palaeozoic, (Fig. 58). In contrast to the central Tarim Basin, its margins (where it underthrusts Tibet and the Tien Shan) are seismically highly active (*NEIC,* 2003) and the elastic strength of the lithosphere there is reduced to 30 km. It is possible that the Tarim micro-plate was weakened in these areas by tectonic thinning. That is, the underthrusted Tarim crust was thinned by off scraping and deformation in the foredeeps at its northern and southern margins. Figure 60 shows a seismic profile from the stable central Tarim Basin to southwestern rim (fore-land basin). The downward-dipping part of the reflectors marks this southern foredeep. Southward indentation of the strong Tarim Block causes extensive deformations at the northern margin of the Tibetan Plateau and northward

indentations at the strong Tarim block causes intense deformation of the southern margin of the Tien Shan. These deformations led to a considerable weakening of the lithosphere.

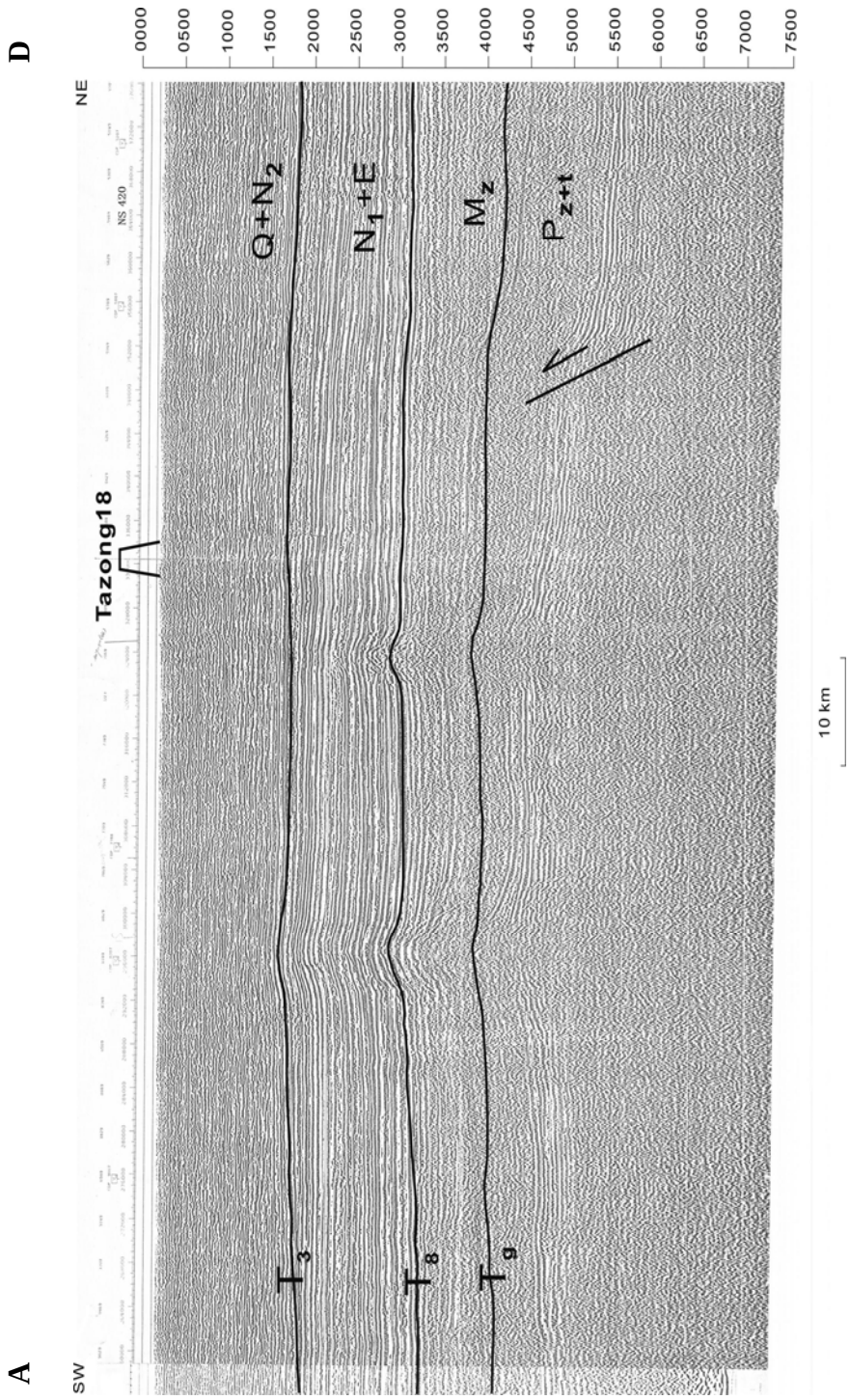

Figure 58. Seismic profile across the Tarim Basin in the NE-SW direction. Profile location is shown in Fig. 59 (profile A-A'). The vertical axis is time in ms. This profile is surveyed by the Shengli Oil Complex in 1983. Within the framework of an agreement in scientific cooperation between the Ocean University of China and the Shengli Oil Complex, this and another profile (BB',. Fig. 60) were provided for ourresearch project. Q = Quaternary, N_2 = Miocene, E = Eocene, M_z = Mesozoic, P_{z+t} = Palaeozoic,. T_3, T_8 and T_g are seismic unconformities. See text for discussions.

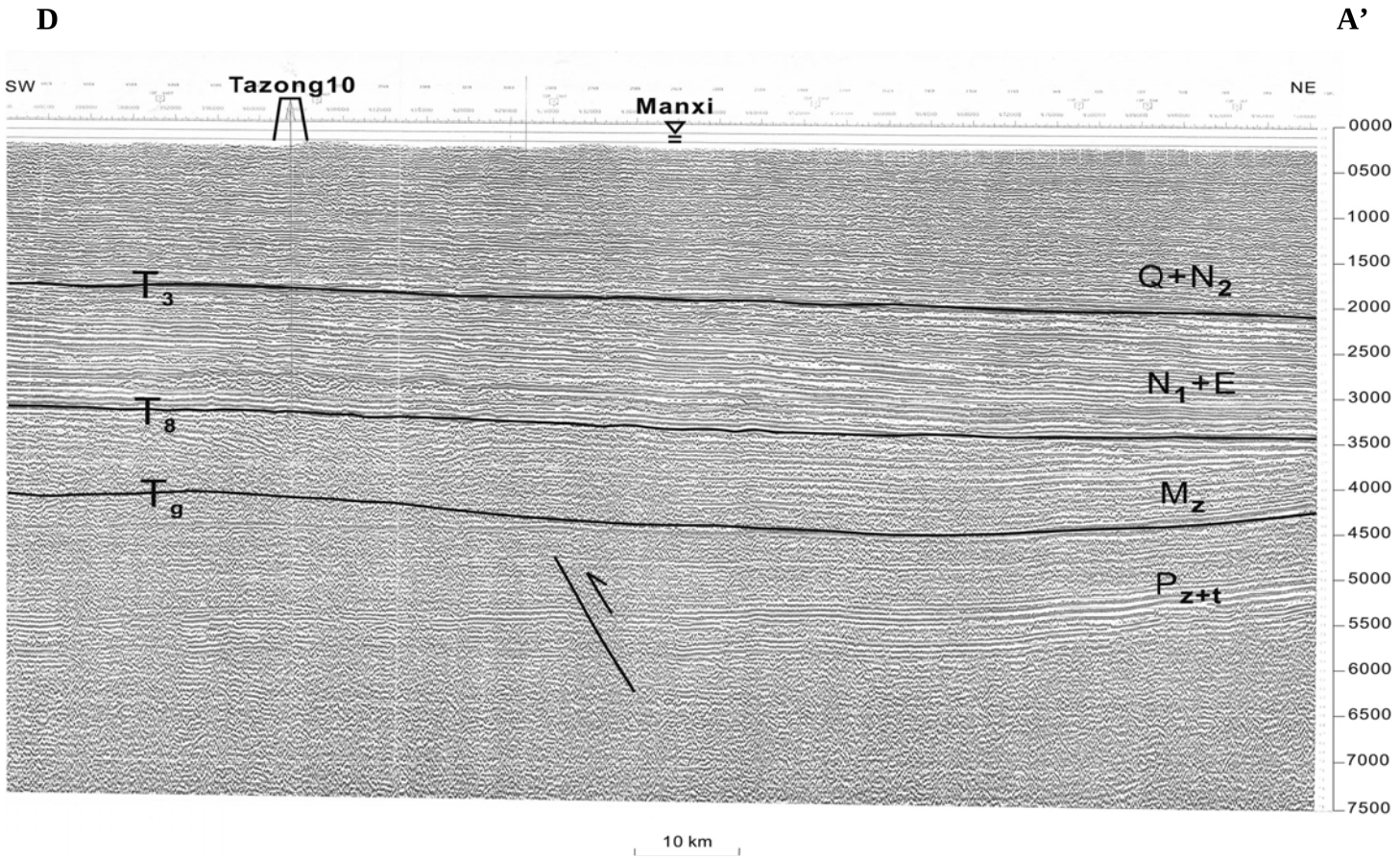

Figure 58. Continued.

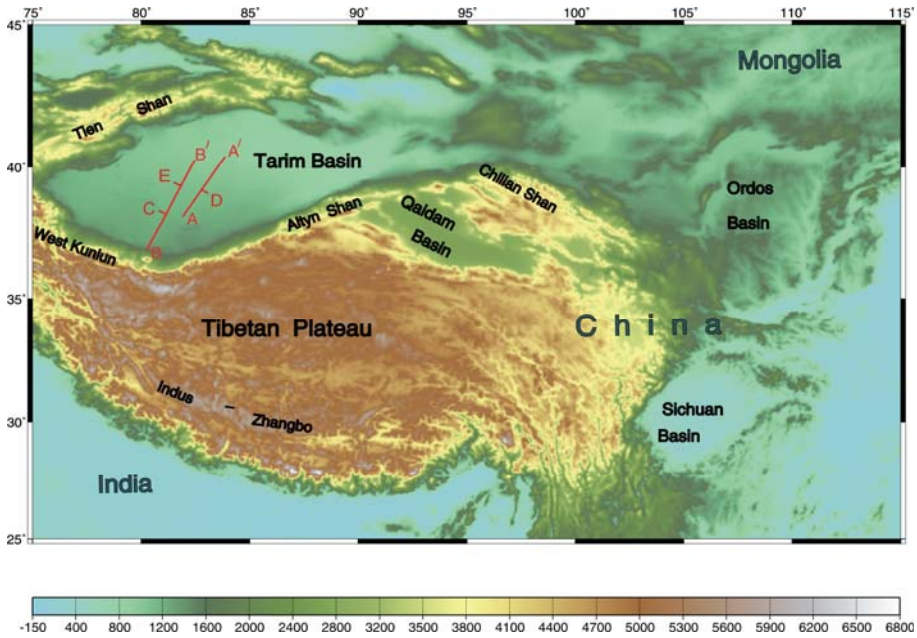

Figure 59. The locations of seismic profiles A-A' and B-B' in the Figs. 58 and 60.

Our results suggest that the elastic thickness of the Tibetan Plateau is generally <40 km, although the crustal thickness may reach 60-80 km (*e.g., Molnar and Tapponnier,* 1975). *Jin et al.* (1994) showed that the Tibetan crust becomes progressively stronger with increasing overburden pressure down to a depth of about 15 km, at which point ductile creep of diabase becomes the dominant mechanism of failure. In the uppermost mantle beneath the Tibetan Plateau, another relatively strong zone exists because of the higher strength of olivine. Between the upper crust and the upper mantle is a weak ductile channel. Maximum crustal thickening occurs beneath the Tibetan Plateau, while the mantle (75% of the lithosphere) did not thicken (*Tapponnier et al.,* 2001). Upwelling of the hot asthenosphere could not have taken place beneath the plateau. Seismic velocity studies (*Bourjot and Romanowicz,* 1992*; Griot et al.,* 1998*; Revenangh and Sipkin,* 1994*; Zeng et al.,* 1995) show that beneath the Tibetan Plateau between depths of 100 and 300 km, the mantle has a higher P-wave velocity and is hence colder than in adjacent regions. In contrast, the crustal velocities are lower beneath Tibet (*Bourjot and Romanowicz,* 1992*;*

Owens and Zandt, 1997). It implies widespread lower crustal partial melting. When subjected to moderate stresses from vertically-directed surface and subsurface loads, the

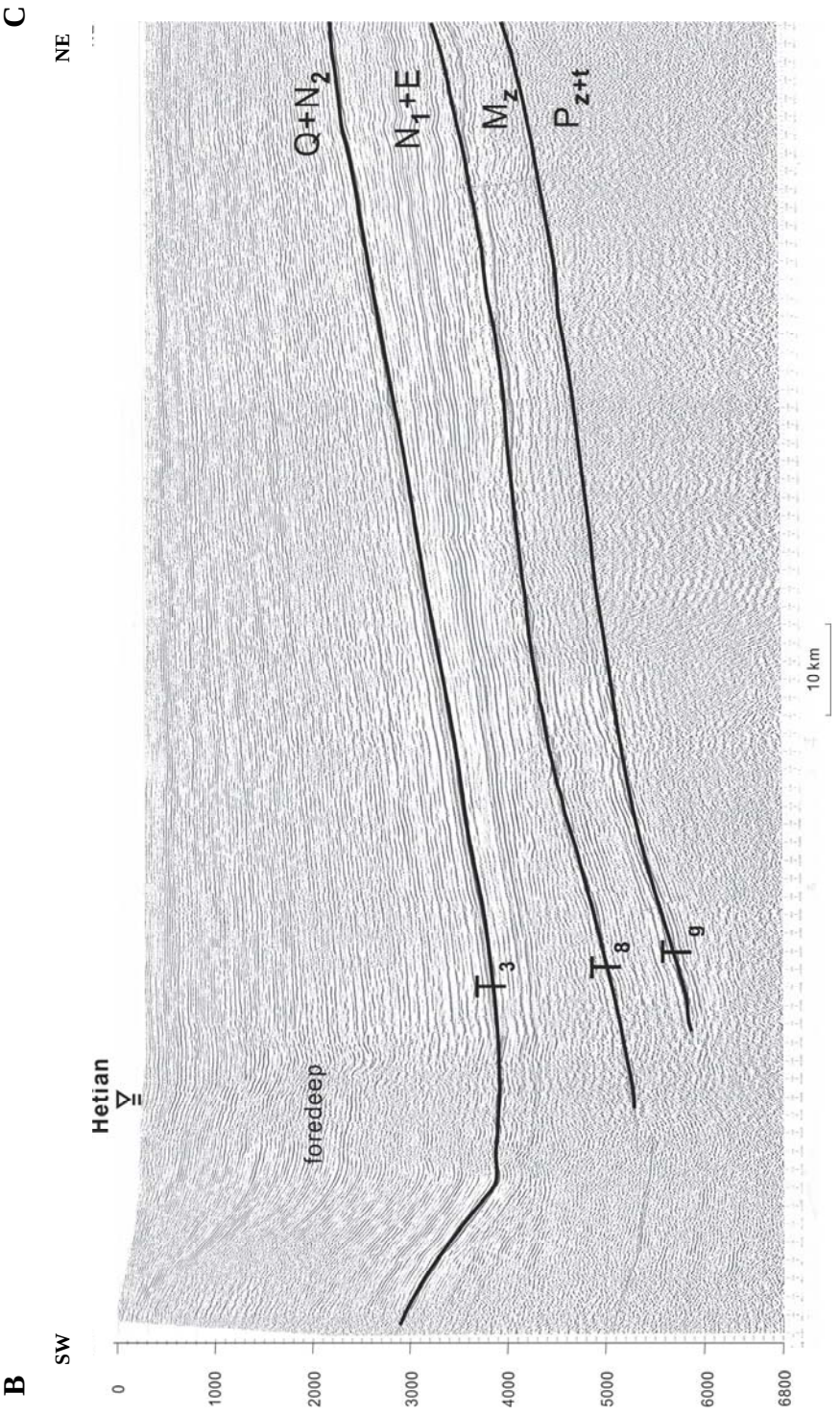

Figure 60. Seismic profile across the Tarim Basin in the NE-SW direction. Profile location isshown in Fig. 59 (profile B-B'). The vertical axis is time in ms. This profile is surveyed by th eShengli Oil Complex in 1998.

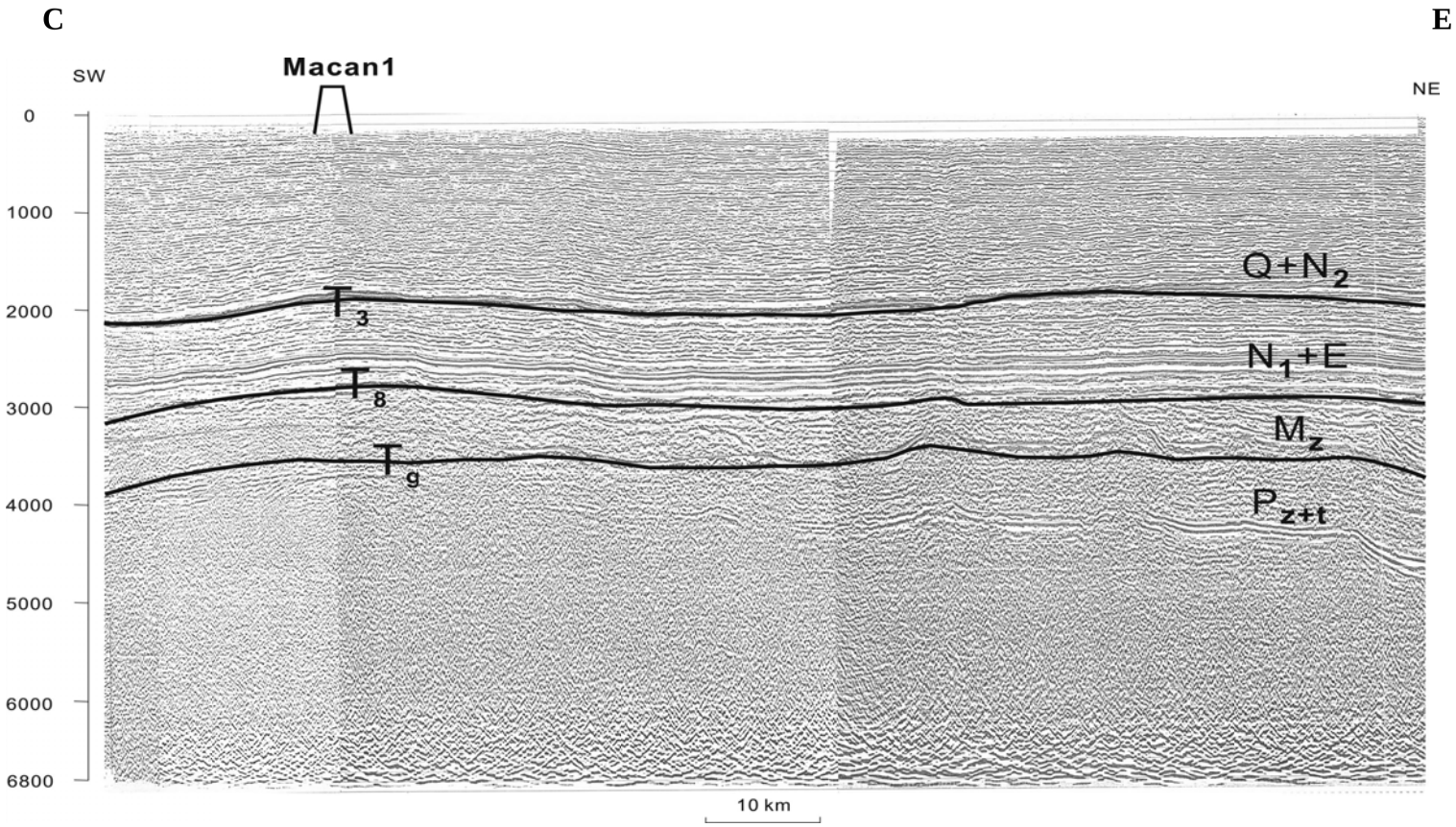

Figure 60. Continued.

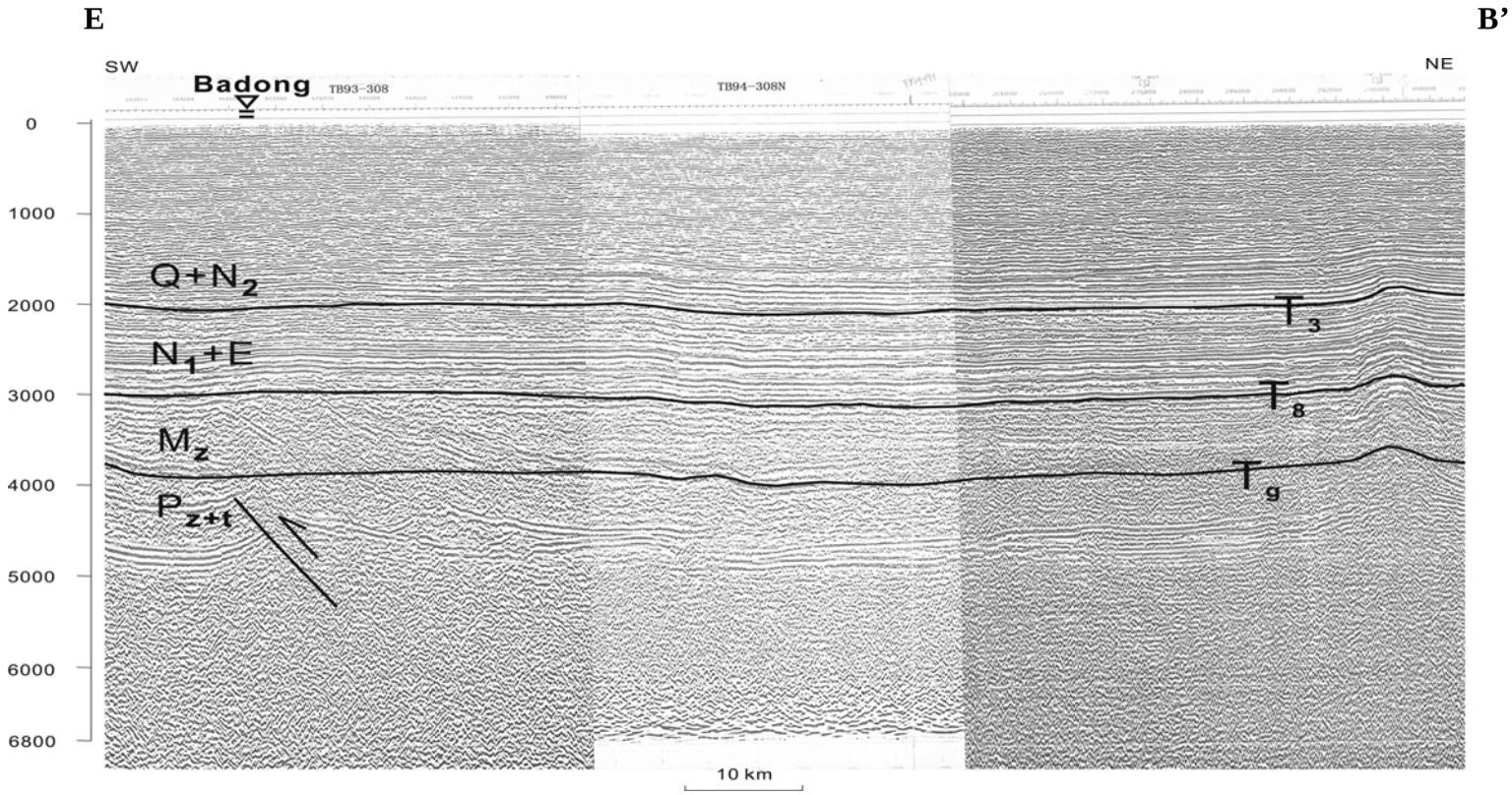

Figure 60. Continued.

overall mechanical behaviour of the two rheologically strong regions separated by a ductile channel is governed by an effective elastic thickness given by $(Tc^3 + Tm^3)^{1/3}$ (*McNutt et al.,* 1988*,* where *Tc* denotes upper crust rigidity and *Tm* the upper mantle rigidity). In our case, it is slightly more than the effective elastic thickness of the stronger of the two layers. Thus, our moderate rigidity model of the Tibetan Plateau is plausible.

The elastic thickness *Te* stays more-or-less constant for the area south of the Zhangbo suture and for India. Some of the young N-S trending rifts extend across the Zhangbo suture into the Greater Himalayas (*Armijo* 1986*; Armijo et al.,* 1989*; Monlar and Lyon-Caen,* 1989), a region underlain by the bending Indian-continental mantle (*Lyon-Caen and Molnar,* 1984*; Zhao et al.,* 1993). Lithospheric thinning did not occur here. Extension south of Tibet is interpreted to have resulted from a combination of dextral strike-slip and high topography along the Main Frontal Thrust (*Armijo et al.,* 1989*; McCaffre and Nabelek,* 1998).

Our results indicate that the interior and eastern parts of Tibet have the same elastic strength as the Yangtze block and the eastern lowlands. If central and eastern Tibet originally belonged to the same tectonic unit as the Yangtze block or if the two units have been welded together long enough, then the similarity in the lithospheric strength of these two tectonic units is understandable. However, northern Tibet was not accreted to the Sino-Korean and Yangtze blocks until the Late Jurassic or Early Cretaceous (*Yin,* 1996), and the Lhasa block was not welded to the Yangtze block until the Eocene or later. The flat topography over large areas in the interior of the plateau has been taken to indicate a lack of Tertiary shortening. However, studies show that thrusting and sinistral strike-slip faulting have been dominant here and are equivalent to crustal deformation processes in Tibet since the Eocene, *viz*. thrusting and strike-slip faulting north and east of the Indus-Zangbo suture (*Achache et al.,* 1984*; Métivier et al.,* 1998). In the central plateau between the Kunlun and Tanggula ranges, strong folding of the Paleogene red beds unconformably overlain by more gently-warped Neogene sandstones implies a certain amount of shortening (*Chang et al.,* 1986*; Yin et al.,* 1994)**.**

The drastic variations in *Te* in the study area and with it the local strength reduction near the suture zone are related to differences in the composition of the crust or to the presence of major faults, as suggested by *Burov et al.* (1998). Our 2D model shows that the lithospheric strength beneath the West Kunlun and Altyn ranges decreases gradually from the Tarim Basin to the Tibetan Plateau.

Gravity modelling is not unique. Thus, it is possible to model the gravity lows in the foredeeps as caused by either flexure of a relatively weak plate with denser sediments, or flexure of a stiffer plate with lighter sediments. Fortunately, density logs remove some of the ambiguities in the interpretation.

As we have demonstrated along the western Yecheng-Songxi profile, the West Kunlun Fault may be interpreted as a zone of intra-plate deformation within the Eurasian plate, while the Altyn Tagh Fault is assumed to cut through the crust into the mantle. This result is unexpected given the presumed intra-plate setting of the Altyn Tagh, but is supported by other studies (*Edward and Arnaud,* 1999; *Lyon-Caen and Molnar,* 1984; *Wittling et al.,* 1998). It is possible that the Altyn Tagh Fault extends south of the West Kunlun Fault and then merges with the Karakorum Fault in western Tibet (*Tapponnier et al*., 2001). It might also have been initiated or reactivated by lower crustal flow as the material moves to the east and south where a leakage exists (*Westaway,* 1995). Fig. 61 is a cartoon showing the relationship between the subducting Tarim plate, the West Kunlun Fault, and the strike-slip Altyn Tagh Fault down to the deep lithosphere.

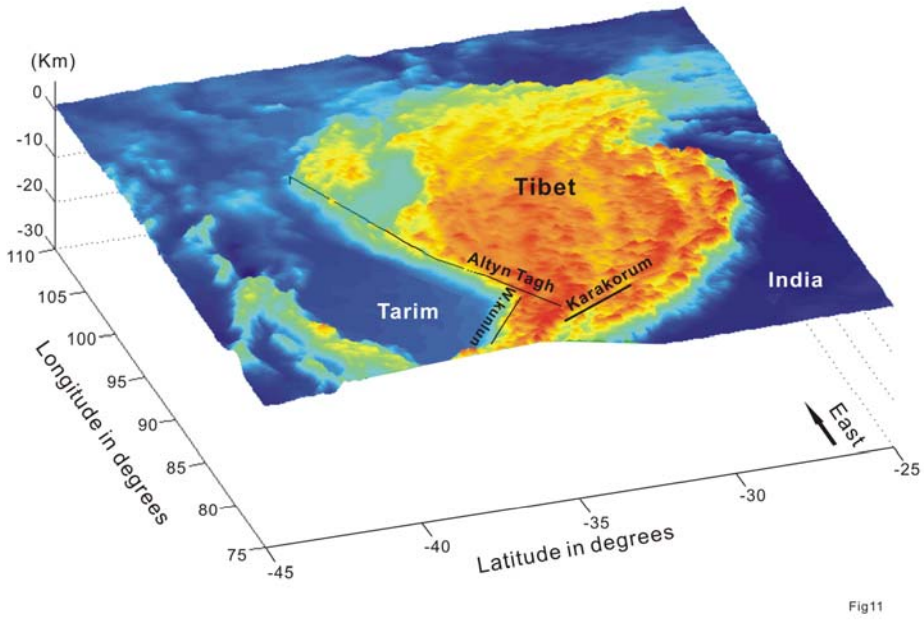

Figure 61. Lithospheric model showing the relationship between the subducting Tarim plate, the overthrusting West Kunlun Fault and the strike-slip Altyn Tagh Fault. W. Kunlun denotes the West Kunlun Fault. 'Slab' is the subducting Tarim plate.

Our results show that the southeastern Tarim block is underthrusted more and deeper along the Altyn Tagh Fault than the southwestern Tarim block along the West Kunlun Fault. We interpret this to imply blocking of southward subduction by the strong crust of the Qaidam Basin, which led to severing of the Tarim lithosphere. The large strike-slip component of the Altyn Tagh Fault is responsible for the fact that the foredeep basins along the south-eastern Tarim are not well-developed. In contrast, the Tarim plate is subducted to a lesser extent along the West Kunlun Fault. Stronger flexure of the Tarim plate here led to a more advanced development of foredeep basins.

The deep structure and kinematics of deformation of the Tien Shan has been quantified using high-resolution gravity data and topographic data to define and quantify their lateral heterogeneities in order to test various hypotheses for dynamic processes in the crust and mantle responsible for the lateral heterogeneities in our study area. On the basis of our model, the elastic thickness in the Tarim and Zungar basins and on the Kazakh Platform is about 40-45 km, which reflects a moderately rigid continental plate. The elastic thickness at the edge of the Tarim Basin is moderate and is consistent with previous results (*Braitenberg et al.,* 2003; *Jin*, 1996; *Lyon-Caen and Molnar*, 1984), but is somewhat lower than that of *Watts* (2001). The reasons for the latter observation have been discussed above (see section 5.2). Analogously, the Zungar Basin has an old and stable continental core (*Yin and Nie*, 1996) and the sediments at its centre are undeformed (*Li*, 2002). Its southern margin where it underthrusts the Tien Shan has a larger sediment thickness and was weakened by tectonic thinning (*Li and Mooney*, 1998; *Sun et al.*, 2004), presumably as a result of stripping of the top of the Zungar crust during underthrusting, while the core of the block remains more rigid than the 40-45 km elastic thickness suggests. The Kazakh Plat - form, an old and stable continental structure, has a moderate rigidity according to our model. Because India is subducted northwards, the northern part of the southern margin of central Asia is under NE-directed compression. The rigid Tarim plate propagated this compressional stress and deformed only at its edge where it underthrusts the Tien Shan to the north (e.g., *Neil and Houseman*, 1997). In turn, the southward motion of the rigid Zungar and Kazakh plates is resisted by the Asian continent. Underthrusting of the Tarim, Zungar, and Kazakh plates beneath the Tien Shan (e.g., *Allen et al*., 1999; *Li and Mooney*, 1998; *Me' tivier and Gaudemer*, 1998; *Molnar et al.,* 1994*; Sun et al.*, 2004; *Thompson et al.,* 2002) has led to a low elastic thickness of the Tien Shan ranges relative to its vicinity, a result which is supported by a higher S-wave velocities for the lower crust of the Tarim

Basin than for the Tien Shan (*Kosarev et al.*, 1993; *Roecker et al.*, 1993). Thus, it is reasonable that our best-fit model to the gravity data across the Tien Shan requires that the plate be very weak or be broken at the thrust faults.

Figure 62 shows the epicentre distribution of earthquakes with magnitudes larger than 2.5 for the period January 1, 1978 to May 31, 2003, recorded by the China Digital Seismic network (*CDSN*). It indicates that seismicity is low within the Tarim, Zungar, and Kazakh plates where the lithosphere has a large elastic thickness, but is high in the Tien Shan ranges where the lithospheric elastic thickness is small. This result supports our gravity model, which suggests underthrusting along the margins of the rigid Tarim, Zungar and Kazakh plates beneath the Tien Shan while their centres remain undeformed. A similar situation occurs in the Tibetan Plateau and to the north (*Braitenberg et al.,* 2003).

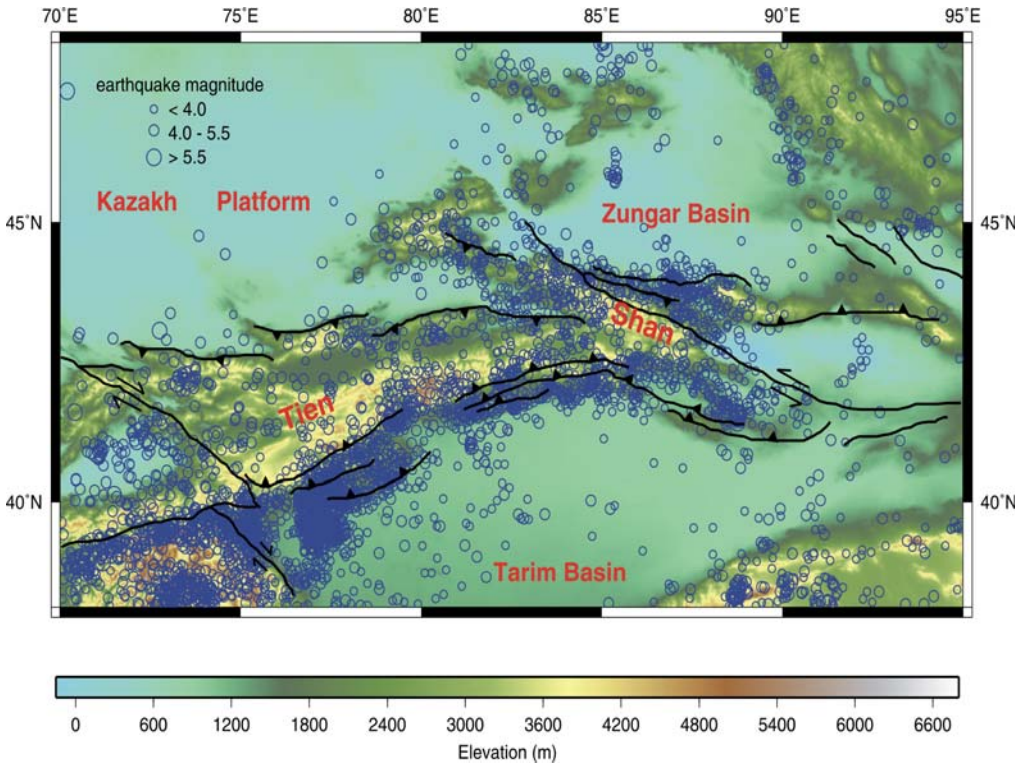

Figure 62. Epicentre distribution of earthquakes with magnitudes larger than 2.5 for the period January 1, 1978 to May 31, 2003, recorded by the China Digital Seismic network (*CDSN*).

Our results indicate that deformation of the Tien Shan is dominated by underthrusting of the Tarim, Zungar, and Kazakh plates. The amount of this underthrusting may be sufficient to support the topography of the Tien Shan. Thrusting skimmed the lighter and lower-density crust of the thrusting plates off their lithosphere to become surface loads of the Tien Shan lithosphere, leading to crustal thickening there. The series of surficial reverse faults along the northern and southern margins of the Tien Shan support our interpretation (*Thompson et al.,* 2002). Loading caused the Tien Shan lithosphere to bend, which in turn increased uplift. The stress field calculations demonstrate that the Tien Shan mountain belt is under large compression (*Jin,* 1997).

Deformation of the Tien Shan is not uniform according to our model. It is confined to the crust along profiles 1 and 2, while it involves the entire lithosphere along profiles 3 and 4. Figures 63 and 64 are 3-D cartoons illustrating this point. Current shortening of the Tien Shan occurs throughout the entire lithosphere in western Tien Shan but is only crustal in the eastern Tien Shan. Geological features and GPS measurements also suggest that shortening across the Tien Shan is inhomogeneous and spatially dependent (*Burchfiel et al.*, 1999; *Wang et al.*, 2001). We hypothesize that the oblique collision between India and Asia (*Tapponnier et al.,* 2001), which is a major controlling factor for the tectonic development of Central Asia, may have also resulted in inhomogeneous deformations in the Tien Shan. Thus, uplift of the Tien Shan orogenic belt is a consequence of the Indian-Asian collision. Although this conclusion is not new, our Bouguer gravity analysis provides a means to map the thrusting occurring beneath the Tien Shan.

Our result is not consistent with previous gravity studies (*Burov et al.,* 1990). By analysing $1° \times 1°$ gravity data in Central Asia, *Burov et al.* (1990) showed that western Tien Shan is close to Airy isostatic equilibrium and eastern Tien Shan is over-compensated. They suggest that in the eastern Tien Shan a deep mass, or a dynamic flow in the asthenosphere, is pulling down the mountain root. Further investigations, especially deep seismic imagery, are need for a better understanding of mountain building and intra-continental deformations.

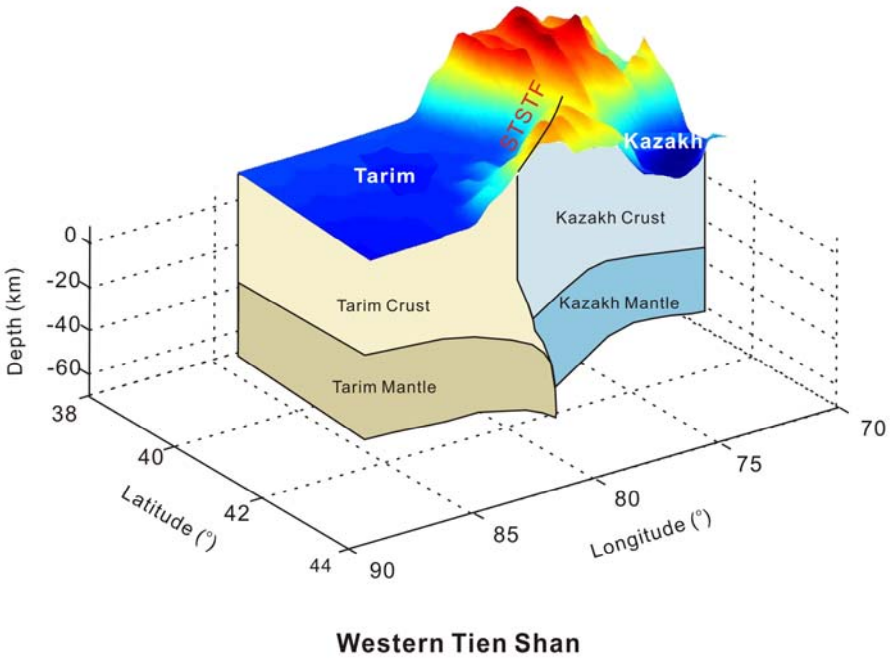

Figure 63. Schematic lithospheric model of western Tien Shan showing the relationship between the underthrusting Tarim plate (labeled *Slab*) and the Southern Tien Shan Thrust Fault (STSTF).

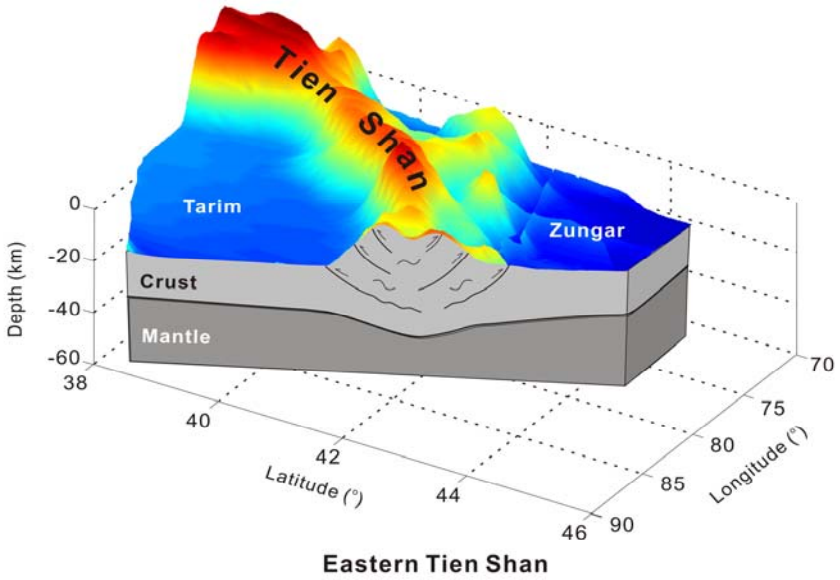

Figure 64. Schematic lithospheric model of eastern Tien Shan showing deformations confined to the crust beneath the Tien Shan and crustal thinning due to the underthrusting Tarim and Zungar plates.

Two important geodynamic questions are: Why are deformations in the Tien Shan distributed without a dominant direction (*e.g.*, *Tapponnier and Molnar,* 1979*; Yin et al.,* 1998*; Burchfiel et al.,* 1999)? And why does the Tien Shan stress field (*Flesch et al.,* 2001) differ significantly from the regional stress field that includes the boundary force and the gravity potential stress field?

We compared our stress results with the World Stress Field released in 2003 (Fig. 48b; *Reinecker et al.,* 2003*; Zoback,* 1992). This comparison shows that our local stress field is consistent with the direction and style of major deformations in the Tien Shan area and it is also in good agreement with the world stress field derived using various methods.

Our results suggest that almost the entire Tien Shan region is dominated by a large local compressional stress field. The largest compressional zone is in central and parts of western Tien Shan. Earthquake focal mechanisms, geodetic GPS measurement and geological evidence also suggest that the Tien Shan is still under compression and that thrust faulting is prevalent (*Abdraknmatov et al.,* 1996*; England and Molnar,* 1997*a; Holt et al.,* 2000). We propose that thrusting of the old and strong Tarim Basin and Kazakh Platform (and Zungar Basin) towards the Tien Shan occurs at large depths beneath the mountain belt, causes crustal thickening, and leads to compression in the Tien Shan. Our gravity study shows positive Airy isostatic anomalies in the Tien Shan (compression) which can be interpreted as a result of intracontinental subduction due to local compressional stress.

In our model, extensional stress is predicted in the Tarim and Zungar basins and in the Kazakh Platform. The direction of extension is roughly consistent with the background stress field caused by the Indian-Eurasian collision. This is consistent with the dominance of normal faults in the Tarim and Zungar basins found in industrial seismic profiles (*Li,* 2002), and with weak extension in these basins as suggested by the Harvard CMT earthquake focal mechanism solutions (Fig. 65). Thus, the old and strong Tarim and Zungar basins and the Kazakh Platform must have resisted deformation and thickening, and the strong Tarim plate must have transferred the stress into the Tien Shan causing reactivation and significant crustal thickening of this mountain range (*e.g.*, *England and Houseman,* 1985).

Figure 55 shows that major strike-slip stress is found along the flanks of the Tien Shan mountain belt, where most historical large-magnitude earthquakes occurred (*e.g.*, *Molnar*

and Ghose, 2000). The extension compensates for the compression due to plate interaction, and stress transition from compression to extension takes place along the flanks. Thus, we suggest that the flanks of the Tien Shan are tectonically more active than the mountain ridges themselves. This result is supported by other studies (*Burchfiel et al.,* 1999*; Thompson et al.,* 2002).

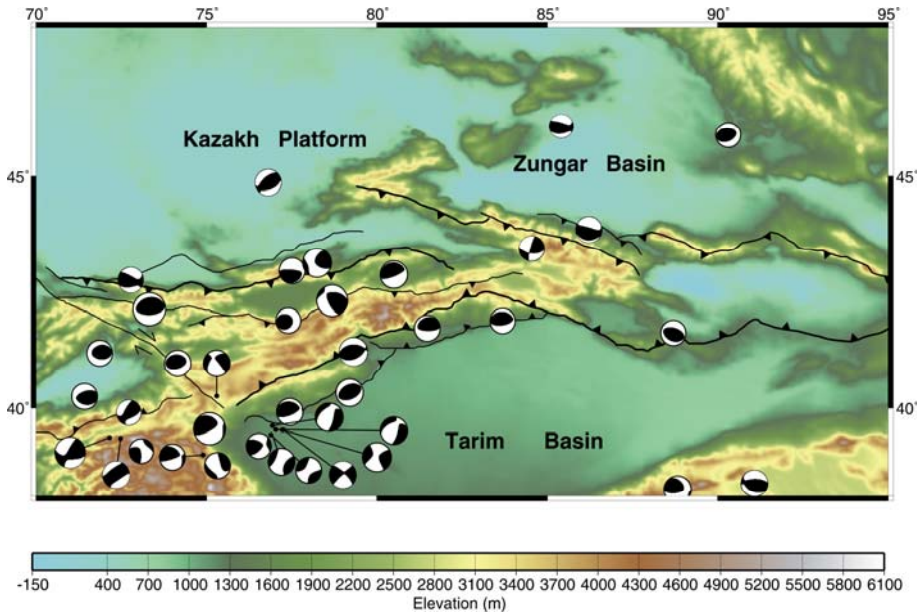

Figure 65. Earthquake focal mechanism solutions (*Harvard, CMT*) and major faults in the Tien Shan area.

We estimated the stress field resulting from a number of possible tectonic forces acting on Tien Shan in order to determine which force exerts dominant control on the intra-continental stress field. Our analysis demonstrates that the flexural stress field resulting from bending of the lithosphere beneath the Tien Shan is the major contributor to the total stress field. This implies that *local* stress due to high topography and surface loading rather than *regional* stress resulting from the collision between India and Eurasia plays the dominant role in the Tien Shan lithospheric deformations. The stress fields derived from topography and flexure are negligible until significant uplift of the Tien Shan occurred. The larger this uplift becomes, the more important are the roles of flexural and topographic stresses in the total stress field. The magnitude of the flexural stress due to lithospheric bending and of stress resulting from gravity potential can be significantly larger than the

background stress (*i.e.*, the stress field due to the collision between India and Eurasia) because they accumulate in response to loads at long geological time scales.

In order to understand how the old orogenies are correlated with the reactivation of the Tien Shan under the present tectonic regime, *Jin* (1997) calculated the stress field in Central Asia assuming that the Tien Shan had either 0 %, 20 % or 40 % of the present topography. His results show that there is no concentration of stress at the location of the Tien Shan in the first case, that a small deflection occurs in the elastic plate underlying the proto-Tien Shan in the second case, and that plate flexural stress is concentrated beneath the Tien Shan in the last case. We propose that it is the combination of intra-continental subduction and a low-relief mountain belt that concentrates the stress from the elevated plateau and triggered the latest rejuvenation of this mountain belt.

Chapter 7. Conclusions

Based on the elastic plate theory, two- and three-dimensional governing equations of flexure are analysed in the space domain in order to test various hypotheses for dynamic processes in the crust and mantle responsible for the lateral heterogeneity in the study area of this dissertation in Central Asia.

Our results show that the mechanical strength of the lithosphere in Central Asia varies significantly from a weak elastic strength of less than 15 km to a moderate strength of 40-50 km. Weak zones exist in the major mountain building areas such as Tien Shan, Altyn Shan, West Kunlun Shan, Qilian Shan and the Indus-Zhangbo suture zone. Stronger zones are located in the less-deformed basin areas such as the Tarim, Qaidam, and Sichuan basins as well as certain topographically lower areas (< 2500 m). The lithosphere beneath Tibet has a small elastic thickness, varying from Te = 10 to 40 km. The low values in the Indus-Zhangbo suture zone (with Te values of 10-20 km or less) are ascribed to weakening during the suturing process. Although the Tibetan crust is much thicker than average, it has a low elastic thickness. This is consistent with other geophysical observations which suggest the presence of a partially molten mid-lower crust (*e.g., Nelson et al.,* 1996; *Owens and Zandt,* 1997). In contrast, the central and the eastern parts of the Tibetan plateau has a considerable elastic strength close to the elastic thickness of the lowlands. Even the steep transition from the high eastern plateau to its adjacent lowland (Sichuan Basin) does not significantly weaken the lithosphere underneath. Our mechanical modelling of the elastic strength of the lithosphere is implemented in the space domain to accommodate the considerably irregular geometries of the tectonic units due to strong compression from the Indian plate, and the calculated strength variations generally fit well to the geometric shapes of the various tectonic blocks. The final RMS fit between the observed and calculated Bouguer gravity is 24.54 mgal.

Our results suggest that the Altyn Tagh Fault possibly cuts through the entire lithosphere of Asia and accommodates motion between Asia and the Tibetan plate. If the Altyn Tagh Fault defines the northern boundary of the eastward extrusion of Tibet, then the extrusion will not only affect the Tibetan crust, but also its upper mantle lithosphere. In contrast, it is possible to fit the gravity data across the West Kunlun Fault with a continuous elastic plate model. Our preferred model for the lithospheric structure beneath the West Kunlun Fault includes a moderately stiff Tarim plate underthrusting the Tibetan Plateau. The Eurasian plate is weakened during this underthrusting from an elastic thickness of about

40-45 km in the Tarim Basin to about 30-35 km beneath the Tibetan Plateau. Based on our models, the magnitude and scale of the southward-directed underthrusting of the Tarim plate is larger in the west beneath the West Kunlun Fault than in the east beneath the highland north of the Altyn Tagh Fault.

Modelling of gravity data suggests that the Tarim, Zungar, and Kazakh plates are moderately rigid. The Tien Shan ranges have an elastic thickness lower than that of its adjacent areas. Gravity data across the eastern Tien Shan are best fitted by a continuous elastic plate model. Here, the moderately stiff Tarim and Zungar plates underthrust the mountains, thereby weakening from *Te* = 40-45 km to about 20-25 km beneath the mountains. In contrast, we suggest that the Southern Tien Shan Thrust Fault cuts the entire lithosphere at the western Tien Shan. Here, shortening involves the crust as well as the upper mantle lithosphere.

Our analysis of the stress field for a number of possible tectonic forces acting on the Tien Shan demonstrates that the flexural stress field resulting from bending of the lithosphere beneath the Tien Shan is the major contributor to the total stress field. This implies that the local stress due to high topography and surface loading but not regional stress resulting from the collision between India and Eurasia plays the most important role in Tien Shan lithospheric deformations. The stress fields derived from topography and flexure are negligible until significant uplift of the Tien Shan occurred. The larger this uplift becomes, the more important are the roles of flexural and topographic stresses in the total stress field. The magnitude of the flexural stress due to lithosphere bending and of stress resulting from gravity potential can be significantly larger than the background stress (*i.e.*, the stress field due to the collision between India and Eurasia) because they accumulate over time. Furthermore, our stress field results in Tien Shan suggest that the Tien Shan uplifted in response to a local intra-continental stress field.

References

Abdrakhmatov, K. Y., Aldazhanov, S. A., Hager, B. H., Hamburger, M. W., Herring, T. A., Kalabarv, K. B., Makarov, V. I., Molnar, P., Panasyuk, S. V., Prilepin, M. T., Reilinger, R. E., Sadybakasov, I. S., Souter, B. J., Trapeznikov, Y. A., Tsurkov, V. Ye. and A. V. Zubovich, 1996. Relatively recent construction of the Tien Shan inferred from GPS measurements of present-day crustal deformation rates, *Nature*, 384, 450–453.

Achache, J., Courtillot, V. and Y. X. Zhou, 1984. Paleogeographic and tectonic evolution of southern Tibet since middle Cretaceous time: new paleomagnetic data and synthesis, *J. Geophys. Res.,* 89, 10,311–10,339.

Ahern, J. L. and R. C. Ditmars, 1985. Rejuvenation of continental lithosphere beneath an intracratonic basin, *Tectonophys*., 120, 21-35.

Akhber, D. Ya. and I. V. Mushkin, 1976. The Kyzyl-Kum-Nurata deep fault, Tien Shan, *Geotectonics*, 10, 58-62.

Allegre C. J. and 35 others, 1984. Structure and evolution of the Himalaya-Tibet orogenic belt, *Nature*, 307, 17-22.

Allen, M. B., Windley, B. F., Zhang, C., Zhao, Z. Y. and G. R. Wang, 1991. Basin evolution within and adjacent to the Tien Shan Range, NW China, *J. Geol. Soc. Lond.,* 148, 369-378.

Allen, M. B., Vincent, S. J. and P. J. Wheeler, 1999. Late Cenozoic tectonics of the Kepingtage thrust zone Interactions of the Tien Shan and Tarim Basin, Northwest China, *Tectonics*, 18, 639-654.

Alsdorf, D. and K. D. Nelson, 1999. Tibetan satellite magnetic low: Evidence for widespread melt in the Tibetan crust? *Geology*, 27, 943-946.

An, Z. S., Kutzbach, J. E., Prell, W. L. and S. C. Porter, 2001. Evolution of Asian monsoons and phased uplift of the Himalaya-Tibetan plateau since Late Miocene times, *Nature,* 411, 62-66.

Armijo, R., 1986. Quaternary extension in southern Tibet: Field observations and tectonic implications, *J. Geophys. Res.*, 91, 13,803-13,872.

Armijo, R., Tapponnier P. and T. Han, 1989. Late Cenozoic right-lateral strike-slip faulting in southern Tibet, *J. Geophys. Res.*, 1989, 94, 2787-2838.

Armstrong, G. D. and A. B. Watts, 2001. Spatial variations in *Te* in the southern Appalachians, eastern United states, *J. Geophys. Res*., 106, 22,009-22,026.

Arnauld, N. O., Vidal, P., Tapponnier, P., Matt, W. M. and W. M. Deng, 1992. The high K_2O volcanism of northwestern Tibet: Geochemistry and tectonic implication, *Earth and Planet. Sci. Lett.,* 111, 351-367,

Avouac, J. P. and G. Peltzer, 1993. Active tectonics in southern Xinjing, China: Analysis of terrace riser and normal fault scarp degradation along the Hotan-Qira fault system, *J. Geophys. Res.,* 98, 21,773-21,807.

Avouac, J. P., Tapponnier, P., Bai, M., You, H., Wang, G., 1993. Active faulting and folding in the northern Tien Shan and rotation of Tarim relative to Dzungaria and Kazakhstan, *J. Geophys. Res.*, 98, 6755-6769.

Bailey, G. B. and P. D. Anderson, 1982. Applications of Landsat imagery to problems of petroleum exploration in the Qaidam basin, China, *Amer. Assoc. Petrol. Geol. Bull.*, 66, 1348-1354.

Bank, R. J., Parker, R. L. and S. P. Huetis, 1977. Isostatic compensation on a continental scale: local versus regional mechanisms, *Geophys. J. R. Astron. Soc.*, 51, 431-452.

Barazangi, M. and J. Ni, 1982. Velocities and propagation characteristics of Pn and Sn waves beneath the Himalayan Arc and Tibetan Plateau: Possible evidence for underthrusting of Indian continental lithosphere beneath Tibet, *Geology*, 10, 179-185.

Barth, S., Oberli, F. and M. Meier, 1994. Th-Pb versus U-Pb isotope systematics in allanite from co-genetic rhyolite and granodiorite: implications for geochronology, *Earth and Planet. Sci. Lett.*, 124, 149-159.

Bechtel, T. D., Forsyth, D. W. and C. J. Swain, 1987. Mechanisms of isostatic compensation in the vicinity of the East African Rift, Kenya, *Geophys. J. R. Astron. Soc.,* 90, 445-465.

Bechtel, T. D., Forsyth, D. W., Sharpton, V. L. and R. A. Grieve, 1990. Variations in effective elastic thickness of the North American lithosphere, *Nature*, 343, 636.

Beloussov, V. V. and 11 others, 1980. Structure of the lithosphere along deep seismic sounding profile: Tien Shan-Pamirs-Karakorum-Himalayas, *Tectonophysics*, 70, 193-221.

Bendick, R., Bilham, R., Freymueller, J., Larson, K. and G. Yin, 2000. Geodetic evidence for a low slip rate in the Altyn Tagh Fault System, *Nature,* 404, 69-72.

Bendick, R. and R. Bilham, 2001. How perfect is the Himalaya? *Geology*, 29, 791-794.

Bilham, R., Larson, K. and J. Freymueller, 1997. GPS measurements of present-day convergence across the Nepal Himalaya, *Nature*, 386, 61-64.

Bilham, R., Gaur, V. K. and P. Molnar, 2001. Himalayan seismic hazard, *Science*, 293, 1,442-1,444.

Bird, P., 1978. Initiation of intracontinental subduction in the Himalaya. *J. Geophys. Res.*, 83, 4975-4987.

Bourjot, L. and B. Romanowicz, 1992. Crust and upper mantle tomography in Tibet using surface waves, *Geophys. Res. Lett.*, 19, 881-884.

Boulin, J., 1981. Afghanistan structure, Greater India concept and eastern Tethys evolution, *Tectonophysics,* 72, 261-287.

Braitenberg, C., Wang, Y., Fang, J., Hsu, H. T. 2003. Spatial variations of flexure parameters over the Tibet-Quighai Plateau, *Earth Planet. Sci. Lett.*, 205, 211-224.

Brown, L. D., Zhao, W., Nelson, K. D., Hauck, M., Alsdorf, D., Ross, A., Cogan, M., Clark, M., Liu, X. and J. Che, 1996. Bright spots, structure, and magmatism in southern Tibet from INDEPTH seismic reflection profiling, *Science*, 274, 1,688-1,690.

Brown, E. T., Bourles, D. L., Burchfiel, B. C., Deng, Q., Li, J., Molnar, P., Raisbeck, G. M. and F. Yiou, 1998. Estimation of slip rates in the southern Tien Shan using cosmic ray exposure dates of abandoned alluvial fans, *Geol. Soc. Am. Bull.*, 110, 377–386.

Bukharin A. K., 1978. Two tectonic sectors of the southern Tien Shan geosynclinal system, *Int. Geol. Rev.*, 3, 331-334.

Bullen, M. E., Burbank, D. W., Abdrakhmatov, K. Y. and J. Garver, 2001. Late Cenozoic tectonic evolution of the northwestern Tien Shan: Constraints from magnetostratigraphy, detrital fission track, and basin analysis, *Geol. Soc. Am. Bull*., 113, 1544-1559.

Burbank, D. W., 1996, Bedrock incision, rock uplift and threshold hillslopes in the northwestern Himalayas, *Nature*, 379, 505-510.

Burbank, D. W., Derry, L. A. and C. France-Lanord, 1993. Reduced Himalayan sediment production 8 Myr ago despite an intensified monsoon, *Nature*, 364, 48-50.

Burbank, D. W., McLean, J. K., Bullen, M., Abdrakhmatov, K. Y., Miller, M. M., 1999. Partitioning of intermontane basins by thrust-related folding, Tien Shan, Kyrgyzstan, *Basin Res.,* 11, 75–92.

Burchfiel, B. C. and L. H. Royden, 1985. North-south extension within the convergent Himalayan region, *Geology*, 13, 679-682.

Burchfiel, B. C., Deng, Q., Molnar, P., Royden, L., Wang, Y. and W. Zhang, 1989. Intracrustal detachment within zones of continental deformation, *Geology*, 17, 748-752.

Burchfiel, B. C., Brown, E. T., Deng, Q., Feng, X., Li, J., Molnar, P., Shi, J., Wu, Z. and H. You, 1999. Crustal shortening on the margins of the Tien Shan, Xinjiang, China, *Int. Geol. Rev*., 41, 665– 700.

Burov, E. B., Kogan, M., Lyon-Caen, H. and P. Molnar, 1990. Gravity anomalies, the deep structure, and dynamic processes beneath the Tien Shan, *Earth Planet. Sci. Lett.,* 96, 367-383.

Burov E. B., Lobkovsky L. I., Cloetingh, S. and A. M. Nikishin, 1993. Continental lithosphere folding in Central Asia (Part II): constraints from gravity and topography, *Tectonophysics*, 226, 74-87.

Burov, E. B. and M. Diament, 1995. The effective elastic thickness (*Te*) of continental lithosphere: What does it really mean? *J. Geophys. Res*., 100, 3905-3927.

Burov, E. B., Jaupart, C. and J. C. Mareschal, 1998. Large-scale crustal heterogeneities and lithospheric strength in cratons, *Earth and Planet., Sci. Lett.*, 164, 205-219.

Burtman, V. S., Skobelev, S. F. and P. Molnar, 1996. Late Cenozoic slip on the Talasa-Ferghana Fault, the Tien Shan, Central Asia, *Geol. Soc. Am. Bull.,*108, 1004–1021.

Calais E., Vergnolle, M., Déverchère, J., Lukhnev, A., San'kov, V. and S. Amarjargal, 2002. Are post-seismic effects of the M = 8.4 Bolnay earthquake (July 12, 1905) still influencing GPS velocities in the Mongolia-Baikal area? *Geophys. J. Int.,* 149, 157-168.

Carroll, A. R., Graham, S. A., Hendrix, M. A., Yang, D. and D. Zhou, 1995. Late Paleozoic tectonic amalgamation of northwestern China: sedimentary record of the northern Tarim, northwestern Junggar Basins, *Bull. Geol. Soc. Am*., 107, 571-594.

Chang, C. and 26 others, 1986. Preliminary conclusions of the Royal Society and Academia Sinica 1985 geotraverse of Tibet, *Nature*, 323, 501–507.

Chemenda, A. I., Burg, J. P. and M. Mattauer, 2000. Evolutionary model of the Himalaya-Tibet system: geopoem based on new modelling, geological and geophysical data, *Earth and Planet. Sci. Lett.*, 174, 397-409.

Chen, J., Burbank, D. W., Scharer, K., Sobel, E., Yin, J., Rubin, C. M. and R. Zhao, 2002. Magnetostratigraphy of the Upper Cenozoic strata in the southwestern Chinese Tian Shan: rates of Pleistocene folding and thrusting, *Earth and Planet. Sci. Lett.,* 195, 113-130.

Chen, L., Booker, J. R., Jones, A. G., Wu, N., Unsworth, M. J., Wei, W. and H. Tan, 1996. Electrically conductive crust in southern Tibet from INDEPTH magnetotelluric surveying, *Science,* 274, 1,694-1,696.

Chen, W. P. and P. Molnar, 1981. Constraints on the seismic wave velocity structure beneath the Tibetan Plateau and their tectonic implications, *J. Geophys. Res*., 86, 5937-5962.

Chen, Z., 1985. 1:2,000,000 geologic map of Xinjiang Uygur Autonomous region, China, *Geological Publishing House,* Beijing (in Chinese).

Chen, C., Lu, H., Jia, D., Cai, D. and S. Wu, 1999. Closing history of the southern Tianshan oceanic basin, western China: an oblique collisional orogeny, *Tectonophysics*, 302, 23–40.

Chen, Z., Burchfiel, B.C., Liu, Y., King, R.W., Royden, L. H., Tang, W., Wang, E., Zhao, J. and X. Zhang, 2000. Global Positioning System measurements from eastern Tibet and their implications for India/Eurasia intercontinental deformation. *J. Geophys. Res.,* 105, 16,215-16,277.

China Digital Seismic Network (CDSN), http://www.eq-igp.ac.cn/bdcndsn/index.html

Coblentz, D. D. and R. M. Richardson, 1996. Analysis of the South American intraplate stress field, *J. Geophys. Res*., 101, 8643-8657.

Coblentz, D. D., Sandiford, M., Richardson, R. M., Zhou, S. and R. Hillis, 1995. The origins of the intraplate stress field in continental Australia, *Earth and Planet. Sci. Lett.*, 133, 299-309.

Coleman, M. E. and K.V. Hodges, 1998. Contrasting Oligocene and Miocene thermal histories from the hanging wall and footwall of the South Tibetan detachment in the central Nepal Himalaya from $^{40}Ar/^{39}Ar$ thermochronology, Marsyandi Valley, central Nepal, *Tectonics*, 17, 726-740.

Cowgill, E., Yin, A., Rumelhart, P., Xiao-Feng, W. and Z. Qing, 1997. Kinematics of the central Altyn Tagh fault system, NW China, *EOS, Trans. AGU*, 78, Fall Meet. suppl., F173.

Darby, B. J. and B. D. Ritts, 2002. Mesozoic contractional deformation in the middle of the Asian tectonic collage: the enigmatic Western Ordos fold-thrust belt, China, *Earth and Planet. Sci. Lett*., 205, 13-24.

Delville, N., Arnaud, N., Montel, J. M., Brunel, M. and E. Sobel, 2001. Paleozoic to Cenozoic deformation along the Altyn-Tagh Fault in the Altun Shan range, Eastern Qilian Shan, NE Tibet China, in Hendrix, M. S. and Davis, G. A., ed., Paleozoic and Mesozoic Tectonic Evolution of Central and Eastern Asia: From Continental Assembly to Intracontinental Deformation, *Geol. Soc. Am. Mem.* 194, 269-292.

DeMets, C., Gordon, R. G., Argus, D. F. and S. Stein, 1990. Current plate motions, *Geophys. J. Int*., 101, 425-478.

DeMets, C., Gordon, R. G., Argus, D. F. and S. Stein 1994. Effect of recent revisions to the geomagnetic reversal time scale on estimates of current plate motions, *Geophys. Res. Lett*., 21, 2191–2194.

Derry L. A. and C. France-Lanord, 1996. Neogene Himalayan weathering history and river $^{87}Sr/^{86}Sr$: Impact on the marine Sr record, *Earth and Planet. Sci. Letts.*, 142, 59-76.

Dewey, J. F. and K. C. Burke, 1973. Tibetan, Variscan, and Precambrian basement reactivation: Products of continental collision, *Journal of Geology*, 81, 683-692.

Dewey, J. F., Shackleton, R. M., Chang, C. F. and Y. Y. Sun, 1988. The tectonic evolution of the Tibetan plateau, *Phil. Trans. R. Soc. London A,* 327, 379-413.

Dupont-Nivet, G., Butler, R. F., Yin, A. and X. Chen, 2002. Paleomagnetism indicates no Neogene rotation of the Qaidam Basin n Tibet during Indo-Asian collision, *Geology,* 30, 263-266.

Edwards, M. A. and T. M. Harrison, 1997. When did the roof collapse? Late Miocene north-south extension in the High Himalaya revealed by Th-Pb monazite dating of the Khula Kangri granite, *Geology*, 25, 543-546.

Edward, R. S. and N. Arnaud, 1999. A possible middle Paleozoic suture in the Altyn Tagh, NW China, *Tectonics,* 18, 1, 64-74.

England, P. and G. Houseman, 1985. Role of lithospheric strength heterogeneities in the tectonics of Tibet and neighbouring regions, *Nature,* 315, 297-301.

England, P. C. and G. Houseman, 1989. Extension during the continental convergence, with application to the Tibet Plateau, *J. Geophys. Res.,* 94, 17,561-17,579.

England, P. and P. Molnar, 1997. The field of crustal velocity in Asia calculated from Quaternary rates of slip on faults, *Geophys. J. Int*., 130, 551-582.

England, P. and P. Molnar, 1997a. Active deformation of Asia: From kinematics to dynamics, *Science*, 278, 647-650.

Faure M, Lin, W. and L. N. Breton, 2001. Where is the North China-South China block boundary in eastern China? *Geology*, 29, 119-122.

Fielding, E., Isacks, B., Barazangi, M. and C. Duncan, 1994. How flat is Tibet? *Geology,* 22, 163-167.

Finlayson, D. P., Montgomery, D. R. and B. Hallet, 2002. Spatial coincidence of rapid inferred erosion with young metamorphic massifs in the Himalayas, *Geology,* 30, 219–222.

Flesch, L. M., Haines, A. J. and W. E. Holt, 2001. Dynamics of the India-Eurasia collision zone, *J. Geophys. Res.*, 106, 16435-16460.

Forsyth, D. W.,1985. Subsurface loading and estimates of the flexural rigidity of continental lithosphere, *J. Geophys. Res.,* 90, B14, 12,623-12,632.

Gahagan, L. M., Scotese, C. R., Royer, J.-Y., Sandwell, D. T., Winn, J. K., Tomlins, R. L., Ross, M. I., Newman, J. S., Mueller, R. D., Mayes, C. L., Lawver, L. A. and C. E. Heubeck, 1988. Tectonic fabric of the ocean basins from satellite altimetry data, in C.R. Scotese and W. W. Sager (eds), Mesozoic and Cenozoic Plate Reconstructions, *Tectonophysics,* 155, 1-26.

Gansser, A., 1974. Himalaya, in Mesozoic-Cenozoic Orogenic Belts, edited by A. M. Spencer, *Geological Society of London, Scottish Academic Press*, Edinburgh, 267-278.

Gao, J., Li, M. S., Xiao, X. C., Tang, Y. G. and G. Q. He, 1998. Paleozoic tectonic evolution of the Tien Shan Orogen, northwestern China, *Tectonophysics*, 287, 213-231.

Garzanti, E., Casnedi, R. and F. Jadoul, 1986. Sedimentary evidence of a Cambro-Ordovician orogenic event in the northwestern Himalaya, *Sediment. Geol*., 48, 237-265.

Gehrels, G., Yin, A., Chen, X. and X. Wang, 2000. Constraints on the offset of the eastern Altyn Tagh fault, western China: *EOS, Trans. AGU* 81, F1093.

Gilder, S. and V. Courtillot, 1997. Timing of the north-south China collision from new Middle to Late Mesozoic palaeomagnetic data from the North China Block, *J. Geophys. Res.,* 102, 17,713-17, 727.

Griot, D., Montagner, J. P. and P. Tapponnier, 1998. Phase velocity structure from Rayleigh and Love waves in the Tibet and its neighboring regions, *J. Geophys. Res*., 103, 21, 215-21,232.

Grujic, D., Casey, M., Davidson, C., Hollister, L. S., Kündig, R., Pavlis, T. and S. Schmid, 1996. Ductile extrusion of the High Himalayan Crystalline in Bhutan: evidence from quartz microfabrics, *Tectonophysic*s, 260, 21-43.

Hacker, B. R., Wang, X., Eide, E. A. and L. Ratschbacher, 1996. Qinling-Dabie ultrahigh-pressure collisional orogen: a critical review of existing data and suggestions for future research, An Yin and T.M. Harrison, eds., *The Tectonics of Asia*: Prentice-Hall Publishers, 345-370.

Hacker, B.R., Ratschbacher, L., Webb, L. E., Ireland, T., Walker, D. and S. Dong, 1998. U/Pb zircon ages constrain the architecture of the ultrahigh-pressure Qinling-Dabie Orogen, China, *Earth and Planet. Sci. Lett.*, 161, 215-230.

Hacker, B. R., Ratschbacher, L., Webb, L. E., McWilliams, M., Ireland, T., Dong, S., Calvert, A. and H. R. Wenk, 2000. Exhumation of the ultrahigh-pressure continental crust in east-central China: Late Triassic-Early Jurassic extension. *J. Geophys. Res.,* 105, 13,339-13,364.

Hanson, A. D., 1999. Organic geochemistry and petroleum geology, tectonics and basin analysis of southern Tarim and northern Qaidam basins, northwest China, *Ph. D. dissert*., Stanford University, Stanford California, 388 pp.

Harris, N. and J. Massey, 1994. Decompression and anatexis of Himalayan metapelites, *Tectonics*, 13, 1,537-1,546.

Harrison, T. M., Copeland, P., Kidd, W. S. F. and A. Yin, 1992. Raising Tibet, *Science* 255, 1,663-1,670.

Harrison, T. M., Ryerson, F. J., Le-Fort, P., Yin, A., Lovera, O. M. and E. J. Catlos, 1997. A late Miocene-Pliocene origin for the central Himalayan inverted metamorphism, *Earth and Planet. Sci. Lett.*, 146, 1-2, E1-E7.

Hendrix, M. A., Dumitra, T. A. and S. A. Graham, 1994. Late Oligocene-early Miocene unroofing in the Chinese Tien Shan: An early effect of the India-Asia collision, *Geology*, 22, 487-490.

Herquel, G., Wittlinger, G. and J. Guilbert, 1995. Anisotropy and crustal thickness of northern Tibet, new constraints of tectonic modelling, *Geophys. Res. Lett.,* 22, 1,925-1,928.

Hirn, A., Nercessian, A, Sapin, M., Jobert, G., Xin, X. Z., Yuan, G. E. and T. J. Wen, 1984. Lhasa block and bordering sutures: a continuation of the 500-km Moho traverse through Tibet, *Nature*, 307, 25-27.

Hodges, K., Bowring, S., Davidek, K., Hawkins, D. and M. Krol, 1998. Evidence for rapid displacement on Himalayan normal faults and the importance of tectonic denudation in the evolution of mountain ranges, *Geology*, 26, 483-486.

Hodges, K., 2000. Tectonics of the Himalaya and southern Tibet from two perspectives, *Geol. Soc. Am. Bull*., 112, 324–350.

Hoffman, P. F., 1991. Did the breakout of Laurentia turn Gondwanaland inside out? *Science*, 252, 1409-1412.

Holt, W. E. and T. C. Wallace, 1990. Crustal thickness and upper mantle velocities in the Tibetan Plateau region from the inversion of regional Pn1 waveforms: Evidence for a thick upper mantle lid beneath southern Tibet, *J. Geophy. Res.,* 95, 12,499-12,526.

Holt, W. E. and A. J. Haines, 1993. Velocity fields in deforming Asia from the inversion of earthquake-released strains, *Tectonics*, 12, 1-20.

Holt, W. E., Chamot-Rooke, N., Le Pichon, X. and A. J. Haines, 2000. Velocity field in Asia inferred from Quaternary fault slip rates and Global Positioning System observations, *J. Geophys. Res*., 105, 19,185–19,209.

Hsu, K. J., Sun, S. and J. L. Li, 1988. Huanan Alps, not South China platform, *Scientia Sinica* (*Series B*), 1, 109-119 (in Chinese).

Hua, Q., 1992. 33 Ma rock was first found in North Tarim Xinjiang, *Science Bull.,* 7, 627-630 (in Chinese).

Huang, H. Ch., 1996. *Geology of Qaidam Basin and its Petroleum Prediction*, *Geological Publishing house,* Beijing, 30-36 (in Chinese).

Jahn, B. M., Zhou, X. H. and J. L. Li, 1990. Formation and tectonic evolution of southeastern China and Taiwan: isotopic and geochemical constraints, *Tectonophysics*, 183, 145-160.

Jain, A. K., Kumar, D., Singh, S., Kumar, A. and N. Lal, 2000. Timing, quantification and tectonic modelling of Pliocene-Quaternary movements in the NW Himalaya: evidence from fission track dating, *Earth and Planet. Sci. Lett*., 179, 437-451.

Ji, X. and P. J. Coney, 1985. Accreted terranes of China, in Howell, D.G. (ed.), *Tectono-stratigraphic Terranes of the Circum-Pacific Region. Circum-Pacific Council for Energy and Mineral Resources Earth Science Series*, Number 1. Houston, Texas, U.S.A., 349-361.

Jia, C., Yao, H., Wi, G. and L. Li, 1991. Plate tectonic evolution and characteristics of major tectonic units of Tarim basin, In: The Tarim Basin, ed., Tong, X. and Liang, D., *Xingjiang Scientific Publishing House, Wulumiqi*, 207-255 (in Chinese).

Jin, Y., McNutt, M. K. and Y. S. Zhu, 1994. Evidence from gravity and topography data for folding of Tibet, *Nature,* 371, 669-674.

Jin, Y., McNutt, M. K. and Y. S. Zhu, 1996. Mapping the descent of Indian and Eurasian plates beneath the Tibetan plateau from gravity anomalies, *J. Geophys. Res.,* 101, B5, 11,275-11,290.

Jin, Y., 1997. State-of-Stress and Rheology of Tibet and its Vicinity from Gravity Anomalies and Numerical Models, *MIT*, *Ph. D. dissert.*, 40-46.

Jin, Y. and X. D. Jiang, 2002. Lithosphere Dynamics, *Scientific Publishing House,* Beijing, 59-67 (in Chinese).

Jolivet, M., Brunel, M., Seward, D., Xu, Z., Yang, J., Roger, F., Tapponnier, P., Malavieille, J., Arnaud, N. and C. Wu, 2001. Mesozoic and Cenozoic tectonics of the northern edge of the Tibet plateau: fission-track constraints, *Tectonophysics*, 343, 111-134.

Judge, A. V. and M. K. McNutt, 1991. The relationship between plate curvature and elastic plate thickness: A study of the Peru-Chile trench, *J. Geophys. Res*., 96, 16,625-16,640.

Kaneoka, I. and M. Kono, 1981. $^{40}Ar/^{39}Ar$ dating of Himalayan rocks from the Mount Everest region, *J. Geophys. Res.*, 49, 207-211.

Kao, H., Gao, R., Rau, R. J., Shi, D. N., Chen, R. Y., Guan, Y. and F. Wu, 2001. Seismic image of the Tarim Basin and its collision with Tibet, *Geology*, 29, 575-578.

Karner, G. D. and A. B. Watts, 1983. Gravity anomalies and flexure of the lithosphere at mountain ranges. *J. Geophys. Res*., 88, 10,449-10,477.

Kind, R., Ni, J., Zhao, W., Wu, J., Yuan, X., Zhao, L., Sandvol, E., Reese, C., Nabelek, J. and T. Hearn, 1996. Evidence from earthquake data for a partially molten crustal layer in southern Tibet, *Science*, 274, 1,692-1,694.

Kind, R., Yuan, X., Saul, J., Nelson, D., Sobolev, S. V., Mechie, J., Zhao, W., Kosarev, G., Ni, J., Achauer, U. and M. Jiang, 2002. Seismic images of crust and upper mantle beneath Tibet: evidence for Eurasian plate subduction, *Science,* 298, 1219-1221.

Klootwijk, C. T., Gee, J. S., Pierce, J. W., Smith, G. M. and P. L. McFadden, 1992. An early India-Asia contact: palaeomagnetic constraints from Ninetyeast Ridge, ODP Leg 121, *Geology*, 20, 395-398.

Kogan, M. G. and M. K. McNutt, 1993. Gravity field over northern Eurasia and variations in the strength of the upper mantle, *Science,* 259, 473-479.

Kong, X., Yin, A. and T. M. Harrison, 1997. Evaluating the role of pre-existing weaknesses and topographic distributions in the Indo-Asian collision by use of a thin-shell numerical model, *Geology*, 25, 527-530.

Kosarev, G. L., Peterson, N. V., Vinnik, L. P. and S. W. Roecker, 1993. Receiver functions for the Tien Shan analog broadband network: Contrasts in the evolution of structures across the Talasso-Fergana fault, *J. Geophys. Res*., 98, 4437-4448.

Larson, K. M., Burgmann, R., Bilham, R. and J. T. Freymueller, 1999. Kinematics of the India-Eurasia collision zone from GPS measurements, *J. Geophys. Res.,* 104, 1,077-1,093.

Lavé, J. and J. P. Avouac, 2000. Active folding of fluvial terraces across the Siwalik Hills, Himalayas of central Nepal. *J. Geophys. Res.*, 105, 5735-5770.

Le Fort, 1996. Evolution of the Himalaya, in *The Tectonic Evolution of Asia*, Yin, A and T. M. Harrison (eds.), Cambridge University Press, 95-109.

Leven, V., Park, J., Brandon, T. M. and W. Menke, 2000. Thinning of the upper mantle during late Paleozoic Appalachian orogenesis, *Geology*, 3, 239–242.

Li, C. Y., Liu, Y., Zhu, B. C., Feng, Y. M. and H. C. Wu, 1978. Structural evolution of Qinling and Qilian Shan, In Scientific Papers on Geology and International Exchange, *Geological Publishing House,* Beijing, 174-197 (in Chinese).

Li, J. G., 2002. Geology of Tarim and Zungar basins and their Petroleum Prediction, *Shengli Oil Complex, Dongying* (internal publication, in Chinese).

Li, S. L. and W. D. Mooney, 1998. Crustal structure of China from deep seismic sounding profiles, *Tectonophysics,* 288, 105-113.

Li, Y.,1990. An apparent polar wander path from the Tarim block, China, *Tectonophysics,* 181, 31-41.

Liu, L. B. and M. D. Zoback, 1992. The effect of topography on the state of stress in the crust: application to the site of the Cajon Pass Scientific Drilling Project, *J. Geophys. Res.,* 97, 5095-5108.

Liu X., Yao, J. X. and Y. Wang, 1997. The review of tectonic attribution of the Tarim plate, *Geological Review,* 43, 1-9 (in Chinese).

Lowry, A. R. and R. B. Smith, 1994. Flexural rigidity of the Basin and Range-Colorado Plateau-Rocky Mountain transition from coherence analysis of gravity and topography, *J. Geophys. Res.,* 99, B10, 20,123-20,140.

Lu, X. X., Zhang, Y. W. and Z. Jin, 1997. Reservoir formation cycle of Tarim Basin, *Chinese Science Bulletin*, 42, 245-247 (in Chinese).

Lyon-Caen, H. and P. Molnar, 1983. Constrains on the structure of the Himalayas from an analysis of gravity anomalies and a flexural model of the lithosphere, *J. Geophys. Res*., 88, 8171-8192.

Lyon-Caen, H. and P. Molnar, 1984. Gravity anomalies and the structure of western Tibet and the southern Tarim basin, *Geophys. Res. Lett.,* 11, 1251-1254.

Makovsky, Y., Klemperer, S. L., Ratschbacher, L., Brown, L. D., Li, M., Zhao, W. and F. Meng, 1996. INDEPTH wide-angle reflection observation of P-wave-to-S-wave conversion from crustal bright spots in Tibet, *Science*, 274, 1690-1691.

Masek, J. G., Isacks, B. L. and E. J. Fielding, 1994. Rift flank uplift in Tibet: Evidence for a viscous lower crust, *Tectonics,* 13, 2, 659-667.

Mattauer, M., Matte, P., Malavieille, J., Tapponnier, P., Maluski, H., Xu, Q., Lun, L. and Q. Tang, 1985. Tectonics of the Qinling belt: Build-up and evolution of eastern Asia, *Nature*, 317, 496-500.

McAdoo, D. C. and D. T. Sandwell, 1985. Folding of oceanic lithosphere, *J. Geophys. Res*., 90, B10, 8563-8569.

McCaffrey, R. and J. Nabelek, 1998. Role of oblique convergence in the active deformation of the Himalayas and southern Tibet plateau, *Geology*, 26, 691-694.

McGarr, A., 1988. On the state of lithospheric stress in the absence of applied tectonic forces, *J. Geophys. Res.*, 93, 13609-13617.

McNamara, D. E., T. J. Owens, P. G. Silver and F. T. Wu, 1994. Shear wave anisotropy beneath the Tibetan plateau, *J. Geophys. Res*., 99*,* 13,655-13,665.

McNamara, D. E., T. J. Owens and W. R. Walter, 1995. Observations of regional phase propagation across the Tibetan Plateau, *J. Geophys. Res*., 100, 22,215-22,229.

McNutt, M. K. and H. W. Menard, 1978. Lithospheric flexure and uplifted atolls, *J. Geophys. Res*., 83 , 1206-1212.

McNutt, M. K. and H. W. Menard, 1982. Constraints on yield strength in the oceanic lithosphere derived from observations of flexure, *Geophys. J. R. Astron. Soc.,* 71, 363-394.

McNutt, M. K., 1983. Influence of plate subduction on isostatic compensation in northern California, Tectonics, 2, 399-415.

McNutt, M. K., Diament, M. and M. G. Kogan, 1988. Variations of elastic plate thickness at continental thrust belts, *J. Geophys. Res.,* 93, B8, 8825-8838.

Meigs, A. J., Burbank, D. W. and R. A. Beck, 1995. Middle-late Miocene [>10 Ma] formation of the Main Boundary Thrust in the Western Himalaya, *Geology*, 23, 423-426.

Meng, Q. R. and G. W. Zhang, 1999. Timing of collision of the north and south China blocks: Controversy and reconciliation, *Geology*, 27, 2, 123-126.

Me′ tivier, F. and Y. Gaudemer, 1997. Mass transfer between eastern Tien Shan and adjacent basins (central Asia), constraints on regional tectonics and topography, *Geophys. J. Int.*, 128, 1-17.

Me′ tivier, F. and Y. Gaudemer, 1998. Mass transfer between eastern Tien Shan and adjacent basins (central Asia): constraints on regional tectonics and topography, *Geophys. J. Int*., 128, 1–17.

Meriaux, A., Tapponnier, P., Ryerson, F. J., Ven der Woerd, J., King, G., Meyer, B., Finkel, R. and M. Caffee, 1997. Application of cosmogenic ^{10}Be and ^{26}Al dating to neo-tectonics of the Altyn Tagh fault in central Asia, *EOS, Trans. AGU*, 78, Fall Meeting Suppl., F173.

Meyer, B., Tapponnier, P., Gaudemwe, Y., Peltzer, G., Guo, S. and Z. Chen, 1996. Rate of left-lateral movement along the easternmost segment of the Altyn Tagh fault, east of 96°E (China), *Geophys. J. Int.,* 124, 29-44.

Molnar, P. and P. Tapponnier, 1975. Cenozoic tectonics of Asia: effects of a continental collision, *Science*, 189, 419-426.

Molnar, P. and P. Tapponnier, 1978. Active tectonics of Tibet, *J. Geophys. Res.,* 83, 5361-5375.

Molnar, P., 1984. Structure and tectonics of the Himalaya, *Ann. Review of Earth and Planet. Sci.*, 12, 489–518.

Molnar, P., 1988. A review of geophysical constraints on the deep structure of the Tibetan plateau, the Himalayas and Karakorum, and their tectonics, *Phil. Trans. R. Soc. Lond*., A326, 33-88.

Molnar, P. and H. Lyon-Caen, 1989. Fault plane solutions of earthquakes and active tectonics of Tibetan plateau and its margins, *Geophys. J. Int.,* 99, 123-153.

Molnar, P., Brown, E. T., Burchfiel, B. C., Deng, Q., Feng, X., Li, J., Raisbeck, G. M., Shi, J., Wu, Z., Yiou, F. and H. You, 1994. Quaternary climate change and the formation of river terraces across growing anticlines on the north flank of the Tien Shan, China, *J. Geol.*, 102, 583–602.

Molnar, P. and S. Ghose, 2000. Seismic moments of major earthquakes and the rate of shortening across the Tien Shan, *Geophys. Res. Lett., 27*, 2377-2380.

Moore, J. C., Diebold, J., Fisher, M. A., Sample, J., Brocher, T., Talwani, M., Ewing, J., Huene, R. V., Rowe, C., Stone, D., Stevens, C. and D. Sawyer, 1991. EDGE deep seismic reflection transect of the eastern Aleutian arc-trench layered lower crust reveals underplating and continental growth, *Geology*, 19, 420-424.

Mukhin, P. A., Abdullaev, K. A., Minaev, V. E., Khristov, S. E. and S. A. Egamberdyev 1989. Paleozoic geodynamics of Central Asia, *Int. Geol. Rev.*, 31, 1073-1083.

NEIC, 2003. USGS National Earthquake Information Center, http://neic.usgs.gov/neis/epic/epic.html.

Neil, E. A. and G. A. Houseman, 1997. Geodynamics of the Tarim Basin and the Tian Shan in Central Asia, *Tectonics,* 16, 571-584.

Nelson, K. D., Zhao, W. J., Brown, L. D., Kuo, J., Che, J., Liu, X., Klemperer, S. L., Makovsky, Y., Meissner, R., Mechie, J., Kind, R., Wenzel, F., Ni, J., Nabelek, J., Chen, L., Tan, H., Wei, W., Jones, A. G., Booker, J., Unsworth, M., Kidd, W. S. F., Hauck, M., Alsdorf, D., Ross, A., Cogan, M., Wu, C. D., Sandvol, E. and M. Edwards, 1996. Partially molten middle crust beneath southern Tibet: Synthesis of Project INDEPTH results, *Science*, 274, 1684-1687.

Ni, J. and M., Barazangi, 1984. Seismotectonics of the Himalayan collision zone: Geometry of the underthrusting Indian plate beneath Himalaya, *J. Geophys. Res.*, 89, 1147-1164.

Nie, S., Rowley, D. B. and A. M. Ziegler, 1990. Constraints on the location of the Asian microcontinents in the Palaeo-Tethys during the Late Palaeozoic, In: W. S. McKerrow and C. R. Scotese, eds., *Palaeozoic Biogeography and Palaeogeography,* Geological Society of London, Memoir 12, 397-410.

Noble, S. R. and M. P. Searle, 1995. Age of crustal melting and leucogranite formation from U-Pb zircon and monazite dating in the western Himalaya, Zanskar, India, *Geology*, 23, 1135-1138.

Northern Arizona University home page, 2001. http://jan.ucc.nau.edu/~rcb7/globaltext2.html.

Oberhänsli, R., Marlinotli, G., Schmid, R. and X. Liu, 2002. Preservation of primary volcanic textures in the ultrahigh-pressure terrain of Dabie Shan, *Geology*, 30, 699-702.

Okabe, M., 1979. Analytical expressions for gravity anomalies due to homogeneous poly-hedral bodies and translations into magnetic anomalies, *Geophysics,* 44, 730-741.

Owens, T. J. and G. Zandt, 1997. The implications of crustal property variations on models of Tibetan Plateau evolution, *Nature*, 387, 37-43.

Parker, R. L. 1972. The rapid calculation of potential anomalies, *Geophys, J. R. astr. Soc.*, 31, 447-455.

Patzelt, A., Huami, L., Wang, J. and E. Appel, 1996. Palaeomagnetism of Cretaceous to Tertiary sediments from southern Tibet: evidence for the extent of the northern margin of India prior to the collision with Eurasia, *Tectonophysics*, 259, 259-284.

Pêcher, A., 1991. The contact between the Higher Himalayan crystallines and the Tibetan sedimentary series: Miocene large-scale dextral shearing, *Tectonics*, 10, 587-598.

Peltzer, G. and P. Tapponnier, 1988. Formation and evolution of strike-slip faults, rifts and basin during the Indian-Asia collision: An experimental approach, *J. Geophys. Res.*, 93, 15,085-15,117.

Peltzer, G., Tapponnier, P. and R. Armijo, 1989. Magnitude of Late Quaternary left-lateral displacements along the north edge of Tibet, *Science*, 246, 1285-1289.

Petit, C., Déverchère, J., Calais, E., San'kov, V. and D. Fairhead, 2002. Deep structure and mechanical behavior of the lithosphere in the Hangai-Hövsgöl region, Mongolia: New constraints from gravity modeling, *Earth and Planet. Sci. Lett.,* 197, 133-149.

Powers, P. M., Lillie, R. J. and R. S. Yeats, 1998. Structure and shortening of the Kangra and Dehra Dun reentrants, Sub-Himalaya, India, *Geol. Soc. Am. Bull*., 110, 1010-1027.

Powell, C. McA., 1993. Assembly of Gondwanaland - Open forum, in Findlay, R. H., Unrug, R., Banks, M. R., and Veevers, J. J., eds., *Gondwana Eight: Assembly, Evolution and Dispersal,* Balkema, Rotterdam, 218-237.

Qinghai BGM (Qinghai Bureau of Geology and Mineral Resource), 1989. Geology History of Qinghai Region, *Geological Publishing House*, 79-88 (in Chinese).

Ratschbacher, L., Hacker, B. R., Webb, L. E., McWilliams, M. O., Ireland, T., Dong, S., Calvert, A., Chateigner, D. and H. R. Wenk, 2000. Exhumation of the ultrahigh-pressure continental crust in East-Central China: Cretaceous and Cenozoic unroofing and the Tan-Lu Fault, *J. Geophys. Res*., B6, 105, 13,308-13,338.

Reigber, B., Michel, G. W., Galas, R., Angermann, D., Klotz, J., Chen, J. Y., Papschev, A., Arslanov, R., Tzurkov, V. E. and M. C. Ishanov, 2001. New space geodetic constraints on the distribution of deformation in Central Asia, *Earth and Planet. Sci. Lett.,* 191, 157-165.

Reinecker, J., Heidbach, O. and B. Mueller, 2003. The 2003 release of the World Stress Map (available online at www.world- stress-map.org).

Ren, J. X., Wang, Z. X., Chen, B. W. and C. Jiang, 1999. Tectonic Map of China, *Geological Publishing House,* Beijing (in Chinese).

Revenaugh, J. and S. A. Sipkin, 1994. Mantle discontinuity structure beneath China, *J. Geophys. Res.*, 99, 21,911-21,927.

Richardson, R. M., Solomon, S. C. and N. H. Sleep, 1976. Intraplate stress as an indicator of plate tectonic driving forces, *J. Geophys. Res.*, 81, 1847-1856.

Ritts, B. D. and U. Biffi, 2001. Mesozoic northeast Qaidam basin: response to contractional reactivation of Qilian Shan, and implications for extent of Mesozoic intracontinental deformation in central Asia, In Hendrix, M. S. and Davis, G. A., ed., Paleozoic and Mesozoic Tectonics of Central Asia -- From Continent Assembly to Intracontinental Deformation, *Geol. Soc. of Am. Mem.* 194, 293-316.

Ritts, B. D., Darby, B. J. and T. Cope, 2001. Early Jurassic extensional basin formation in the Daqing Shan segment of the Yinshan belt, northern North China Block, Inner Mongolia, *Tectonophysics,* 339, 235-253.

Roecker, S. W., Sabitova, T. M., Vinnik, L. P., Burmakov, Y. A., Golvanov, M. I., Mamatkanova, R. and L. Munirova, 1993. Three-dimensional elastic wave velocity structure of the western and central Tien Shan, *J. Geophys. Res.*, 98, B9, 15,779-15,795.

Rong, Y. and D. D. Jackson, 2000. Kinematics of Tibetan Plateau from GPS measurements (abstract), *EOS Trans. AGU*, Fall Meeting Supplement, F122.

Rong J., Johnson, M. E., Baarli, B. G., Li, W., Su, W. and J. Wang, 2001. Continental island from the Upper Silurian (Ludlow) Sino-Korean Plate, *Chinese Science Bulletin*, 46, 238-241 (in Chinese).

Rothery, D. A. and S. A. Drury, 1984. The neotectonics of the Tibetan Plateau, *Tectonics*, 3, 19-26.

Rowley, D. B., 1996. Age of initiation of collision between India and Asia: a review of stratigraphic data, *Earth and Planet. Sci. Lett.*, 145, 1-13.

Royden, L. and B. C. Burchfiel, 1995. Crustal thickening in eastern Tibet without surface shortening: A natural result of flow within a weak lower crust, *EOS Trans. AGU,* 76, Fall Meeting Supplement, F567.

Royden, L. H., Burchfiel, B. C., King, R. W., Wang, E., Chen, Z., Shen, F. and Y. Liu, 1997. Surface deformation and lower crustal flow in eastern Tibet, *Science*, 276, 788-790.

Rumelhart, P. E., 1999. Cenozoic Basin Evolution of Southern Tarim, Northwestern China: Implications for the Uplift History of the Tibetan Plateau, *Ph. D. dissert*., University of California, Los Angeles, 268 pp.

Sandwell, D. T. and W. H. F. Smith, 1997. Marine gravity anomaly from Geosat and ERS 1 satellite altimetry, *J. Geophys. Res.,* 102, 10,039-10,054.

Savage, W. Z. and R. H. Morin, 2002. Topographic stress perturbations in southern Davis Mountains, west Texas 1. Polarity reversal of principal stress, *J. Geophys. Res.*, ETG5.

Scotese, C. R. and W. W. Sager, 1988. Mesozoic and Cenozoic plate tectonic reconstructions, *Tectonophysics,* 155, 27-48.

Scotese, C. R. and S. F. Barrett, 1990. Gondwana's movement over the south pole during the Palaeozoic: evidence from lithological indicators of climate, in W. S. McKerrow and C. R. Scotese, eds*., Palaeozoic Biogeography and Palaeogeography,* Geological Society of London, Memoir 12, 75-86.

Sengör, A. M. C., 1996. Paleotectonics of Asia: fragments of a synthesis, in An Yin and Mark Harrison (eds.), *The Tectonic Evolution of Asia*, 486-641.

Sheffels, B. and M. K. McNutt, 1986. Role of subsurface loads and regional compensation in the isostatic balance of the Transverse Ranges, California: Evidence for intercontinental subduction*, J. Geophys. Res.,* 91, 6,419-6,431.

Shen, F., Royden, L. H. and B. C. Burchfiel, 2001. Large-scale crustal deformation of the Tibetan Plateau, *J. Geophys. Res*., 106, 6,793-6,816.

Sinha-Roy, S., 1982. Introductions of Tethyan blocks and evolution of Asian fold belt*, Tectonophysics, 82*, 277-297.

Sobel, E. R., 1995. Basin Analysis and Apatite Thermochronology of the Jurassic-Paleogene Western Tarim Basin, *Ph. D. dissert.,* Stanford, California, Stanford University, 308 pp.

Sobel, E. R. and T. A. Dumitru, 1997. Exhumation of the margins of the western Tarim basin during the Himalayan orogeny, *J. Geophys. Res*., 102, 5043-5064.

Sobel, E. R., Arnaud, N., Jolivet, M., Ritts, B. D. and M. Brunel, 2001. Jurassic exhumation history of the Altyn Tagh, NW China. In Hendrix, M. S. and Davis, G. A., eds., *Paleozoic and Mesozoic Tectonics of Central Asia -- From Continent Assembly to Intracontinental Deformation,* Geological Society of America Memoir 194, 247-268.

Song, T. and X. Wang, 1993. Structural styles and stratigraphic patterns of syndepositional faults in a contractional setting; example from Qaidam Basin, northwestern China, *Am. Assoc. Pet. Geol. Bull.*, 77, 102-117.

Song, H. B. and Z. L. Lou, 1995. The study of the basement and deep geological structures of Sichuan Basin, China, *Earth Science Frontiers*, 3-4, 231-237 (in Chinese).

Stephen C. T., Weldon, R. J., Rubin, C. M., Abdrakhmatov, K., Molnar, P. and G. W. Berger, 2002. Late Quaternary slip rates across the central Tien Shan, Kyrgyzstan, central Asia, *J. Geophys. Res.*, 107, ETG 7.

Sun, W. K., 1989. Bouguer Gravity Anomaly Map of the People's Republic of China, Chinese Academy of Geoexploration, Beijing (in Chinese).

Sun, J. M., Zhu, R. X. and J. Bowler, 2004. Timing of the Tianshan Mountains uplift onstrained by magnetostratigraphic analysis of molasse deposits, *Earth Planet. Sci. Lett.*, 219, 239-253

Tapponnier, P. and P. Molnar, 1977. Active faulting and tectonics in China, *J. Geophys. Res.*, 82, 2,905-2,930.

Tapponnier, P. and P. Molnar, 1979. Active faulting and Cenozoic tectonics of the Tien Shan, Mongolia, and Baikal regions, *J. Geophys. Res.*, 84, 3425–3459.

Tapponnier, P., Peltzer, G. and A. Y. Ledain, 1982. Extrusion tectonics in Asia: new insights from simple experiments with plasticine, *Geology,* 10, 611-616.

Tapponnier, P., Peltzer, G. and R. Armijo, 1986. On the mechanics of the collision between India and Asia, Coward, M. P. & Ries, A. C., eds., *Collision Tectonics*, *Geol. Soc. Amer. Special Publication,* 19, 115-157.

Tapponnier, P., Xu, Z. Q., Roger, F., Meyer, B., Arnaud, N., Wittlinger, G. and J. S. Yang, 2001. Oblique stepwise rise and growth of the Tibet Plateau, *Science,* 294, 1671-1677.

Teng, J., Yang, H., Wang, Q., Ge, R., Dong, P., Jia, S. and X. Li, 1991. Hydrocarbon in the Tarim Basin Based on Geophysical Data, *Scientific Publishing House*, Beijing. p. 20 and 60.

Thompson, S. C., Weldon, R. J., Rubin, C. M., Abdrakhmatov, K., Molnar, P. and G. W. Berger, 2002. Late Quaternary slip rates across the central Tien Shan, Kyrgyzstan, central Asia, *J. Geophys. Res.*, 107, ETG7.

Turcotte, D. L., McAdoo, D. C. and J. G. Caldwell, 1978. An elastic-perfectly plastic analysis of the bending of the lithosphere at a trench, *Tectonophysics,* 47, 193-205.

Turcotte, D. L. and G. Schubert 1982. *Geodynamics*: *Application of Continuum Physics to Geological Problems,* John Wiley and Sons, 115-140.

Van der Voo, R., Spakman, W. and H. Bijwaard, 1999. Tethyan subducted slabs under India, *Earth and Planet. Sci. Lett.*, 171, 7-20.

Vannay, J. C. and A. Steck, 1995. Tectonic evolution of the High Himalayan Crystalline and of the Tethyan Zone in Upper Lahul (NW Himalaya, India), *Tectonics*, 14, 253-263.

Vening Meinesz, F. A., 1941. Gravity over the Hawaiian archipelago and over the Madeira area, *K. Ned. Akad. Wet.*, 44.

Walcott, R. I., 1970. Flexure of the lithosphere over the Hawaiian Islands, *Tectonophysics*, 9, 435-446.

Wang, L., 1984. Elastic Theory, *Science Publishing House*, Beijing, 380-385 (in Chinese).

Wang, H., 1985. Atlas of the Paleogeography of China, Institute of Geology, Chinese Academy of Sciences, Wuhan College of Geology, *Cartographic Publishing House*, Beijing, 143 (in Chinese).

Wang, Q., Zhang, P. Z., Freymueller, J. T., Bilham, R., Larson, K. M., Lai, X., You, X., Niu, Z., Wu, J., Li, Y., Liu, J., Yang, Z. and Q. Chen, 2001. Present-day deformation in China constrained by global positioning system measurements, *Science,* 294, 574-577.

Wang, Y. H. and J. C. Mareschal, 1999. Elastic thickness of the lithosphere in the Central Canadian Shield, *Geophys. Res. Lett*. 26, 3033-3036.

Watts, A. B. and J. R. Cochran, 1974. Gravity anomalies and flexure of the lithosphere along the Hawaiian-Emperor seamount chain, *Geophys. J. R. astron. Soc*., 38, 119-141.

Watts, A. B., Bodine, J. H. and M. S. Steckler, 1980. Observations of flexure and the state of stress in the oceanic lithosphere, *J. Geophys. Res.,* 85, 6,369-6,376.

Watts, A. B., Karner, G. D., Wessel, P. and J. Hastings, 1985. Global Gravity Bank System, Technical Report 4, CU-1-85, *Office of Naval Research*, Washington D. C.

Watts, A. B. and U. S. T. Brink, 1989. Crustal structure, flexure, and subsidence history of the Hawaiian Islands, *J. Geophys. Res*., 94, 10,473-10,500.

Watts, A. B. and E. B. Burov, 2003. Lithospheric strength and its relationship to the elastic and seismogenic layer thickness, *Earth and Planet. Sci. Lett.,* 213, 113-131.

Webb, L. E., Graham, S. A., Johnson, C. L., Badarch, G. and M. Hendrix, 1999. Occurrence, age, and implications of the Yagan–Onch Hayrhan metamorphic core complex, southern Mongolia, *Geology*, 27, 143-146.

Wees, J. D. van and S. Cloetingh, 1994. A finite-difference technique to incorporate spatial variations in rigidity and planar faults into 3-D models for lithospheric flexure, *Geophys. J. Int.,* 117, 179-195.

Wei, W., Unsworth, M., Jones, A., Booker, J., Tan, H., Nelson, D., Chen, L., Li, S., Solon, K., Bedrosian, P., Jin, S., Deng, M., Ledo, J., Kay, D. and B. Roberts, 2001. Detection of widespread fluids in the Tibetan crust by magnetotelluric studies, *Science,* 292, 716-718.

Westaway, R., 1995. Crustal volume balance during the India-Eurasia collision and altitude of the Tibetan plateau: A working hypothesis, *J. Geophys. Res.,* 100, 15,173–15,192.

Willett, S. D. and C. Beaumount, 1994. Subduction of Asian lithospheric mantle beneath Tibet inferred from models of continental collision, *Nature,* 369, 642-645.

Wittke, J. H., http://jan.ucc.nau.edu/~wittke/Tibet/Himalaya.html, 2002.

Wittlinger, G., Tapponnier, P., Poupinet, G., Jiang, M., Shi, T. N., Herquuel, G. and F. Masson, 1998. Tomographic evidence for localized lithospheric shear along the Altun fault, *Science,* 282*,* 74-76.

Wu, H., Zhau, R., Liu, C. and C. Chang, 1990. Paleomagnetic observation in North China Block from Late Paleozoic to Triassic, *Acta Geophysical Sinica*, 33, 694-701 (in Chinese).

Xia, X. C. and S. Y. Fang, 2000. Research progress of desert science in China, *Chinese Science Bulletin,* 24, 2209-2213 (in Chinese).

Yang, Q. and Y. Jin, 1984. Integrated Geophysical Data Interpretation of Northern China Basin, *Tech. Rept., Publ. of BGP*, Ministry of Petroleum, P. R. China, 22-30 (in Chinese).

Yang, Z. and J. Besse, 2001. New Mesozoic apparent polar wander path for South China: tectonic consequences, *J. Geophys. Res.,* 106, 8493-8520.

Yang, Z. Y., Chen, Y. Q. and H. Z. Wang, 1986. The Geology of China, *Oxford, Clarendon Press*, 112-135.

Yang, Z. Y., Otofuji, Y.-I., Sun, Z. M. and B. C. Huang, 2002. Magnetostratigraphic constraints on the Gondwana origin of North China: Cambrian/Ordovician boundary results, *Geophys. J. Int.* 151, 1-10.

Yeats, R. S., Nakata, T., Farah, A., Fort, M., Mirza, M. A., Pandey, M. R. and R. S. Stein, 1992. The Himalayan Frontal Fault System, *Annales Tectonicae*, 6, 85-98.

Yin, A. and S. Nie, 1993. Development of the Tan-Lu fault as a transform system during collision of the north and south China blocks, east-central China, *Tectonics*, 12, 801-813.

Yin, A., Harrison, T. M., Ryerson, F. J., Chen, W. J., Kidd, W. S. F. and P. Copeland, 1994. Tertiary structural evolution of the Gangdese thrust system, southeastern Tibet, *J. Geophys. Res.,* 99, B9, 18,175-18,201.

Yin, A., and S. Nie, 1996. A Phanerozoic palinspastic reconstruction of China and its neighboring regions, *The Tectonic Evolution of Asia*, in An Yin and Mark Harrison (eds.), 442- 481.

Yin, A., Nie, S., Craig, P., Harrison, T. M., Ryerson, F. J., Qian, X. and G. Yang, 1998. Late Cenozoic tectonic evolution of the southern Chinese Tien Shan, *Tectonics*, 17, 1-27.

Yin, A., 2000. Mode of Cenozoic east-west extension in Tibet suggests a common origin of rifts in Asia during Indo-Asian collision, *J. of Geophys. Res.*, 105, 21,745-21,759.

Yin A. and T. N. Harrison, 2000. Geologic evolution of the Himalayan-Tibetan orogen, *Annu. Rev. Earth. Planet. Sci*., 28, 211-280.

Yu, Z. and K. M. McNutt, 1995. Development of intracontinental orogens: The Tien Shan, *EOS, Trans*., 76, F567.

Yue, Y. and J. G. Liou, 1999. A two-stage evolution model for the Altyn Tagh fault, China, *Geology*, 27, 227–230.

Yue, Y., Ritts, B. D. and S. Graham, 2001. Initiation and long-term slip history of the Altyn Tagh fault, *International Geology Review*, 43, 1087-1093.

Zeng, R. S. and R. Gao, 1995. A review on the studies of lithosphere structures and dynamics in Tibetan Plateau, *China National Report on Seismology and Physics of the Earth's Interior for the XXIst General Assembly of IUGG,* China Meteorological Press, Beijing, 41-53 (in Chinese).

Zhai, G. M., 1992. Petroleum Geology of China, *Petroleum Industry Publishing House*, Beijing, 33-59 (in Chinese).

Zhang, P. Z., 2003. Late Cenozoic tectonic deformation in the Tien Shan and foredeep basins, *Science Bull.*, 48, 2499-2500 (in Chinese).

Zhao, R., Liu, C. and H. Song, 1997. Comprehensive geological study report and appraisal of the Tarim exploration area, internal publication of the *Geological Research Institute* of the *Shengli Oil Complex*, 23-35.

Zhao, W. J., Nelson, K. D. and Project INDEPTH Team, 1993. Deep seismic reflection evidence for continental underthrusting beneath southern Tibet, *Nature,* 366, 9, 557-559.

Zhao, W. L. and W. J. P. Morgan, 1987. Injection of Indian crust into Tibetan lower crust; a two-dimensional finite element model study, *Tectonics,* 6, 489-504.

Zhou S. W., 1992. China Provincial Geography, *Foreign Languages Press,* Beijing, 58-80 (in Chinese).

Zhou, Z. and P. Chen, 1990. Paleontology, Stratigraphy, and Geologic Evolution of the Tarim Basin, *Science Publishing House,* Beijing, 78-117 (in Chinese).

Zhu, L. and D. V. Helmberger, 1998. Moho offset across the northern margin of the Tibetan Plateau, *Science*, 281, 1170-1172.

Zoback, M. L., Zoback, M. D., Adams, J., Assumpcao, M., Bell, S., Bergman, E. A., Blürnling, P., Brereton, N. R., Denham, D., Ding, J., Fuchs, K., Gay, N., Gregersen, S., Gupta, H. K., Gvishiani, A., Jacob, K., Klein, R., Knoll, P., Magee, M., Mercier, J. L., Müller, B. C., Paquin, C., Rajendran, K., Stephansson, O., Suarez, G., Suter, M., Udias, A., Xiao, Z. H. and M. Z. Zhin, 1989. Global patterns of tectonic stress, *Nature*, 28, 291-296.

Zoback, M. L., 1992. First- and second-order patterns of stress in the lithosphere: The world stress map project, *J. Geophys. Res.,* 97, 11,703-11,728.

Zuber, M. T., 1987. Compression of oceanic lithosphere: An analysis of intraplate deformation in the Central Indian basin, *J. Geophys. Res*., 92, 4817-4825.

Zuber, M. T., Bechtel, T. D. and D. W. Forsyth, 1989. Effective elastic thickness of the lithosphere and mechanisms of isostatic compensation in Australia, *J. Geophys. Res.,* 94, 9353-9367.

Zusammenfassung

In dieser Dissertation soll eine Studie der Deformationsprozesse der Lithosphäre in Zentralasien vorgestellt werden. Diese wird durch zahlreiche spektakuläre tektonische Einheiten, wie das Tibetanische Plateau, den intrakontinentalen Gebirgsgürtel des Tien Shan oder das Altyn Tagh *strike-slip* Störungssystem. Ein Großteil des bearbeiteten Gebiets liegt in der Volksrepublik China. Darüber hinaus wurden im Süden Nepal und Nordindien erfasst, im Norden die Mongolei. Das Relief im Arbeitsgebiet wurde und wird bis heute im Zuge der Konvergenz zwischen Indien und Eurasien tief greifend modifiziert. Topographische Hochlagen bilden das Tibetanische Plateau sowie der Tien Shan. Das Tibetanische Plateau ist die größte Hochebene der Welt und weist eine durchschnittliche Höhe von ca. 5000 m bei einer Krustenmächtigkeit von ca. 70 km. Der Tien Shan ist eines der höchsten, jüngsten und seismisch aktivsten intrakontinentalen Gebirge in Zentralasien. In dieser Dissertation wird versucht die folgenden Fragen zu beantworten: In welchem Umfang schwächen tektonische Einheiten der oberen Kruste, die im Zuge der Konvergenz zwischen Indien und Eurasien gebildet wurden, die unterlagernde Lithosphäre? Wie wird das Tibetanische Plateau entlang seiner nördlichen Grenze gravitativ kompensiert? Setzen sich die Altyn Tagh oder West Kunlun Störungen als vertikale *strike-slip* Systeme durch die Kruste bis in die Mantellithosphäre fort und stellen somit fundamentale Plattengrenzen dar? Welche dynamischen Prozesse in Kruste und Mantel sind verantwortlich für die intrakontinentale Gebirgsbildung im Bereich des Tien Shan? Wie kann das lokale Stressfeld im Tien Shan charakterisiert werden und was bewirkt die Deformationsprozesse in diesem Gebirge?

Um diese Fragen zu beantworten, wurde die Theorie der elastischen Platten angewandt, um gravimetrische und topographische Daten zu interpretieren und daraus spezifische Charakteristika der Lithosphärenstruktur in Zentralasien ableiten zu können. Die folgende Leitgleichung zur Flexur einer elastischen Lithosphäre mit lateral inhomogenen Festigkeiten wurde gelöst:

$$\frac{\partial^2}{\partial x^2}\left\{D\ (x,y)\left[\frac{\partial^2 w}{\partial x^2}+\nu\frac{\partial^2 w}{\partial y^2}\right]\right\}+\frac{\partial^2}{\partial y^2}\left\{D\ (x,y)\left[\frac{\partial^2 w}{\partial y^2}+\nu\frac{\partial^2 w}{\partial x^2}\right]\right\}$$

$$+2\frac{\partial^2}{\partial x\ \partial y}\left[D\ (x,y)(1-\nu)\frac{\partial^2 w}{\partial x\ \partial y}\right]+N_{11}\frac{\partial^2 w}{\partial x^2}+N_{22}\frac{\partial^2 w}{\partial y^2}+\Delta\rho g w(x,y)=\rho_c g h_t$$

In der w die Plattenflexur, h_t die Topographie, ρ_c die Krustendichte, $\Delta\rho$ die Dichteabweichung der Kruste und Mantel, N die tektonischen Hintergrundkräfte in Kraft pro Längeneinheit und D die Biegesteifigkeit der Lithosphäre (beschreibt die physische Stärke der elastischen Platte) darstellen. Diese Gleichung wurde mit Hilfe der 3D und 2D finite-Differenzen Methoden gelöst. Platten von variabler Festigkeit werden je nach ihrer geologischen Beschaffenheit vertikalen und horizontalen Auflasten, Scherspannungen und endständigen Biegemomenten ausgesetzt. Mit Hilfe der theoretischen Abweichungen der elastischen Platten von den finite-Differenzen Lösungen konnten theoretische gravimetrische Anomalien berechnet werden; dazu wurden die 2D Formel nach *Okabe* oder die 3D Formel nach *Parker* benutzt. Der Fehler der theoretischen im Vergleich zur gemessenen Bouguer Gravimetrie wurde zur Justierung Biegesteifigkeitsparameter der modellierten Lithosphäre eingesetzt. Durch eine iterative Berechnung konnte ein *best-fit* Modell erzeugt werden (zusammen mit optimierten Werten für D und w), das eine minimierte gravimetrische Anomalie aufweist.

Die Datenbasis dieser Dissertation bilden Bouguer Gravimetrie und topographische Daten. Die Oberflächentopographie aus dem Topo30- Datenset wurde als vertikale Auflast benutzt, um die Flexur der elastischen Lithosphäre zu berechnen. Gravimetrische Daten aus China wurden von der Karte ’Regional Bouguer Gravity of China’ im Maßstab 1:4.000.000 digitalisiert. Diese Karte wurde zwischen 1987 und 1988 vom Institut für Geophysikalische und Geochemische Exploration sowie dem Technischen Zentrum für Regionale Gravimetrie des Ministeriums für Geologie und Mineralische Rohstoffe (MGMR) erstellt. Gravimetrische Daten, die im Auftrag des MGMR seit 1979 zu Prospektionszwecken gewonnen wurden, sind in die Karte integriert. Die Messungen wurden den technischen Standards des MGMR entsprechend in Maßstäben von 1:100.000, 1:200.000 und 1:500.000 durchgeführt. Ergänzend wurden der Datenbasis 468 neue Messpunkte hinzugefügt, die 1997 und 1998 im Bereich des Altyn Tagh im Norden Tibets sowie des West Kunlun Gebirges im Nordwesten gewonnen wurden. Gravimetrische Daten aus Indien stammen aus der Lamont Geobase, solche aus der Mongolei wurden *McNutt et al.* entnommen.

Die Ergebnisse der Modellierung zeigen, dass die mechanische Festigkeit der Lithosphäre in Zentralasien deutlich schwankt, zwischen kleinen, elastischen Mächtigkeiten von weniger als 15 km zu moderaten Werten von 40-50 km. Schwächezonen existieren in den großen Gebieten der Gebirgsbildung wie dem Tien Shan, Altyn Shan, West Kunlun Shan, Qilian Shan oder der Indus-Zhangbo Sutur. Stärkere Zonen befinden sich in den weniger deformierten Beckenbereichen, z.B. in den Tarim, Qaidam oder den Sichuan Becken

oder in bestimmten, niedrig gelegenen Gebieten (< 2500 m). Von besonderem Interesse ist das zentrale und das östliche Tibetanische Plateau. Hier liegt eine hohe elastische elastische Festigkeit vor, ähnlich der in topographisch niedrigen Gebieten. Auch der steil abfallende Übergang vom östlichen Plateau zum angrenzenden Tiefland (Sichuan Becken) schwächt die darunter liegende Lithosphäre nicht maßgeblich. Die gewonnenen Resultate zeigen, dass die Deformationsprozesse in weiten Bereichen Tibets nur in der Kruste, nicht aber durch die gesamte Lithosphäre stattfinden und das die hohe Krustenmächtigkeit in Tibet in erster Linie durch Spröddeformation und Faltung in der Oberkruste hervorgerufen wird. Die mechanische Modellierung der elastischen Festigkeit der Lithosphäre wurde räumlich implementiert um die irreguläre Geometrie der tektonischen Einheiten zu berücksichtigen; die berechneten Variationen der elastischen Festigkeit stimmen dabei gut mit den geometrischen Formen der verschiedenen tektonischen Blöcke überein.

Neue gravimetrische und topographische Daten aus den Gebieten der Altyn Tagh und West Kunlun Störungssysteme wurden benutzt, um Schüsselstellen des oben beschriebenen tektonischen Modells für die nördliche Grenze des Tibetanischen Plateaus zu testen. Die gemessene Gravimetrie entlang dreier Profile wurde in Bouguer-Anomalien konvertiert, um flexurale Modelle der isostatischen Kompensation des großen Reliefunterschieds an den Störungssystemen ableiten zu können. Alle Versuche, die wesentlichen Merkmale der gravimetrischen Anomalien anhand eines isostatischen Modells nachzubilden, das eine Flexur der Moho als Hauptursache für das beobachtete gravimetrische Muster ansieht, scheiterten. Eine Anzahl plausibler Modelle der Krustenstruktur wurden dann mit Hilfe von Informationen aus explorationsseismischen Daten über die Sedimentsäule in den Tarim und Qaidam Becken erstellt. Eine Betrachtung des gravimetrischen *best-fit* Modells zeigte, das die elastische Festigkeit über das Altyn Tagh Störungssystem Null beträgt, was zur Annahme berechtigt, das dieses Störungssystem die gesamte Lithosphäre durchschlägt und zur Zeit und in der Vergangenheit nur eine vernachlässigbar kleine aufschiebende Komponente aufweist. Das Ergebnis stimmt mit tektonischen Modellen überein, die annehmen, das die Bildung der verdickten Kruste in Nord-Tibet durch thick-skinned Deckenüberschiebungen hervorgerufen wird, die sich fortschreitend nach Nordosten über Asien schieben während das Altyn Tagh Störungssystem im Sinne einer klassischen Transformstörung in die gleiche Richtung propagiert. Weiter westlich können die gravimetrischen Beobachtungen am West Kunlun Störungssystem am besten durch deutliches *underthrusting* der hoch gelegenen Gebiete durch eine elastische Platte mit einer effektiven Mächtigkeit zwischen 30 und 40 km erklärt

werden. Diese Interpretation stimmt mit der Modellierung früher gemachter gravimetrischer Beobachtungen überein, die jedoch eine sehr geringe Messdichte aufwiesen.

Eine Korrektur der Sedimentsäule in den Zungar und Tarim Becken im Norden und Süden des Tien Shan sowie eine 2D Modellierung entlang von vier Profilen wurde durchgeführt. Plausible Modelle der Lithosphärenstruktur wurden ebenso getestet, um die wesentlichen Merkmale der Bouguer Gravimetrie und der Topographie räumlich nachzuvollziehen. Die Resultate legen nahe, das die elastische Festigkeit über den westlichen Tien Shan Null beträgt, was für ein Fortbestehen der südlichen Tien Shan Aufschiebung durch die gesamte Lithosphäre spricht. Tektonische Verkürzungsprozesse im westlichen Tien Shan umfassen die gesamte Lithosphäre. Im Gegensatz dazu passen die gravimetrischen Daten am besten zu einer unterschiebenden elastischen Platte mit einer effektiven Mächtigkeit von 40-45 km im Bereich der Tarim und Zungar Becken, die auf 20-25 km unter dem östlichen Tien Shan abnimmt. Für diesen Bereich sagt das *best-fit* Modell einer kontinuierlichen elastischen Platte geringere elastische Mächtigkeiten im Tien Shan Gebirge als in den benachbarten Gebieten vorraus. Wir schlagen vor, das die Deformationsprozesse im Tien Shan vom underthrusting einer starren Platte unter das Gebirge hervorgerufen werden.

Der Tien Shan wurde im Durchschnitt um ca. 3 km im Verlauf der letzten 10 Millionen Jahre angehoben, obwohl er in 1200-2000 km Entfernung zur Kollisionszone zwischen Indien und Eurasien liegt. Dies kann mit Hilfe der Theorie der Plattentektonik nicht erklärt werden. Darüber hinaus kann das lokale Stressfeld im Tien Shan nicht aus dem regionalen Stressfeld abgeleitet werden, das durch Kompression an der Plattengrenze hervorgerufen wird. In dieser Dissertation wurde das lokale Stressfeld im Tien Shan untersucht und der Zusammenhang zwischen einer älteren Phase der Gebirgsbildung und der Reaktivierung des Tien Shan unter dem heutigen tektonischen Regime analysiert. Die Summe der Stressfelder wurde Anhand der folgenden Faktoren berechnet: (1) Interaktion zwischen der Indischen und Eurasischen Platte, (2) die erhöhte gravitative Potentialenergie und (3) Biegung der Lithosphäre im Tien Shan. Dieses zusammengesetzte Stressfeld stimmt mit Vorhersagen anhand von seismischen Herdflächenlösungen, GPS-Messungen und der Oberflächengeologie überein. Die Resultate zeigen, das der tektonische Biegestress, der aus der Biegung der Lithosphäre unterhalb des Tien Shan resultiert, maßgeblich zum Gesamtstressfeld beiträgt. Darüber hinaus legen sie nahe, das die Hebung des Tien Shan eher in Folge eines lokalen intrakontinentalen Stressfeldes erfolgte, als von der Kollision zwischen Indien und Eurasien hervorgerufen wurde.

Acknowledgments

I would like first of all to express my deep gratitude to all those who have encouraged and helped me to finish my dissertation, although I feel rather lost in finding the proper English words to express myself.

I would also like to express my sincere thanks to my supervisor, Professor How Kin Wong. Many geological terminologies in English were new to me. I feel very lucky that during my Ph. D. studies at the University of Hamburg, Professor Wong has always been very patient and understanding in discussions and is always sympathetic to problems that I encountered.

I owe my gratitude to Professor Marcia K. McNutt at the Monterey Bay Aquarium Research Institute. She ignited my interest in lithosphere dynamics. From May to August, 1997, and June to October, 1999, I worked in her laboratory at MIT and at the University of California Santa Cruz, and learnt the theory and method of using Bouguer gravity and topographic data to describe the dynamics of the lithosphere.

Special thanks are due to my former classmate Dr. Yu Jin of the Chevron Petroleum Company, U.S.A. The initial program code I used came from him. He also offered me his patient help in model design, programming and choice of model parameters.

The warmth of all members of the research group of Professor Wong, especially that of Dr. Thomas Lüdmann, Philipp Konerding and Kai Berglar, has been a great source of comfort for me during my stay in Hamburg far away from home.

My thanks go also to Ms. Fang Ye, Haiying Gao and Haiyan Long, who helped me in the preparation of several maps with GMT.

And, last but not least, my most hearty thanks to my husband for his love. He has been waiting for me for such a long time.